Physical-Biogeochemical Couplings in the Land-Ocean Transition Zone

Cara Nissen

June 2014

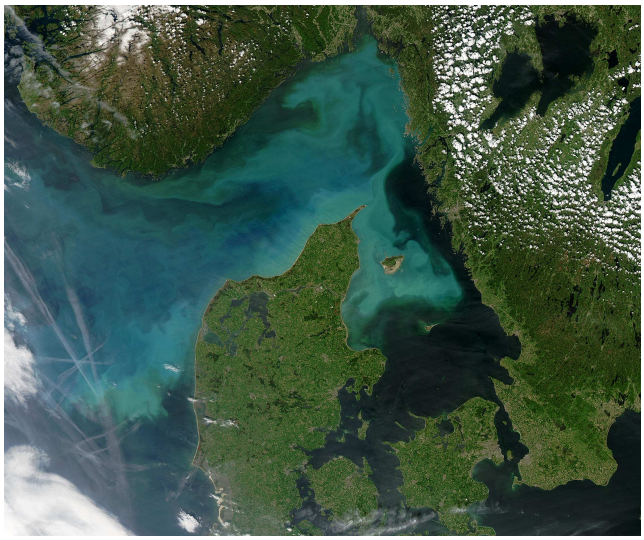

Joint Nordic Master's Program in Marine Ecosystems and Climate (MARECLIM)

Specialization: Physical Oceanography

UNIVERSITY OF THE FAROE ISLANDS

The picture on the title page shows a phytoplankton bloom off the coasts of Denmark. It was taken by the "Moderate Resolution Imaging Spectroradiometer (MODIS)" on NASA's Aqua satellite on June 1, 2004. The picture was downloaded from: http://www.redorbit.com/images/pic/75184/denmark-a2004153-1145-250m/

Physical-Biogeochemical Couplings in the Land-Ocean Transition Zone

Cara Nissen

June 2014

SUPERVISORS:

Corinna Schrum [1,2]

Ute Daewel [1,2]

Katja Fennel [3]

[1] Geophysical Institute, University of Bergen, Norway
[2] Nansen Environmental and Remote Sensing Center, Bergen, Norway
[3] Department of Oceanography, Dalhousie University, Halifax, NS, Canada

Abstract

A significant fraction of global primary production takes place on continental shelves. Due to their interactions with the open oceans, they are highly relevant for the cycling of nutrients, oxygen, and carbon, not only on a regional, but also on a global scale. Coastal areas are to a regionally varying extent impacted by atmospheric, oceanic, and terrestrial forcings, and benthic-pelagic coupling is especially important for the cycling of organic matter in these regions.

In this study, the role of different processes controlling the benthic-pelagic coupling are assessed for the North and Baltic Sea, two regions of fundamentally different characteristics. While the North Sea is characterized by strong tides, exchange with the Atlantic Ocean, and no permanent stratification, the Baltic Sea is mostly influenced by freshwater runoff from land and a limited exchange with open ocean water masses, both leading to a permanent stratification of the water column causing frequent anoxia in the deep basins.

The coupled hydrodynamic–sea ice–NPZD–carbonate–model ECOSMO is used to quantify the role of dissolved and particulate fluxes across the sediment-water column interface for the cycling of nutrients, oxygen and carbon in both North and Baltic Sea by performing sensitivity studies.

A new parametrization of sedimentary respiration is implemented accounting for the anoxic nature of sediments below a thin oxygenated surface layer, and the resulting nutrient and oxygen concentrations are opposed to the former parametrization and validated against observations. The new parametrization improves the model's performance in the Baltic Sea while the North Sea is insensitive to changes in the parametrization.

Subsequently, the importance of resuspension for primary production is demonstrated. At first, the effect of resuspension on the nutrient availability is quantified, without including its effect on the light climate. Generally, the North Sea reacts more sensitively to neglecting resuspension which can be attributed to the stronger tidal forcing. Primary production is locally reduced by up to 45% thereby also significantly changing surface pH and surface flux of CO_2. In a second step, the parametrization of light attenuation is changed to include light attenuation due to water, phytoplankton, dissolved organic matter (DOM), and detritus to address the effect of resuspended matter on light availability. The resuspension experiment is repeated with this new parametrization and results in a significant change in the seasonality of primary production.

Acknowledgements

There is a lot of people I have to thank for their contribution to this thesis. Without each and every one of them, this thesis would not be what it is today. A big thanks ...

- to my supervisors:
  - to Corinna for all the feedback throughout the year, for spending so much time discussing my results or any question I had, and for invaluable comments on earlier versions of this thesis
  - to Ute for patiently answering all my questions, especially about the ECOSMO code
  - to Katja for the collaboration, for all advice, both scientifically and personally
- to Rocío for all the help when I was getting impatient with the code or couldn't figure out the units of a variable in ECOSMO
- to my family for always supporting me
- to my friends all over the world for trying to keep track of all my travelling in those crazy past two years
- to the whole Marine Environmental Modeling Group at Dal for the warm welcome during both of my stays and for the inspiring discussions, especially at the lunch meetings
- to all other master students at UiB for helping me to get my mind off my thesis for at least a few minutes during all those funny coffee & lunch breaks
- to everybody involved in the MARECLIM program for making the past two years as exciting as they were
- to the POME exchange program for financing my stays at Dalhousie University
- to the DAAD for the financial support during the past two years in Norway
- last, but not least to my boyfriend Christoph for always being there for me

Contents

List of Figures

List of Tables

1 Introduction

1.1 Scientific background

Coastal areas are biologically highly productive regions. Generally, between approximately 15% and 30% of the global primary production and approximately 80% of oceanic organic matter burial take place in coastal waters (Gattuso et al., 1998; Borges and Gypens, 2010). Sediment-water exchange is therefore of particular importance when looking at the biogeochemistry of coastal systems. The water column (pelagic environment) is coupled to the seabed (benthic environment) through fluxes of both particulate and dissolved matter. How much organic matter is permanently buried in the sediments is a sensitive balance of rates of sedimentation and organic matter remineralization in both water column and sediments, bioturbation by clams and worms, and resuspension of particulate matter from the seafloor back into the water column (Gruber and Sarmiento, 2006, pp.229ff.).
The coastal ocean represents a transition zone between land and open ocean. In this area, biogeochemical cycling, carbon fluxes, and productivity in the coastal zone are influenced by atmospheric, oceanic and terrestrial forcings. Wind, precipitation, evaporation, advection of open ocean water masses, freshwater runoff from land, and tides are important factors affecting both the physical and biogeochemical properties in coastal areas, but their local relevance might vary significantly (Rodhe et al., 2006; Holt et al., 2014). Moreover, eutrophication due to human activities and climate change have the potential to locally alter, amongst others, the cycling of carbon, oxygen, and nutrients (Neumann et al., 2002; Claussen et al., 2009; Middelburg and Levin, 2009).
Regional bio-physical models are an effective tool to integrate important processes, such as production and degradation of organic matter, the cycling of carbon, nutrients and oxygen, and benthic-pelagic coupling. However, in what way changing climate or anthropogenic forcing is modeled to impact regional ecosystem dynamics, not only depends on the characteristic properties of the region of interest (for example bathymetry, connection to the open ocean, amount of runoff from land), but also on the chosen complexity and parametrizations of the regional biogeochemical model used to study impacts in the respective region (Holt et al.,

2014).

Therefore, it is of high importance to investigate and understand the local dynamics and mechanisms at work in coastal areas and to assess how the chosen setup of the model impacts the representation of important processes.

In the literature, models of different degrees of complexity are employed to study coastal biogeochemical dynamics and their changes under different climatic conditions and eutrophication scenarios (Eilola et al., 2013, 2011; Henson et al., 2013; Neumann et al., 2002). The models differ in the number of functional groups used for phytoplankton and zooplankton, the representation of light attenuation, and the biogeochemical complexity including the representation of sediment respiration processes and sediment-water column coupling. Generally, the respective setup is chosen with regard to the region of interest and the study question to be answered and represents a compromise between accuracy of the representation of the processes of interest and computational demand.

Relevant processes in the coupled benthic pelagic system are benthic and pelagic production, remineralization and sinking speeds, sediment respiration, fluxes of oxygen and nutrients across the sediment water interface under oxic and anoxic conditions, and resuspension (fluxes of particulate organic and inorganic matter). The focus of this study is the role of sediment denitrification and related fluxes of oxygen and dissolved organic nutrients across the sediment-water interface and the fluxes of particulate organic matter from sediments into the water column (resuspension), which both have the potential to impact regional productivity and carbonate chemistry. The region of interest are the North Sea and Baltic Sea. Due to the different geographic setting of the two seas, different processes are expected to be of importance in either of them.

Degradation of organic matter releases nutrients back into the water column, which are again available for photosynthesis and thereby closes the nutrient cycle (Gruber and Sarmiento, 2006, p.173). The relative importance of remineralization processes in the water column compared to those in the sediments depends on the water depth. The shallower it is, the more organic material reaches the sea floor (Treude, 2012). At shallow depths, about 40% of the total respiration takes place in the sediments (Middelburg and Soetaert, 2004; Heip et al., 1995). What directly follows is the importance of including sedimentary processes in bio–physical models. In contrast to this, many biogeochemical models in the past neglected benthic processes completely or only used crude approximations to account for sedimentary processes (Soetaert et al., 2000).

In their review, Soetaert et al. (2000) divide the models into different levels of complexity regarding the benthic-pelagic coupling included (i.e. sediment-water exchange processes). Considering both accuracy and computational demand, they conclude a model including a dy-

namic vertically integrated sediment model coupled to the water column such as implemented in ECOSMO (Daewel and Schrum, 2013) instead of a computationally demanding vertically resolving diagenetic model (highest complexity) to be the best compromise.
Denitrification removes fixed nitrogen from the system, and it is therefore a key process in organic matter degradation. In their study, Fennel et al. (2006) looked at the nitrogen cycling in the Middle Atlantic Bight and underline the importance of denitrification to correctly simulate shelf primary production. Denitrification is especially relevant in low oxygen regimes and regions with high organic sediment portions, such as the Baltic Sea.
Resuspension is forced by strong bottom shear stress and is especially important in regions with a strong tidal or wind forcing (Gruber and Sarmiento, 2006, p.233), such as the North Sea. Particulate matter impacts on primary production are complex and involve both decreasing (light availability) and increasing (availability of dissolved inorganic nutrients) effect. The latter has been demonstrated in Porter et al. (2010).
Tian et al. (2009) investigated the influence of resuspension on primary production through altered light conditions in the German Bight. Testing different parametrizations for light attenuation, the importance of not only considering attenuation due to water and phytoplankton, but also due to other optically active parameters, such as colored dissolved organic matter (CDOM)[1], detritus, and suspended particulate matter (SPM) is demonstrated.
In his study looking at the factors contributing to light attenuation in the North Sea - Baltic Sea transition zone, Lund-Hansen (2004) found an average partitioning of the different factors of 9% for water, 17% for CDOM, 42% for SPM, and 32% for phytoplankton. This is only to a lesser degree considered in current bio-physical models.
Most of the bio-physical models currently used only consider light attenuation due to water (sometimes the combined effect of water and CDOM) and phytoplankton (see e.g. Daewel and Schrum (2013); Fennel et al. (2006); Urtizberea et al. (2013) and Gruber and Sarmiento (2006)).
Urtizberea et al. (2013) investigated the sensitivity of euphotic zone properties to the background turbidity attenuation coefficient (combined effect of water and CDOM) and concluded that when dealing with a model spanning both oceanic and coastal waters (e.g. North Sea and Baltic Sea, see Table 5 in Urtizberea et al. (2013)), varying background turbidity must be accounted for to correctly simulate light conditions.

[1]CDOM is sometimes also denoted as "chromophoric dissolved organic matter" (Lübben et al., 2009)

1.2 Benthic-pelagic coupling

In the remains of this chapter, an overview of key processes in benthic-pelagic coupling which are of particular relevance for the focus of the study are presented. At first, a summary of sedimentary respiration, sediment-water nutrient exchange, and the specific role of denitrification for these are discussed. After this, the exchange of particulate organic matter across the sediment-water interface and its impact on water column properties, such as light attenuation, will be discussed in more detail. Eventually, physical and biogeochemical characteristic properties of the study region will be presented and an outlook on the focus and structure of this thesis will be given.

1.2.1 Sediment respiration & sediment-water nutrient exchange

Organic matter degradation closes the cycling of nutrients (Gruber and Sarmiento, 2006, p.173). Having been incorporated into organic matter by photosynthesis, remineralization re-transforms organic matter into its constituents.

Table 1.1: Stoichiometry for different respiration processes (Gruber and Sarmiento, 2006, Table 6.1.1). Reactions are assuming organic matter (OM) to be composed of $C_{106}H_{175}O_{42}N_{16}P$.

Process	**Stoichiometry**
Aerobic respiration	$OM + 150O_2 \rightarrow 106CO_2 + 16HNO_3 + H_3PO_4 + 78H_2O$
Denitrification	$OM + 104HNO_3 \rightarrow 106CO_2 + 60N_2 + H_3PO_4 + 138H_2O$
Manganese reduction	$OM + 260MnO_2 + 174H_2O \rightarrow 106CO_2 + 8N_2 + H_3PO_4 + 260Mn(OH)_2$
Iron reduction	$OM + 236Fe_2O_3 + 410H_2O \rightarrow 106CO_2 + 16HNO_3 + H_3PO_4 + 472Fe(OH)_2$
Sulfate reduction	$OM + 59H_2SO_4 \rightarrow 106CO_2 + 16HNO_3 + H_3PO_4 + 59H_2S + 62H_2O$
Methane fermentation	$OM + 59H_2O \rightarrow 47CO_2 + 59CH_4 + 16HNO_3 + H_3PO_4$

Decomposition and respiration of organic matter takes place in the water column and the sediments under oxic, but also under anoxic conditions. However, sediment respiration shows different characteristics than respiration in the water column, amongst others due to the

smaller permeability of the sediment, reduced vertical and lateral exchange rates, and higher variety of electron acceptors[2] used (Soetaert et al., 2000). In addition, sediments are mostly a permanently anoxic environment below a thin oxygenated surface layer (Glud, 2008).
In the water column, aerobic respiration and denitrification (if oxygen is absent) are by far the dominant respiration pathways (Soetaert et al., 2000; Peña et al., 2010).
In the sediment, different electron acceptors are used in the degradation of organic matter. The order of consumption of these electron acceptors is determined by their energy yield with oxygen generating the largest energy output, followed by nitrate, manganese, iron, sulfate, and organic matter itself (Treude, 2012; Fennel et al., 2006).
Remineralization in marine sediments is generally sensitive to processes in the overlying water column, especially the amount of organic matter being deposited on the sea floor and bottom water composition, most importantly regarding oxygen and nitrate (Middelburg and Levin, 2009). However, especially in shallow regions, not only is the sediment sensitive to processes in the water column, but also vice versa. This tight two-way-coupling results from the direct effect of sedimentary processes (such as nutrient fluxes) on e.g. primary production (Soetaert et al., 2000).
The equations given in Table 1.1 describing the different pathways of organic matter degradation do not occur simultaneously, but rather consecutively (Gruber and Sarmiento, 2006, p.233f.). This leads to a general vertical profile of the different electron acceptors as shown in Figure 6.1.6 in Gruber and Sarmiento (2006): Oxygen only diffuses into the upper few millimeters (coastal ocean) to decimeters (deeper ocean) of the sediment (Glud, 2008) and is quickly used up by aerobic respiration. Nitrate concentrations increase with depth in the oxygenated part of the sediment due to nitrification of ammonium resulting from organic matter degradation (see Figure 1.1). When oxygen is used up, nitrate is used as the electron acceptor (denitrification, see Figure 1.1) and its concentration decreases with depth.
How much of the produced nitrate in the oxic zone of the sediment diffuses downwards towards the denitrification zone and how much upwards into the overlying water column is the result of a sensitive balance between the amount of nitrate produced in the oxic zone and the concentrations of oxygen and nitrate in the bottom water (Gruber and Sarmiento, 2006; Middelburg and Levin, 2009).
Generally, one distinguishes between coupled nitrification/denitrification referring to denitrification using nitrate that was produced locally in the sediment (nitrate that was produced in the oxic part of the sediment diffuses downwards into the denitrification zone) and direct de-

[2]During respiration processes, an electron acceptor (e.g. oxygen, nitrate, iron, manganese, sulfate or organic matter itself) receives an electron from an electron donor (organic matter) (Gruber and Sarmiento, 2006, p.233)

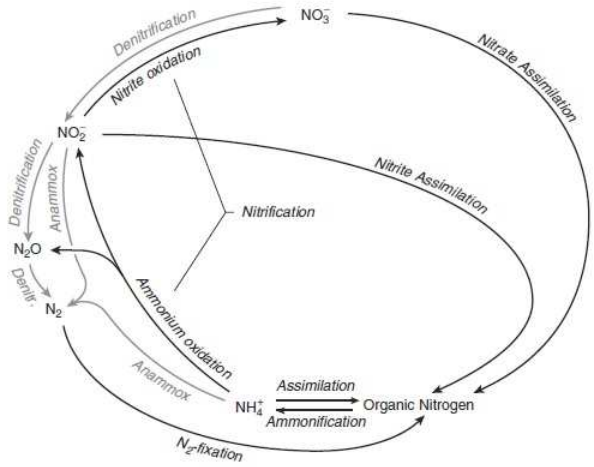

Figure 1.1: Nitrogen cycle (adapted from Gruber (2008)).

nitrification using nitrate diffusing into the sediment directly from the overlying water column (Fennel et al., 2006; Seitzinger et al., 2006).
The relative importance of coupled nitrification/denitrification versus direct denitrification depends on the region looked at. For this study, it is important to note that direct denitrification has been shown to only play a minor role in the North Sea (van Raaphorst et al., 1990; Lohse et al., 1993), but a more important role in the Baltic Sea (Jensen et al., 1990) which frequently becomes (or permanently is) anoxic in its deep basins (see Section 1.3).
Using a diagenetic model, Middelburg et al. (1996) investigated denitrification in marine sediments at different water depths (100 m, 1000 m, and 4000 m). They found qualitatively similar results for sediments at 100 m and 1000 m depth and showed that the contribution of denitrification to overall organic matter degradation is fairly stable in shelf sediments underlying high nitrate bottom water due to a "gradual shift from bottom water nitrate-supported denitrification to nitrification-coupled denitrification" with increasing bottom water oxygen levels.
The importance of the different respiration pathways in marine shelf sediments as a function of bottom water oxygen is shown in Figure 1.2 (Middelburg and Levin, 2009). The general importance of anaerobic processes is obvious easily. The contribution of denitrification to overall respiration is less variable with varying bottom water oxygen ($\approx 5\%$ at $0 - 50 \cdot 10^{-6}$mol O_2 and $\approx 8 - 10\%$ at $50 - 350 \cdot 10^{-6}$mol O_2) than aerobic ($\approx 0 - 8\%$ at $0 - 50 \cdot 10^{-6}$mol O_2 and $\approx 8 - 22\%$ at $50 - 350 \cdot 10^{-6}$mol O_2) and anaerobic respiration (the remaining part).
Anaerobic respiration here includes the reduction of the electron acceptors iron, manganese, sulfate, and organic matter itself. Do these reduced compounds get in contact with oxygen, they are re-oxydized involving a consumption of oxygen (Middelburg et al., 1996; Gruber and Sarmiento, 2006).

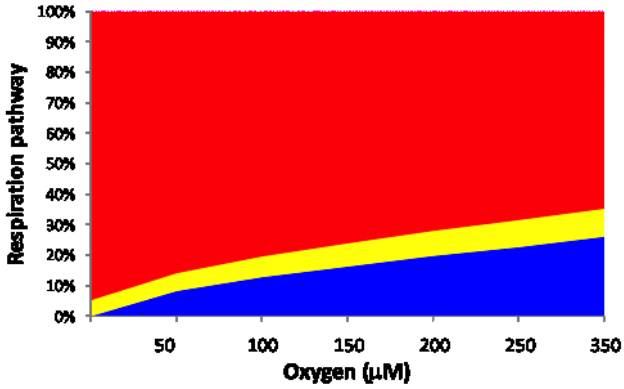

Figure 1.2: Relative importance of different respiratory pathways in shelf sediments (aerobic respiration in blue, denitrification in yellow and anaerobic respiration in red) as a function of bottom water oxygen concentration. Figure is taken from Middelburg and Levin (2009) and is based on model results from (Middelburg et al., 1996).

The dynamics of sediment-water column exchange of phosphate are fundamentally different from that of nitrate/ammonium. A fraction of the phosphate produced by organic matter degradation binds to Fe-oxyhydroxids and is not released. How much of the phosphate is released to the water column and how much stays in the sediment is a function of bottom water oxygen. Under anoxic conditions, the bindings dissolve and all phosphate is relased (Jilbert et al., 2011).

1.2.2 Particle fluxes across the sediment-water interface and light attenuation

Resuspension, the lifting of sediment particles back into the water column, occurs when a critical bottom shear stress τ_{crit} is exceeded (Daewel and Schrum, 2013) and resuspension versus sedimentation is illustrated in Figure 1.3. Resuspension has the power to influence light directly (turbidity) and nutrient conditions indirectly via production and respiration impacts (Schallenberg and Burns, 2004).
Resuspension of sediment particles back into the water column increases the turbidity of the water, thus reduces the amount of light penetrating into the water column.
The intensity of the incoming solar irradiance I_0 at the sea surface decreases exponentially with depth due to absorption and scattering (Wright et al., 1999; Gruber and Sarmiento, 2006). At a depth z, the irradiance $I(z)$ is described by:

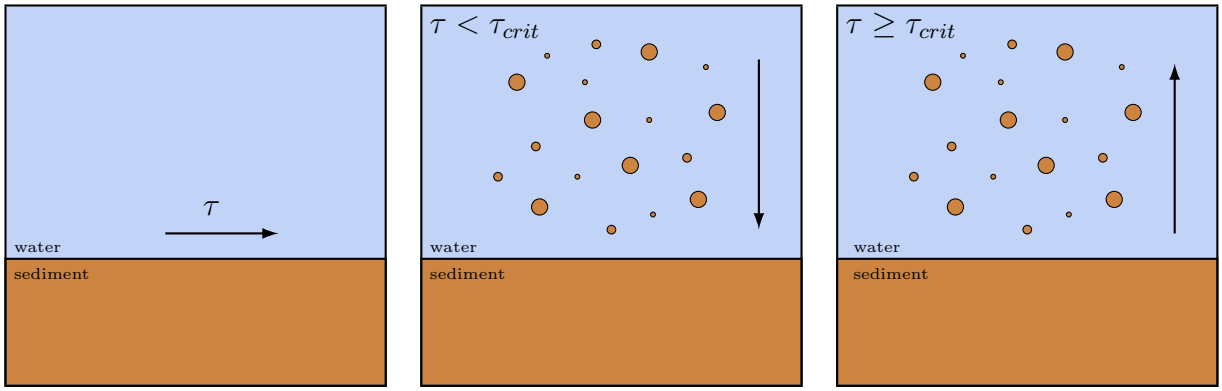

Figure 1.3: Sedimentaion vs. resuspension: Paticles are either deposited on the seabed or lifted up from it depending on the bottom shear stress τ (left). If τ exceeds a critical bottom shear stress τ_{crit} (right), particles get lifted up from the sediment (resuspension), otherwise the particles settle (sedimentation, middle).

$$I(z) = I_0 \cdot exp(-K \cdot z) \tag{1.1}$$

$$K = k_w + k_p \cdot P + k_x \tag{1.2}$$

In this equation, K $[\mathrm{m}^{-1}]$ represents the vertical attenuation coefficient. Attenuation of light is caused by the water itself (k_w $[\mathrm{m}^{-1}]$ is the specific attenuation coefficient of pure water), due to phytoplankton (k_p $[\mathrm{m}^2(\mathrm{mmol\ C})^{-1}]$ scaled with P $[\mathrm{mmol}\, C\, \mathrm{m}^{-3}]$, the concentration of phytoplankton) and due to other particulate and dissolved organic matter (k_x $[\mathrm{m}^{-1}]$).
The specific attenuation coefficients are a function of the wavelength of the incoming radiation. For example, the specific attenuation coefficient of pure water increases from close to zero at 300 nm to $1.8\,\mathrm{m}^{-1}$ at around 700 nm (see Figure 3.3 in Kirk (2011)).
However, most bio-physical models do not include a spectral approach to light representation (see e.g Daewel and Schrum (2013); Neumann et al. (2002); Fennel et al. (2006); Urtizberea et al. (2013); Tian et al. (2009)), but only the integrated effect over all wavelengths of importance for primary production (also called photosynthetically active radiation (PAR) ranging from 400 nm to 700 nm (Wright, 1995, p.70)). Additionally, most models only consider the light attenuation due to phytoplankton and a "background turbidity" (k_{bg} $[\mathrm{m}^{-1}]$) combining the effects of pure water and other particulate and dissolved organic matter (Urtizberea et al., 2013):

$$k_{bg} = k_w + k_x \tag{1.3}$$

Such an approach does not account for any spatial and/or temporal variations in the attenuation characteristics, e.g. due to temporal and spatial variations in CDOM[3].
Dissolved organic matter (DOM) can originate from both the degradation of terrestrial and aquatic plant material (Kirk, 2011; Lübben et al., 2009). While some suggest that CDOM (part of k_x) behaves conservatively in coastal systems, and its effect on light attenuation therefore shows a linear relationship with salinity (Urtizberea et al., 2013), this relationship only holds if all available CDOM originates from river discharge, hence terrestrial plant material. Kirk (2011) pointed out that in productive regions, the marine production of CDOM could be significant. Additionally, terrestrial influence on CDOM was only detected until ≈20 km off the coast in the German Bight in the study conducted by Lübben et al. (2009) suggesting that production in the marine environment is dominating further away from the coast in this area. Coastal regions are dominated by shelf areas with water depths shallower than about 200 m (e.g the North Sea) leading to deeper waters and sediments which often are not fully decoupled from both atmospheric wind and tidal forcing and interfering bottom and surface mixed layers. In these areas, resuspension frequently occurs as a function of wind (occasionally e.g. by autumn storms) and tidal forcing (regularly) and dominantly impacts nutrient recycling pathways, primary production, and carbonate chemistry. The importance of resuspension of sediments for primary production in shallow areas such as lakes (Schallenberg and Burns, 2004) and for phytoplankton spring bloom dynamics (Tian et al., 2009) has been shown before, but its effect on overall primary production on a larger spatial scale has not yet been quantified.

1.3 Study region: North Sea & Baltic Sea

In this study, processes impacting benthic-pelagic coupling will be assessed in ECOSMO, a bio-physical model for the North Sea and Baltic Sea (Daewel and Schrum, 2013). The North Sea and Baltic Sea are two systems with fundamentally different characteristics which will be discussed briefly in the following to provide a hydrodynamic framework for the process discussion.
The topography of the Baltic Sea is made up of three main basins (Bothnian Basin, Gotland Basin, and Bornholm Basin) and numerous narrow and shallow straits interconnecting them (Rodhe et al., 2006; Winsor et al., 2001).
The hydrography of the Baltic Sea is characaterized by large freshwater inputs from adjacent

[3]Colored/Chromophoric dissolved organic matter (CDOM) is often referred to as "yellow substances" in the literature (Wright et al., 1999; Lübben et al., 2009) and describes the optically active fraction of total dissolved organic matter (DOM).

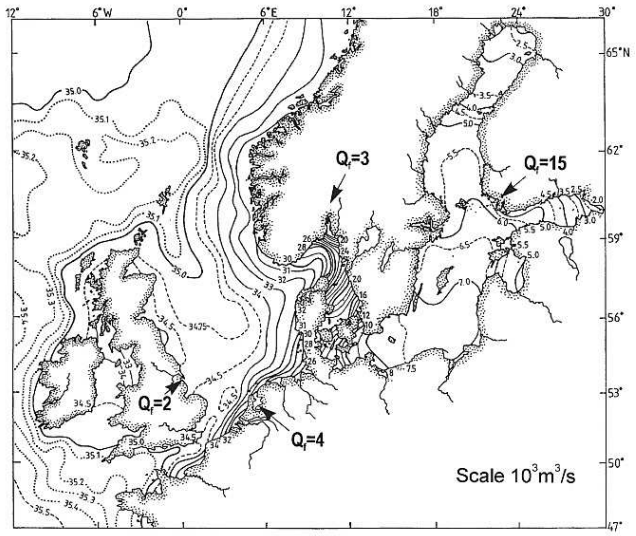

Figure 1.4: Surface salinity in the North Sea and Baltic Sea (Winsor et al., 2001). Additionally, the terrestrial runoff is given by Q_f for four areas: the Baltic Sea, the Kattegat and Skagerrak, the coastal area in the North Sea of Denmark, Germany, the Netherlands, and Belgium, and the east coast of England. Values are given in units of $10^3\,\mathrm{m^3 s^{-1}}$.

rivers and its narrow connection to the open ocean in the Belt Sea and Kattegat restricting the exchange with the open ocean. This leads to comparatively low salinities of $2 - 15$ (brackish water, salinity is gradually increasing from the northern Baltic Sea to the Kattegat, see Figure 1.4 (Winsor et al., 2001)), a low tidal range (in the order of decimeters), and long exchange time scales of $20 - 30$ years (Rodhe et al., 2006; Winsor et al., 2001).

The Baltic Sea generally shows a typical estuarine circulation (sill fjord circulation) with freshwater outflow at the surface and inflow of denser more saline water of oceanic origin through the Kattegat at greater depths[4]. As a result of the circulation, the Baltic Sea can mainly be looked at as a two-layer system. It has a permanent halocline at around 80 m (Winsor et al., 2001) and a thermocline that varies seasonally between on average approximately 20-50 m (summer) and 80 m (winter) (Janssen et al., 1999).

Due to the low salinities and the permanent stratification, sea ice formation plays an important role in the overall Baltic Sea, but especially in the northern areas, which are covered with sea ice every winter and up to almost half a year in the very northern coastal region (indicated in Figure 1.5(b)) (Vihma and Haapala, 2009; Winsor et al., 2001).

This is why primary production in the Baltic Sea is not only controlled by the availability of nutrients and light, but also indirectly by sea ice cover, which controls light availability in

[4]The Mediterranean Sea is another example of a semi-enclosed sea with an estuarine circulation (Colling, 2001, p.205)

spring.
The permanent stratification, weak tidal mixing and weaker wind driven mixing results in only weak coupling of the surface layer to the deep nutrient pool and thus in generally lower primary production levels compared to the North Sea (Daewel and Schrum, 2013, Figure 9).
Air-sea exchange processes rarely result in an oxygenation of deeper layers of the Baltic Sea due to the general characteristics presented above. Low oxygen values or complete oxygen depletion is frequently or even permanently found in certain areas in the Baltic Sea, especially in the deep areas of the Baltic Proper (see Figure 1.5(b) (Rodhe et al., 2006)).

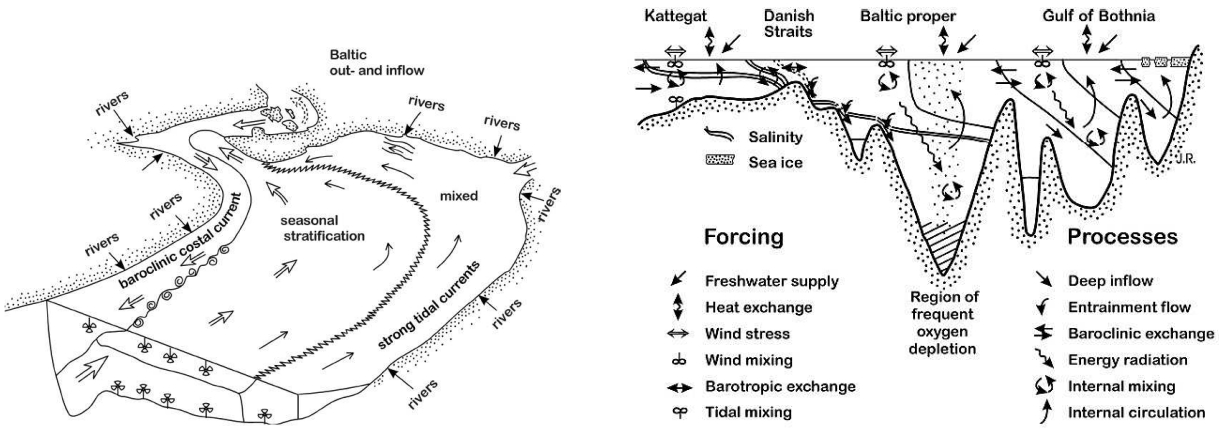

(a) (b)

Figure 1.5: Important physical processes in the North 1.5(a) and Baltic Sea 1.5(b) (Rodhe et al., 2006).

Having a wide opening towards the Atlantic Ocean, the North Sea (about twice the size of the Baltic Sea) is classified as an adjacent sea. The average depth of 93 m is misleading because only a fairly small area around the southern coast of Norway shows depths greater than 500 m while the rest is to a large part shallower than 50 m (Rodhe et al., 2006).
The circulation in the North Sea is dominated by inflow of water of the North Atlantic Current (NAC, $\approx 1-2\ Sv$) on the northern end of the sea (see Figure 1.5(a)), only a small fraction of the inflow comes through the English Channel in the south (inflow about one order of magnitude smaller (Turrell et al., 1996; Winsor et al., 2001)).
The main outflow of water occurs with the freshwater driven baroclinic Norwegian coastal current. Average salinities found in the North Sea are around $34-35$ (see figure 1.4 (Winsor et al., 2001) and Janssen et al. (1999)) leading to large salinity gradients in the Kattegat area (see Figure 1.4).
The prevailing salinity values might seem surprising when looking at the significant input of freshwater by adjacent rivers ($9\,\mathrm{m^3 s^{-1}}$), but they can be explained by the wide opening towards

the Atlantic Ocean leading to a short exchange time scale of one year or less (Rodhe et al., 2006).
Another result of the open connection to the Atlantic Ocean are pronounced co-oscillating semi-diurnal tides that can be found all along the coast in the North Sea. The incoming tidal wave propagates as a Kelvin wave counterclockwise through the North Sea leading to elevated tidal ranges towards the coast (see Figure 1.6).
Tidal ranges at the North Sea coasts can be as high as 6 m in southeastern England (even up to 11 m in the English Channel) and as low as slightly larger than zero at the southern coast of Norway. The latter is due to the proximity to an amphidromic point where the tidal range is zero. Even though the German North Sea coast is relatively close to such an amphidromic point as well, it has larger tidal ranges resulting from the shoaling of the topography with shorter distance to the coast (tidal wave piles up while approaching the coast).
Tides are extremely important to understand the dynamics of the North Sea. The dominant part of the tidal energy entering the oceans is dissipated over the continental shelves where the strongest tidal currents are observed (Thorpe, 2007, ch.6). Figure 1.6(b) (Davies and Kwong, 2000) shows the tidal energy dissipiation (in log_{10}) of the M2 constituent for the North Sea. Highest energy dissipation rates are found in the western and southern North Sea. Vertical mixing of the water column is induced by turbulence resulting from bottom friction due to tidal currents.
During summer, a seasonal thermocline develops over most of the North Sea. Near the coast and in the Southern Bight, the North Sea remains nearly well mixed throughout the year with a tidal mixing front separating these two regimes (e.g. Janssen et al. (1999); Schrum et al. (2003)). Surface mixed layer and bottom mixed layer are uncoupled in the northern North Sea, whereas they frequently interact in the southern North Sea resulting in continuous entrainment of nutrients into the euphotic zone.
The bathymetric and hydrographic characteristics have huge implications for primary production and sea ice formation. As mentioned before, there is no sea ice formation in the North Sea (in contrast to the Baltic Sea), which can be explained by the dynamics of the area and the characteristics of the prevailing water masses. Relatively high salinities (> 24.7) in the North Sea lead to winter convection preventing sea ice formation.
Primary production is generally higher in the North Sea compared to the Baltic Sea due to winter mixing, Atlantic water supply, and more pronounced wind and tidal mixing in the North Sea. The latter enhances productivity especially in the southern North Sea by a permanent re-supply of nutrients from the deep water nutrient pool to the surface leading to extended production. That is why nutrients do not become a limiting factor for primary production throughout the year in those areas (Daewel and Schrum, 2013). Schrum et al. (2006) pointed

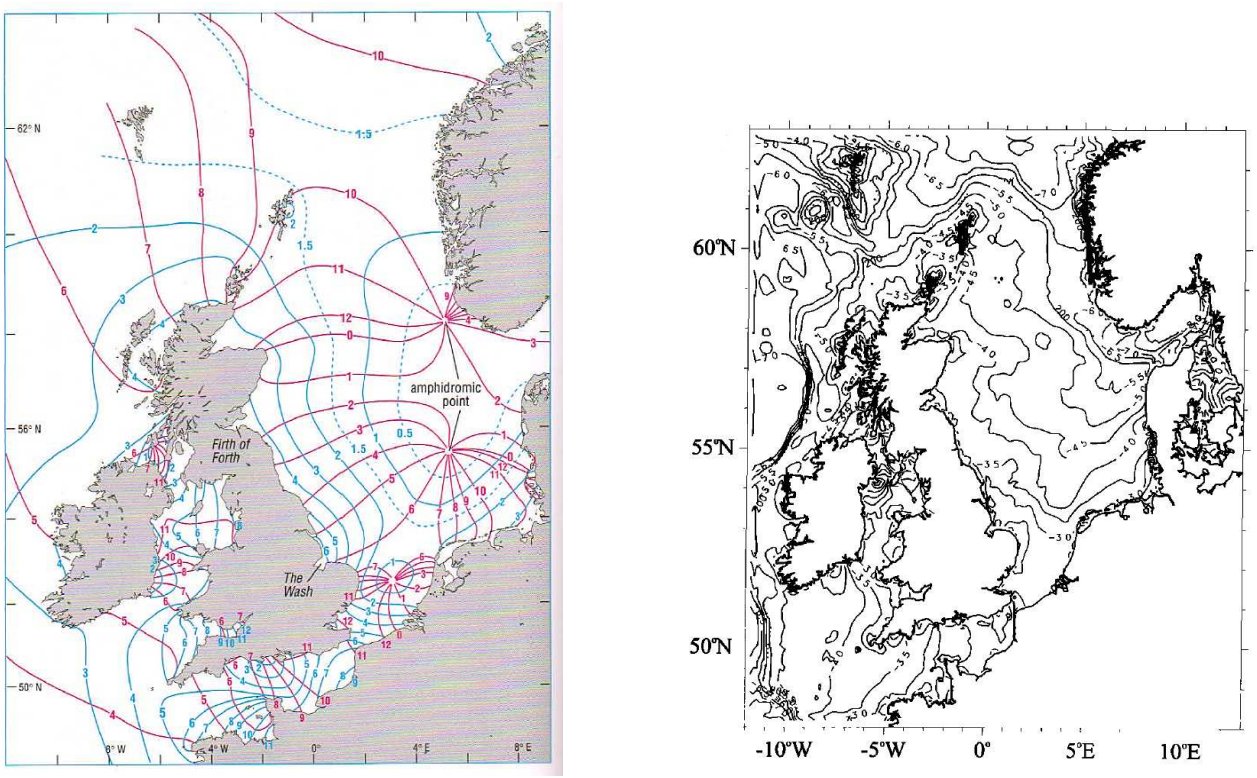

(a) (b)

Figure 1.6: Tides in the North Sea. Amphidromic systems in the North Sea and west of the British Isles in Figure 1.6(a) (Wright et al., 1999). The time of the high water after the Moon has passed the Greenwich meridian is indicated with the co-tidal lines (red) and given in hours. Co-range lines are shown in blue, tidal range is given in meters. Figure 1.6(b) (Davies and Kwong, 2000) shows the log_{10} tidal energy dissipiation of the M2 constituent in $\mathrm{W\,m^{-2}}$.

out that silicate can potentially be a limiting factor for primary production by diatoms in the North Sea with flagellates therefore dominating over diatoms. As can be seen in Figure 10 in Daewel and Schrum (2013), the opposite is the case for the Baltic Sea. Here, cyanobacteria (nitrogen fixers) as a third group of phytoplankton play a not negligible role in the ecosystem. The coupled system North Sea-Baltic Sea covers areas of different characterics in the benthic-pelagic coupling. The Baltic Sea spans a variety of oxygen regimes in the bottom water and thereby influences both the dynamics of phosphate sediment-water column exchange (Jilbert et al., 2011) and the importance of different respiratory pathways in the sediments. Jensen et al. (1990) pointed out that direct denitrification has been shown to be up to equally important as coupled nitrification/denitrification in the Baltic Sea while direct denitrification does not seem to play an important role in the North Sea (van Raaphorst et al., 1990; Lohse et al., 1993). The latter is mainly dominated by resuspension due to the strong tidal influence.

2 Data & Methods

In this chapter, a detailed description of the methods used in this study will be presented. To analyze the role of different processes affecting benthic-pelagic coupling in the North and Baltic Sea, the model ECOSMO (Schrum et al., 2006; Daewel and Schrum, 2013) is used. Here, the version and setup previously described in Daewel and Schrum (2013) provides the basis of the study. Changes in parametrizations described in this chapeter are applied to this version of the model.
First, the focus of this study is outlined. After a brief description of general characteristics of ECOSMO and results from previous validation experiments revealing its strengths and weaknesses in Section 2.2, a description of the most important features of the biogeochemical component (NPZD module, carbonate chemistry and sediments) follows. The model equations of this component are described in detail in the appendix (p.96).
Observational data sets and methods of model validation are presented subsequently, followed by a description of the newly implemented parametrizations into the model in this study. Concluding, an emulator method is presented in Section 2.5 which is used to assess the model's sensitivity to its parametrizations in a computational effective way. Details about all model runs performed in this study are given in Section 3.1 and 4.1.

2.1 Focus of this study

This study focusses on the sediment-water column coupling in the North Sea and Baltic Sea using ECOSMO. Sensitivity experiments are performed to assess the importance of two different ways of exchange of matter at the sediment-water column interface for primary production: the exchange of dissolved and particulate matter, respectively. Regional differences in the importance of different processes will be identified, quantified, and discussed.
Regarding the exchange of dissolved matter at the sediment-water column interface, the release of inorganic phosphate due to resuspension is introduced into the model in this study. Furthermore, a new parametrization of sedimentary respiration processes is implemented. Considering constant percentaged contributions of different respiration pathways to overall respiration, the

changes for the benthic-pelagic coupling induced by this newly developed parametrization are analyzed.
To assess the importance of exchange of particulate matter at the sediment-water column interface, different model experiments are performed. The importance of resuspension on primary production and state variables of the carbonate system is quantified by comparing model runs with and without resuspension of sediment particles. Both the positive effect of resuspended material for primary production (higher nutrient availability) and the negative effect due to decreased light availability are quantified. To include the light effect of resuspended particles, the sensitivity of ECOSMO to the parametrization of light attenuation is analyzed and a new parametrization implemented, accounting for dissolved and particulate matter in light attenuation. To quantify the importance of detritus and DOM in light attenuation and in the model in general, an emulator method is used.
Studying the importance of different processes affecting sediment-water column exchange is especially interesting in ECOSMO. Its model domain comprises both the North and the Baltic Sea - two fundamentally different systems when looking at their dynamics (see Section 1.3). From this, it is expected that the different processes assessed in this study show a fundamentally different importance in the two seas.

2.2 ECOSMO: Model description & setup

ECOSMO[1], which is used in this study, is a coupled hydrodynamic–sea ice–NPZD[2]–carbonate–system (Schrum et al., 2006; Daewel and Schrum, 2013; Daewel et al., 2014)). The hydrodynamic component of ECOSMO is the free-surface 3D baroclinic coupled sea-ice model HAMSOM3, which is described in more detail in Schrum and Backhaus (1999).
The model is implemented for the North Sea & Baltic Sea (incl. boundary and forcing conditions) and has previously been run for a 60 years simulation period (Daewel et al., 2014). ECOSMO is computationally efficient and can easily be integrated for several decades to investigate the impact of the different processes for different climate periods.
In their study, Daewel and Schrum (2013) assessed the model's validity when studying seasonal, inter-annual, and decadal variability in both seas. They conclude that ECOSMO simulates ecosystem variability in both the North and the Baltic Sea sufficiently well, but pointed out some weaknesses as well. The overestimation of summer concentrations of nitrate in some

[1]ECOSMO = ECOSystem MOdel
[2]NPZD = Nutrient Phytoplankton Zooplankton Detritus

parts of the southern North Sea is interpreted as a systematic deficiency of the model and may be induced by a phosphate limitation created by the model, e.g. due to missing tidal flats in ECOSMO. In the Baltic Sea, mis-representations of ecosystem dynamics are linked to stratification and deep water ventilation and are potentially caused by errors introduced by the numerical setup underestimating mixing, the vertical resolution especially in deeper areas of the model domain and the resolution of atmospheric forcing data which both are too coarse. Additionally, river load data are not complete and might lack the temporal resolution needed to correctly simulate nutrient loads from lands.

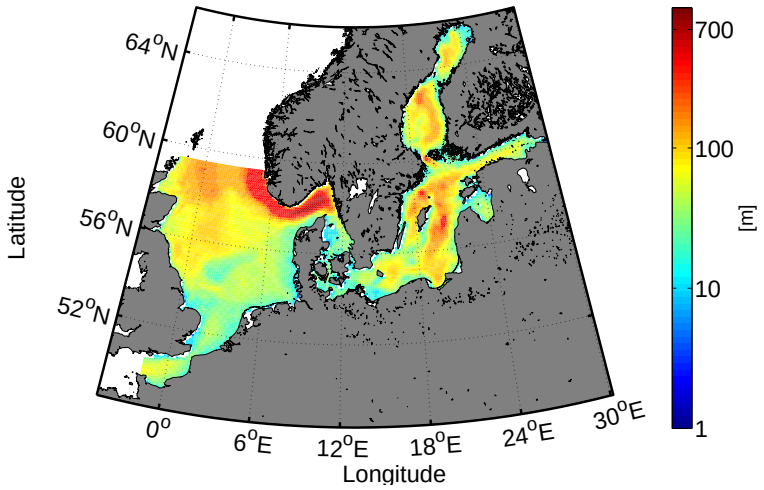

Figure 2.1: Bathymetry of the model domain of ECOSMO, depth given in meters.

The model domain and its bottom topography is shown in Figure 2.1. The model captures the main topographic features of both the North and the Baltic Sea (see Section 1.3). The horizontal resolution of ECOSMO is approximately 10km, its vertical resolution is depth-dependent: 5m for the upper 40m, 8m for the layer between 40m and 88m, and more coarsely below.

In this study, the model is generally forced with the same data as presented in Daewel and Schrum (2013). At the surface, the model is forced with atmopsheric data from the NCEP/NCAR reanalysis project (NCEP/NCAR, 2013) as well as freshwater runoff from land and river nutrient loads. A data set combining different sets of observations was compiled for river runoff as decribed in Daewel and Schrum (2013). Sea surface elevation is prescribed at the open boundaries (North Atlantic, English Channel) from a coarser model for the North Atlantic (Backhaus and Hainbucher, 1987). ECOSMO considers co-oscillating tides forced in the North Atlantic. Tidal sea level variations are prescribed with a time step of 20 minutes for the 8 dominant tidal constituents (M2, S2, N2, K2, μ2, K1, O1, P1) at the northern open boundary and for the English Channel. The model is initialized with gridded climatological

data for temperature and salinity compiled by Janssen et al. (1999) and fields for the nutrients (initial and boundary conditions) are taken from the World Ocean Atlas (Conkright et al., 2001). Sediments are initialized with results from an earlier run. For further details on the model setup and applied bias corrections applied to the atmospheric NCEP forcing, see Daewel and Schrum (2013).
If not indicated differently, model runs in this study are done from 1984-2009, but only the last 11 years (1999-2009) are analyzed.

2.2.1 NPZD module & carbonate chemistry

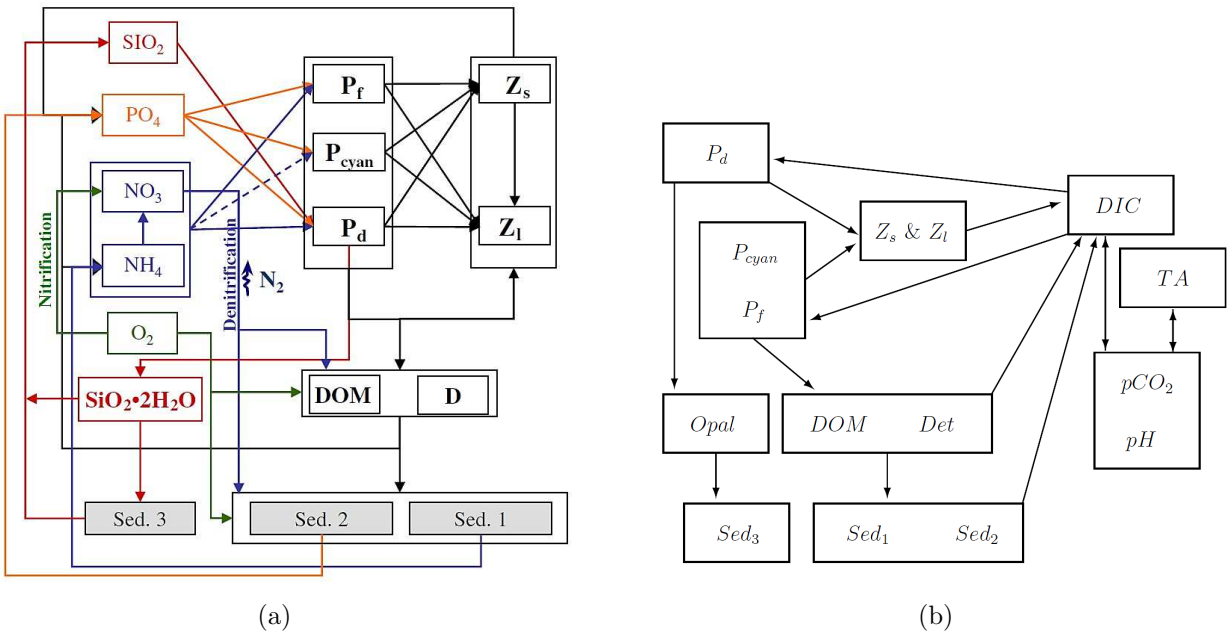

(a) (b)

Figure 2.2: Interactions of state variables in ECOSMO. Figure 2.2(a) taken from Daewel and Schrum (2013), Figure 2.2(b) shows additional interactions with state variables of the carbonate system. P_d (left figure) = P_l (Table 2.1), $P_f = P_s$ and $P_{cyan} = P_{bg}$.

In the NPZD module, biomass and nutrients are described in carbon units according to Redfield stoichiometry (Schrum et al., 2006; Redfield, 1934). This means that the elements carbon, nitrogen, and phosphate are built into organic matter while producing oxygen in the ratio $106:16:1:-138$ $(C:N:P:O_2)$ following the formula

$$\begin{aligned} &106CO_2 + 16HNO_3 + H_3PO_4 + 122H_2O \\ &\rightleftharpoons (CH_2O)_{106}(NH_3)_{16}(H_3PO_4) + 138O_2 \end{aligned} \tag{2.1}$$

Table 2.1: State variables in ECOSMO.

	Abbr.	Variable	Units
1	P_l	Diatoms	mg C m^{-3}
2	P_s	Flagellates	mg C m^{-3}
3	P_{bg}	Cyanobacteria	mg C m^{-3}
4	Z_l	Meso Zooplankton	mg C m^{-3}
5	Z_s	Micro Zooplankton	mg C m^{-3}
6	D	Detritus	mg C m^{-3}
7	DOM	Dissolved Organic Matter	mg C m^{-3}
8	NH_4	Ammonium	mmol N m^{-3}
9	NO_3	Nitrate	mmol N m^{-3}
10	PO_4	Phosphate	mmol P m^{-3}
11	SiO_2	Silicate	mmol Si m^{-3}
12	$Opal$	Biogenic Opal	mmol Si m^{-3}
13	O_2	Oxygen	ml l^{-1}
14	Sed_1	Sediment	mg C m^{-2}
15	Sed_2	Sediment Phosphate	mg C m^{-2}
16	Sed_3	Sediment Silicate	mg C m^{-2}
17	DIC	Dissolved Inorganic Carbon	mg C m^{-3}
18	TA	Total Alkalinity	mg C m^{-3}
19	pCO_2	partial pressure of CO_2	μatm
20	pH	pH	

For diatoms, the only group of phytoplankton requiring silicate besides nitrogen and phosphate, the ratio of $Si:N$ is 1:1 (Brzezinski, 1985)[3].

Currently, 16 state variables are used to model the biogeochemistry and ecosystem dynamics in water column and sediments, and another 4 state variables are used to model carbonate chemistry (see Table 2.1 (Daewel and Schrum, 2013; Daewel et al., 2014)). For each state variable, assuming C to be the respective state variable, prognostic equations of the following form are used in the model (Daewel and Schrum, 2013):

$$\frac{\partial C}{\partial t} + (\vec{v} \cdot \nabla)C + w_D \frac{\partial C}{\partial z} = \frac{\partial}{\partial z}(A_v \frac{\partial C}{\partial z}) + R_C \tag{2.2}$$

Local changes over time of a state variable ($\frac{\partial C}{\partial t}$) are caused by advective transport ($(\vec{v} \cdot \nabla)C$), sinking ($w_d \frac{\partial C}{\partial z}$), vertical sub-scale diffusion ($\frac{\partial}{\partial z}(A_v \frac{\partial C}{\partial z})$), or biological or chemical interactions (R_C). The velocity for advective transport $\vec{v} = (u, v, w)$ and the vertical diffusion coefficient

[3]Gruber and Sarmiento (2006) (p.270) commented that this ratio is only valid for "diatoms with adequate light and nutrients"

A_z are estimated in the hydrodynamic part of ECOSMO. The sinking speed w_D is a non-zero constant only for detritus, opal, and cyanobacteria. The three sediment state variables can only change in time by biological or chemical interactions, all other terms are zero.
The reaction term is different for each state variable and described in detail in the appendix (see p.96).
In ECOSMO, phytoplankton is divided into three functional groups (diatoms, flagellates, cyanobacteria (nitrogen fixers)) and zooplankton into two, based on their feeding behaviour (microzooplankton (herbivorous) and mesozooplankton (omnivorous)). Primary production by phytoplankton is limited by either light or nutrients. Phytoplankton growth is only temperature dependent for cyanobacteria.
Dead organic matter is divided into DOM (Dissolved Organic Matter) and detritus. The pools of DOM and detritus are filled with the fixed percentages 40%/60%, but the ratio can vary after that because DOM is remineralized 10 times faster than detritus and is not sinking, in contrast to detritus. Biogenic opal only includes dead organic matter from diatoms. Detritus sinks to the sea floor where it is sedimented when the critical bottom shear stress $\tau_{crit} = 0.07\ \mathrm{N/m^2}$ is exceeded. Otherwise, sediment is resuspended to the detritus pool in the water column.
Oxygen, phosphate, nitrate, ammonium, and silicate are included as state variables to resolve the three macronutrient cycles including respiratory processes.
Sediment dynamics and sediment-water exchange processes are described in more detail in Section 2.2.2.
The incoming short wave radiation at the sea surface is halved to only account for photosynthetically active radiation (PAR, see Section 1.2.2). The depth dependence of light intensity is then described by Equation 1.1 (p.8). In the current version of ECOSMO (Daewel and Schrum, 2013), only light attenuation due to phytoplankton (specific attenuation coefficient: $0.2\,\mathrm{m^2(mmolC)^{-1}}$) is resolved. The attenuation due to particulate and organic matter and the water itself are parametrized by considering a constant background turbidity coefficient ($0.5\,\mathrm{m^{-1}}$).
Generally, the carbonate chemistry in the ocean can be described by the following reactions (Doney et al., 2009):

$$CO_{2_{atm}} \rightleftharpoons CO_{2_{aq}} + H_20 \rightleftharpoons H_2CO_3 \rightleftharpoons H^+ + HCO_3^- \rightleftharpoons 2H^+ + CO_3^{2-} \tag{2.3}$$

Atmospheric CO_2 ($CO_{2_{atm}}$) which is dissolved in seawater ($CO_{2_{aq}}$) reacts with water (H_2O) to H_2CO_3 (carbonic acid). This dissociates to first form HCO_3^- (bicarbonate ion) and finally CO_3^{2-} (carbonate ion), hereby adding two hydrogen ions (H^+) to the seawater. If more $CO_{2_{aq}}$ is dissolved in seawater, bicarbonate and hydrogen ion concentrations increase, whereas

carbonate ion concentration and the pH of seawater ($pH = -log_{10}[H^+]$) decrease.
There are four measurable variables describing the carbonate system: pH, pCO_2 (partial pressure of CO_2), TA (Total Alkalinity), DIC (Dissolved Inorganic Carbon), amongst which only TA and DIC are conservative and defined as follows (square brackets representing the concentration (Zeebe and Wolf-Gladrow, 2008)):

$$DIC = [CO_2] + [HCO_3^-] + [CO_3^{2-}] \tag{2.4}$$

$$TA = [HCO_3^-] + 2[CO_3^{2-}] + [B(OH_4)^-] + [OH^-] - [H^+] + minor\ compounds \tag{2.5}$$

DIC, TA, pCO_2, and pH are included as state variables in ECOSMO. DIC and TA are prognostic variables, pCO_2 and pH diagnostic, they are calculated from DIC and TA. DIC changes with primary production, degradation of organic matter and excretion by zooplankton. TA depends on river discharge and is parametrized as a function of salinity.
The flux of CO_2 at the surface of the ocean (fCO_2) is calculated as a function of the difference in pCO_2 between atmosphere and ocean, the solubility of CO_2 in seawater and wind speed (Daewel et al., 2014).
For a more complete overview of the exact equations and parameter values used in the original version of ECOSMO, please see the appendix (p.96).

2.2.2 Sedimentary respiration in ECOSMO

In the current version of ECOSMO, sediments are split up into three pools to account for counter-acting dynamics: The 3 groups resolve (1) particulate sediments (containing both nitrogen and phosphorus contributions in Redfield stoichiometry), (2) dissolved phosphorus bound to Fe-complexes, and (3) sedimented biogenic opal (silicate pool).
While the silicate sediment pool interacts with the biogenic opal only, the pool of particulate sediment interacts with detritus. The link between the particulate sediment pool and the one of dissolved phosphorus is established through respiratory processes. Remineralizing organic matter in the first sediment pool leads to a respective addition of phosphorus to the second pool (Daewel and Schrum, 2013).
The release of phosphorus to the overlying water column as phosphate is dependent on the bottom water oxygen concentration as mentioned in Section 1.2.1 (p.4). Under oxic conditions, a fraction of the phosphate in the sediment binds to Fe-oxyhydroxids and is thus not released. The more oxygen is available, the less phosphate is relased. Under anoxic conditions, all phosphate is released into the bottom water (Jilbert et al., 2011; Daewel and Schrum, 2013)

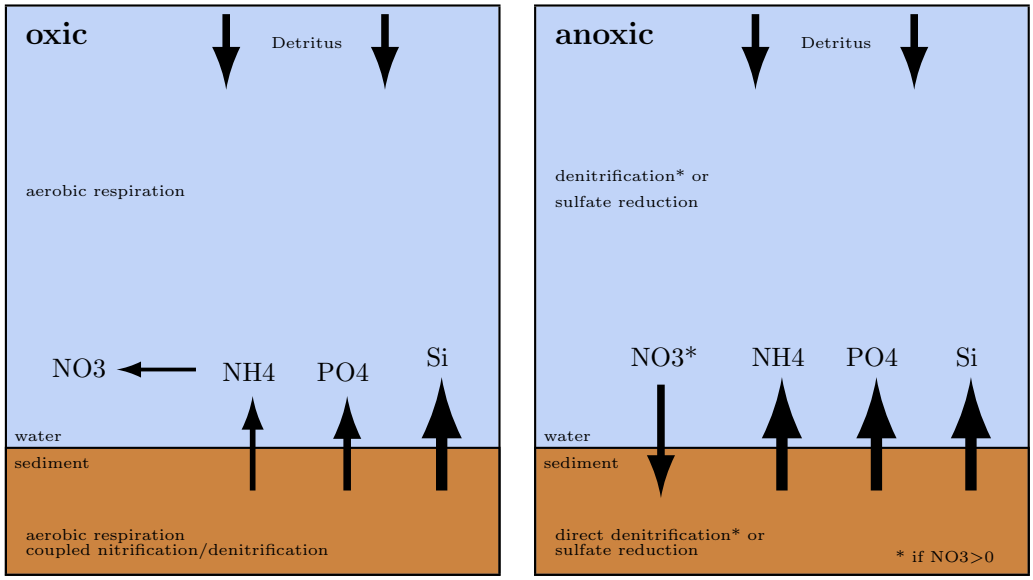

Figure 2.3: Respiratory processes in ECOSMO before changes were applied. It is differentiated between sediments underlying oxic (left) and anoxic (right) bottom water only. More explanation can be found in the text.

(see the appendix on p.96 and Neumann et al. (2002) for the exact parametrization). In the current version of ECOSMO (Daewel and Schrum, 2013), no phosphate release into the water column due to resuspension is considered.

Rates of respiratory processes are temperature dependent. Which electron acceptor is used for respiration depends on the availability of oxygen. Here, it is only differentiated between oxic and anoxic conditions in the water column.

If oxygen is available, aerobic respiration is the only pathway of organic matter degradation in the water column. In this setting, nitrification takes place as well. In the sediment, respiration is done through aerobic respiration and denitrification, which, as long as the bottom water is well oxygenated, are equally important. This is realized by only releasing half of the ammonium produced by overall respiration, assuming that the other half fuels coupled nitrification/denitrification.

Under anoxic conditions, denitrification is the only pathway of organic matter degradation if nitrate is present, otherwise oxidation occurs by sulfate reduction which is accounted for by negative oxygen values. In the sediment, direct denitrification using nitrate from the overlying water column as the source of nitrate is the only active respiratory process until all nitrate is used up. Due to the absence of oxygen both nitrification and thereby also coupled nitrification/denitrification cannot take place. When all nitrate is used up, sulfate reduction sets in.

The release of silicate to the overlying water column does not show a oxygen dependence - all

silicate produced by organic matter degradation is released from the sediment.

2.3 Observational data & validation methods

Observational data from the period 1948-2008 of nitrate, phosphate, and oxygen are downloaded from ICES (2014)[4] to validate the new parametrization of sedimentary respiration processes, which will be presented in the following section, in the ECOSMO model. Additionally, observations from the CANOBA data base (Bozec et al., 2005; Thomas et al., 2005) are used for the North Sea. The latter data are for the seasonal cycle 2001-2002 only (four cruises in one year) and are available on an approximately 1° by 1° grid for the North Sea (97 stations), thus adding stations that are not included in the ICES data set.

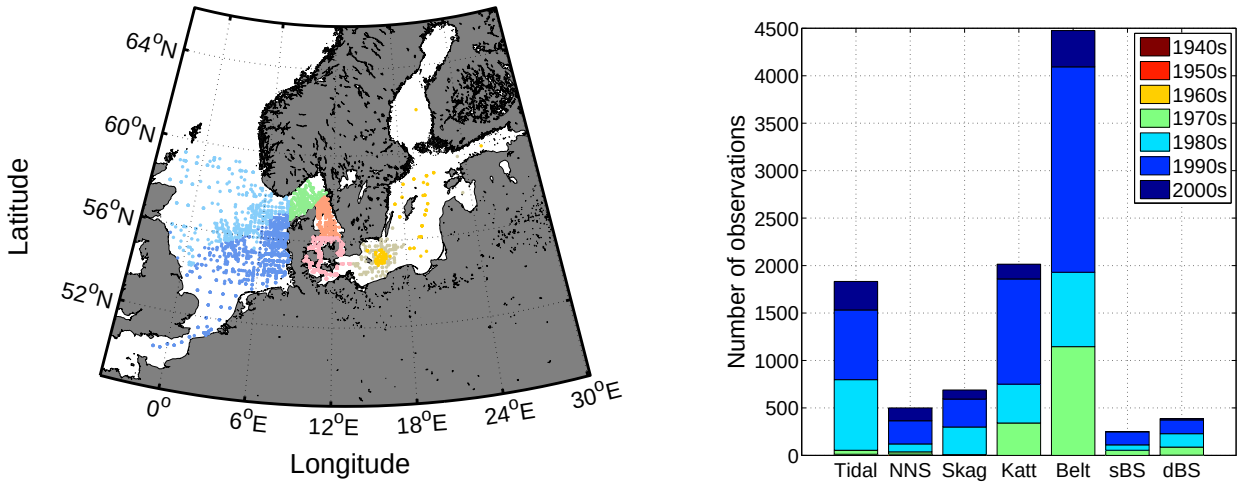

Figure 2.4: Observations of surface nitrate between 1948-2008. Data are combined from the ICES (ICES, 2014) and the CANOBA data set for the North Sea (Bozec et al., 2005; Thomas et al., 2005). Figure 2.4(a) shows the spatial distribution of the data. Colors correspond to regions in Figure 2.5. Figure 2.4(b) shows the average number of observations per year in each region between 1948-2008.

To avoid misinterpretations due to aliasing, model data and observations are co-located. The co-location procedure picks the closest model data point from the ECOSMO results (smallest difference in time and in latidudinal and logitudinal coordinate respectively). The vertical resolution of the observations can differ from the depth levels of ECOSMO. Therefore, the

[4]http://ocean.ices.dk/HydChem/

measured values are linearly interpolated onto the depth levels of ECOSMO[5].
Figure 2.4 shows the spatial (Figure 2.4(a)) and temporal (Figure 2.4(b)) resolution exemplarily for observational surface nitrate data for 1948-2008. While the North Sea shows a good spatial distribution in the observational data base, the Baltic Sea is much less resolved both spatially and temporally. Monitoring of the Baltic Sea state is mainly done using a few monitoring stations in each of the Baltic Sea basins. A dense data set of observations is available in the transition zone between both seas.
For the comparison of model data and observations, different characteristic regions are defined: northern North Sea (north NS/NNS), tidal mixing zone[6], Skagerrak, Kattegat, Belt Sea, shallow Baltic Sea (shallow BS/sBS), and deep Baltic Sea (deep BS/dBS)[7]. The boundaries between the different areas can be seen in Figure 2.5.

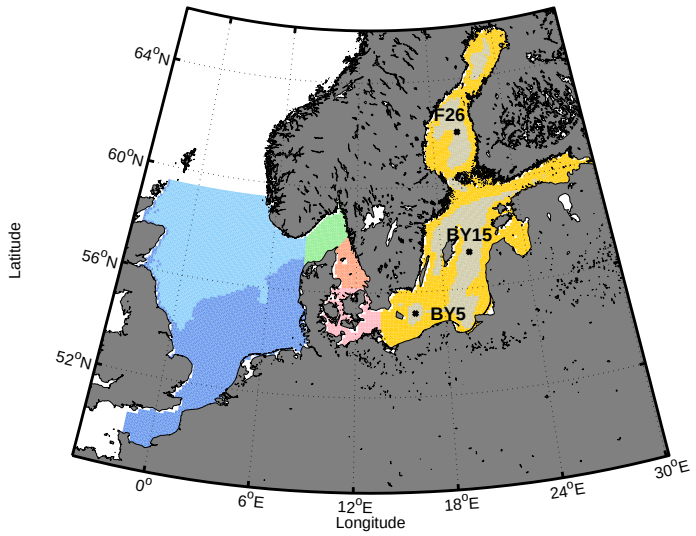

Figure 2.5: Subareas in ECOSMO: northern North Sea (light blue), tidal mixing zone (blue), Skagerrak (green), Kattegat (salmon), Belt Sea (pink), shallow Baltic Sea (yellow), and deep Baltic Sea (light grey). BY5, BY15, and F26 are three monitoring stations in the Baltic Sea which are looked at more closely in this study.

The model results are compared to the observations in different ways: Temporally averaged vertical profiles of nitrate are calculated for the different areas presented in Figure 2.5. Spatial averages of model data are constructed using the co-located subset of model data.
In addition to nitrate profiles, oxygen and phosphate profiles are calculated for the three

[5]The MATLAB function *interp1* is used, see MATLAB documentation for more information (MATLAB, 2013).

[6]Here, the northern NS and the tidal mixing zone are divided by the 48 m isobath in the model. Smaller deeper areas clearly lying within the tidal mixing zone are included in this zone accordingly.

[7]Here, the deep and shallow BS are divided by the 80 m isobath in the model.

monitoring stations locations BY15, BY5 and F26 in the Baltic Sea (see again Figure 2.5). The observational data for these three stations are downloaded from http://apps.nest.su.se/nest/ (Wulff et al., 2008), a data set extracted from the HELCOM data base[8] (HELCOM, 2014).
For the visualization and quantification of statistical differences between model results and observations, Taylor diagrams (Taylor, 2001) are used. The Taylor diagrams are computed following Daewel and Schrum (2013) for surface nitrate concentrations in all areas described in Figure 2.5. Again, only model data which have been co-located in both space and time to the observations are included. To obtain a Taylor diagram, the root mean square difference (RMSD) and the Pearson correlation coefficient (R) between the model data (Mod) and the observations (Obs) are calculated as follows:

$$RMSD = \sqrt{\frac{1}{N}\sum_{n=1}^{N}\left[\left(Obs_n - \overline{Obs}\right) - \left(Mod_n - \overline{Mod}\right)\right]^2} \tag{2.6}$$

$$R = \frac{\frac{1}{N}\sum_{n=1}^{N}\left(Obs_n - \overline{Obs}\right) - \left(Mod_n - \overline{Mod}\right)}{\sigma_{Mod}\sigma_{Obs}} \tag{2.7}$$

with

$$\sigma_X = \frac{1}{N}\sqrt{\sum_{n=1}^{N}(X - \overline{X})^2} \tag{2.8}$$

denoting the standard deviation. N the number of data points and a bar above Mod or Obs denotes the mean of the respective data set as calculated by:

$$\overline{X} = \frac{1}{N}\sqrt{\sum_{n=1}^{N}(X} \tag{2.9}$$

For further explanation, it is referred to Taylor (2001) and Daewel and Schrum (2013).
With respect to interpretation of the model-observation comparison, it has to be pointed out that both the temporal and spatial resolution of model data can lead to reduced comparability of model data and observations. Here, the model results span one model grid box, thus $\approx 10\,\text{km} \cdot 10\,\text{km}$ and are daily means whereas the observations are local in-situ measurements

[8] http://helcom.fi/baltic-sea-trends/data-maps/helcom-map-and-data-service

(Daewel and Schrum, 2013). This is specifically relevant in highly dynamic and frontal regions of the coastal North Sea.

2.4 New parametrizations

To assess improtant processes in the benthic-pelagic coupling in the North Sea and Baltic Sea, several changes are applied to the original version of ECOSMO used by Daewel and Schrum (2013). Changes in the parametrization are introduced for

- phosphate release from the sediment
- sedimentary respiration and
- light attenuation

and will be presented in this section. Details on all model runs performed in this study can be found in sections 3.1 and 4.1.

2.4.1 Phosphate release

In the original version of ECOSMO, no realease of phosphate from the sediment pool of dissolved phosphorus due to resuspension is considered (Daewel and Schrum, 2013). As the first step, this wrongly missing effect of resuspension is considered from now on.
Whenever it is referred to the "baseline run" in the following, phosphate release from the sediment pool of dissolved phosphorus due to resuspension is activated which means that results for the baseline run might deviate from the results presented in Daewel and Schrum (2013).
In Section 3.2, some differences between the "new" baseline run of this study and a run not considering phosphate release due to resuspension will be presented.

2.4.2 Sedimentary respiration

In this study, a new parametrization for sedimentary respiration processes is implemented into ECOSMO based on the modeling results for coastal sediments of Middelburg et al. (1996), which are shown in Figure 1.2.

In contrast to the parametrization of sedimentary respiration currently used, the new parametrization mainly relates to two aspects:

- Sediments are only oxygenated in the upper millimeters in the coastal ocean (see Section 1.2.1, p.4 (Glud, 2008)). Hence, both denitrification and other anaerobic respiratory processes are always contributing to overall organic matter degradation, not only in an anoxic setting.
- To what extent the different respiratory pathways contribute to overall organic matter degradation, has been shown to be a function of bottom water oxygen concentration. Here, a hypoxic regime is introduced in addition to the oxic and anxoxic regime already defined.

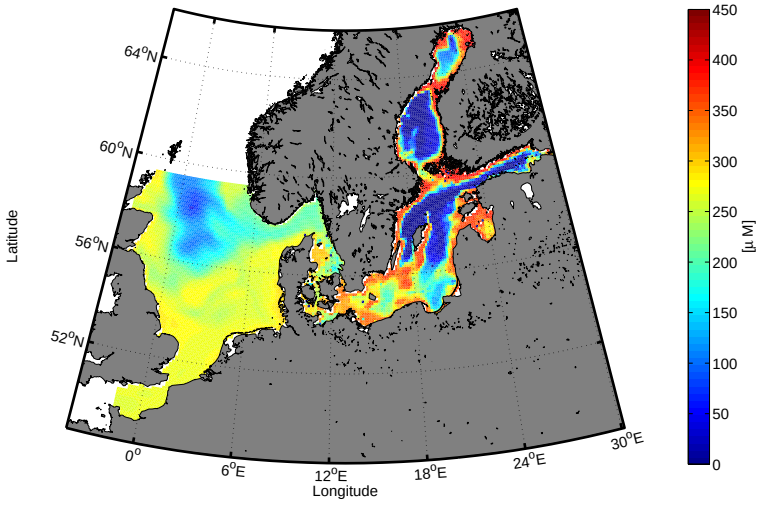

Figure 2.6: Average bottom water O_2 concentrations in the model domain of ECOSMO. Values are taken from the baseline run (run 1 in Table 4.1) and averaged over 1999-2009.

Figure 2.6 shows the bottom water O_2 concentrations for the baseline run in the model domain. Values are averaged over all months of 1999-2009. The model is able to reproduce the main features of the domain: an overall well oxygenated North Sea and a more diverse Baltic Sea with well oxygenated coastal areas and hypoxic or even permanently anoxic deep basins (see also Section 1.3, p.9).
While O_2 concentrations in the North Sea vary between 150-300 $\cdot 10^{-6}$mol, values in the Baltic Sea show a higher spatial variability (between 0-400 $\cdot 10^{-6}$mol). In the whole model domain, O_2 concentrations seem to be related to water depth: the deeper it is, the lower are the O_2 concentrations which can be explained with a reduced atmosphere-ocean coupling at greater depths.

This distribution of bottom water O_2 levels has consequences for sedimentary respiration processes, as mentioned in Section 1.2.1. As can be seen in Figure 1.2 (p.7), bottom water O_2 concentrations determine the contribution of different respiration pathways to overall organic matter degradation.

Table 2.2: Fractions of different pathways of organic matter degradation for the different O_2 regimes. Numbers are based on Figure 1.2 (p.7) (Middelburg and Levin, 2009), resp. = respiration.

Regime	**Aerobic resp.** (*aero*)	**Denitrification** (*denit*)	**Anaerobic resp.** (*anaero*)
oxic	0.22	0.10	0.68
hypoxic	0.05	0.10	0.85
anoxic	0	0.20	0.80

Three oxygen regimes are defined: oxic (O_2 levels above $63 \cdot 10^{-6}$mol), hypoxic (O_2 levels below $63 \cdot 10^{-6}$mol, but still measurable) and anoxic (no measurable O_2 concentrations) (Middelburg and Levin, 2009).
The chosen fractions for the different respiratory pathways (aerobic, denitrification, anaerobic) are taken as an approximate average over the respective regime according to Figure 1.2 and are presented in Table 2.2. It has ben pointed out in Middelburg and Levin (2009) that a carbon loading dependency might mask the bottom water oxygen dependency. In Middelburg et al. (1996), the contribution of denitrification to overall respiration in coastal sediments and estuaries was estimated at $7 - 30\%$ for intermediate carbon loadings, i.e. 0.1-1 $\cdot 10^{-6}$mol C $(\text{cm})^{-2}\text{d}^{-1}$. This estimate agrees well with the estimate of $3 - 37\%$ of Heip et al. (1995). Mattila and Kankaanpää (2006) estimated sedimentation rates in the Baltic Sea. Their lowest estimates were found in the Baltic Proper and were in the same order of magnitude as $1 \cdot 10^{-6}$mol C $(\text{cm})^{-2}\text{d}^{-1}$. This region overlaps with the anoxic region of the Baltic (see Figure 2.6), which is because the fraction of denitrification in overall respiration is set to 20%, which is higher than the values shown in Figure 1.2.
In the earlier version of the sediment module (described in Section 2.2.2, p.20), ammonium fluxes were halved under oxic conditions to account for coupled nitrification/denitrification (organic matter degradation split into 50% aerobic respiration and 50% denitrification). A flux of nitrate from the water column into the sediment was only included for anoxic settings to account for direct denitrification (100% denitrification). If no nitrate was present, sulfate reduction took place (100%).
Now, a nitrate flux is included for all conditions and the presence or absence of oxygen and thereby the rate of nitrification determines whether coupled nitrification/denitrification or direct denitrification takes place. No changes were applied to the parametrization of phosphate

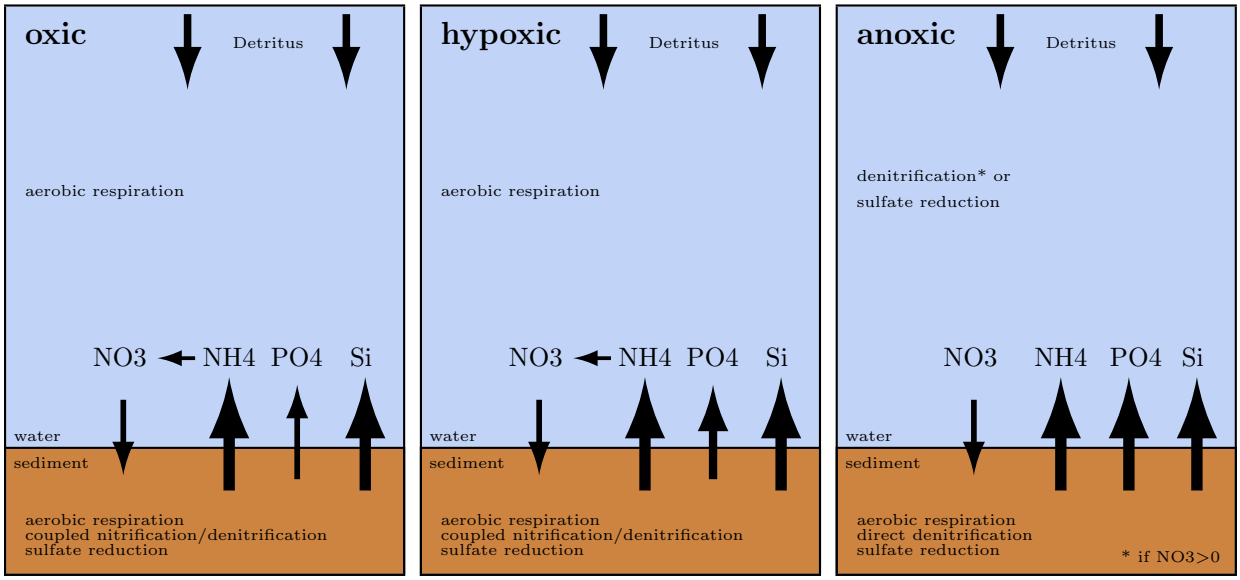

Figure 2.7: Respiratory processes in ECOSMO after changes were applied. It is differentiated between sediments underlying oxic (left), hypoxic (middle) and anoxic (right) bottom water. More explanation can be found in the text.

and silicate sediment-water fluxes.

The equations of sedimentary respiration processes in the current version of ECOSMO are presented in the appendix (see p.99 and p.100). Here, a summary of all changes applied to these equations is given:

The equation for sedimentary respiration processes (see Equation 25 in the appendix on p.99) is split into the three respiration pathways:

$$\epsilon_{Sed_{aero}}(T) = 2 \cdot 0.001\,\mathrm{d}^{-1} \cdot e^{0.15^{\circ}\mathrm{C}^{-1} \cdot T} \cdot aero \tag{2.10}$$

$$\epsilon_{Sed_{denit}}(T) = 2 \cdot 0.001\,\mathrm{d}^{-1} \cdot e^{0.15^{\circ}\mathrm{C}^{-1} \cdot T} \cdot denit \tag{2.11}$$

$$\epsilon_{Sed_{anaero}}(T) = 2 \cdot 0.001\,\mathrm{d}^{-1} \cdot e^{0.15^{\circ}\mathrm{C}^{-1} \cdot T} \cdot anaero \tag{2.12}$$

$$\epsilon_{Sed_{total}}(T) = \epsilon_{Sed_{aero}}(T) + \epsilon_{Sed_{denit}}(T) + \epsilon_{Sed_{anaero}}(T) \tag{2.13}$$

The values for the parameters *aero*, *denit* and *anaero* can be found in Table 2.2.

This means, since the overall respiration rate does not change with this new parametrization, the equations for the different sediment pools do only change by re-writing them (compare

with equations 26 and 27 in the appendix on p.100):

$$\begin{aligned} R_{Sed1} = & SR \cdot D - RR \cdot Sed_1 - \delta_{burial} \cdot Sed_1 \\ & - \epsilon_{Sed_{total}}(T) \cdot Sed_1 \end{aligned} \tag{2.14}$$

$$\begin{aligned} R_{Sed2} = & - RR \cdot Sed_2 + \epsilon_{Sed_{total}}(T) \cdot Sed_1 \\ & - \theta(O_2) \cdot (\epsilon_{Sed_{total}}(T) \cdot Sed_2 \cdot (1 - 0.15\lambda)) \\ & - \theta(-O_2) \cdot (\epsilon_{Sed_{total}}(T) \cdot Sed_2) \end{aligned} \tag{2.15}$$

The equation for the silicate sediment pool R_{Sed3} does not change at all.
Only looking at the parts of the equations of nitrate, ammonium and oxygen interacting with the sediment, these change as follows (compare with equations 31, 32, and 34 in the appendix on p.101):

$$R_{NO3} = \cdots - \theta(NO_3) \cdot a_{denit} \cdot \epsilon_{Sed_{denit}}(T) \cdot \frac{Sed_1}{dz}\Big|_{z=bottom} \tag{2.16}$$

$$R_{NH4} = \cdots + \epsilon_{Sed_{total}}(T) \cdot \frac{Sed_1}{dz})\Big|_{z=bottom} \tag{2.17}$$

$$\begin{aligned} R_{O_2} = \cdots - \Bigg[& \frac{1}{REDF_{C:O_2} REDF_{C:N}} \Bigg(6.625 \cdot \epsilon_{Sed_{aero}} \cdot \frac{Sed_1}{dz} \\ & + 6.625 \cdot \epsilon_{Sed_{anaero}} \cdot \frac{Sed_1}{dz} \Bigg) \Bigg]_{z=botom} \end{aligned} \tag{2.18}$$

The equation of silicate remains unchanged, the equation for phosphate is re-written to:

$$\begin{aligned} R_{PO4} = \cdots & + RR \cdot \frac{Sed_2}{dz} \\ & + \theta(O_2) \cdot (\epsilon_{Sed_{total}}(T) \cdot \frac{Sed_2}{dz} \cdot (1 - 0.15\lambda)) \\ & + \theta(-O_2) \cdot (\epsilon_{Sed_{total}}(T) \cdot \frac{Sed_2}{dz}) \cdot \end{aligned} \tag{2.19}$$

2.4.3 Light attenuation

As has been mentioned in Section 1.2.2, not only phytoplankton and the water itself, but also all other particulate and dissolved organic matter contribute to light attenuation in water.
In the original version of ECOSMO, light is attenuated due to a background turbidity and pyhtoplankton only (Daewel and Schrum, 2013). However, the state variables dissolved organic matter (DOM) and detritus are expected to influence the light climate and thereby primary production significantly as well if accounted for in light attenuation.
To quantify the role of the parametrization of light attenuation in primary production, a sensitivity analysis using different specific attenuation coefficients and even parametrizations of light attnuation is done in this part of the study. This is done to eventually being able to quantify the effect of resuspensed matter on primary production caused by the combined effect of altered nutrient and light availabilty. The original parametrization of light attenuation neglects the effect of resuspended matter (detritus), and hence only the effect of altered nutrient availability can be quantified in such a resuspension experiment.
At first, the model's sensitivity to different background turbidity attenuation coefficients is assessed using the emulator method described in the section following hereafter. Afterwards, DOM and detritus are stepwise accounted for in light attenuation and their effect on primary production is quantified. The vertical attenuation coefficient K is successively defined as:

$$K = k_w + k_p \cdot P + k_x \tag{2.20}$$

$$K = k_w + k_p \cdot P + k_{DOM} \cdot DOM \tag{2.21}$$

$$K = k_w + k_p \cdot P + k_{DOM} \cdot DOM + k_{Det} \cdot Det \tag{2.22}$$

At any time, the specific attenuation coefficient for phytoplankton k_p is kept at $0.2\,\mathrm{m^2(mmolC)^{-1}}$. When including DOM in light attenuation, k_w is set to $0.03\,\mathrm{m^{-1}}$ following Urtizberea et al. (2013). k_w was higher in the original version of ECOSMO ($0.05\,\mathrm{m^{-1}}$) to account for a background turbidity ($k_{bg} = k_w + k_x$). For DOM, the specific attenuation coefficient found for Danish waters by Stedmon et al. (2000), $0.29 \pm 0.11\,\mathrm{m^2(gC)^{-1}}$, is used as a first educated guess to get an idea about its influence on light attenuation (k_{DOM}). To assess the model's sensitivity to the specific light attenuation coefficent of DOM, three runs are performed: one using the average value found by Stedmon et al. (2000) ($0.29\,\mathrm{m^2(gC)^{-1}}$) and two taking into account the standard deviation of this value as given in the study ($0.18\,\mathrm{m^2(gC)^{-1}}$ and $0.40\,\mathrm{m^2(gC)^{-1}}$).
It has been pointed out in Section 1.2.2 (p.7) that CDOM, the optically active part of all

DOM, can be of both terrestrial and oceanic origin. In ECOSMO, only DOM of oceanic origin is included. Even though specific light attenuation coefficients found in the literature are for total CDOM combining terrestrial and oceanic sources and even though not all DOM in ECOSMO necessarily needs to be a part of CDOM, the average coefficient found by Stedmon et al. (2000) is considered an appropriate first guess due to the minor influence of terrestrial CDOM at some distance (in the order of kilometers) from the coast (Lübben et al., 2009) and due to the lack of other values in the literature.
Light attenuation due to detritus is subsequently included using the specific attenuation coefficients $k_{DOM} = 0.29\,\mathrm{m}^2(\mathrm{gC})^{-1}$ and $k_{Det} = 0.2\,\mathrm{m}^2(\mathrm{gC})^{-1}$ as given in Tian et al. (2009).
A detailed overview of the settings of all runs performed in this part of the study can be found in Section 4.1 (see Table 4.1).

2.5 An emulator method: polynomial chaos expansion

The emulator method presented here is a computationally effective tool for parameter optimization and sensitivity analyses in a coupled complex 3D model such as ECOSMO. In this study, it is used to assess the model's sensitivity to the background turbidity attenuation coefficient in the parametrization of light attenuation and to the general representation of detritus and DOM in the model.
Like every bio-physical model, ECOSMO includes numerous constant parameter values, such as for example specific light attenuation coefficients or the sinking speed of detritus (see appendix on p.96). In reality, these values are far from being constant, but vary in both space and time. This variability is typically not included in the model for most parameters either due to a lack of knowledge about its variability or computational restraints. The parameter values used in ECOSMO are supposed to represent the best possible values for the whole model domain, but often, detailed multi-parameter sensitivity analyses are lacking.
The emulator method applied here uses the polynomial chaos expansion, which performs an interpolation of coefficients in parameter space. It was first applied to oceanographic research questions in Mattern et al. (2012a,b). Matlab functions (MATLAB, 2013) for the application of the emulator method were kindly provided by Jann Paul Mattern and are applied here.
At first, a decision has to be made on the parameter the model's sensitivity is to be quantified to. The regional parameter range is estimated from available literature or as an educated guess. Subsequently, based on the knowledge about the spatial and temporal variability, a probability distribution is assigned to the parameter over the range of values it can adopt (in this study: uniform).

This distribution is then sampled at the so-called quadrature points - the parameter values, the model is actually run at (see further down for description on how these points are determined). After running the model at these points, a polynomial chaos expansion in parameter space is performed for an output parameter which depends on the varied input parameter. Through only running the model at certain sample points of the input parameter range, information for the respective output parameter can easily be obtained for the complete range of the input parameter range by this emulation technique.
Mathematically, the emulator method is a basis function expansion. If f is a function describing the model output (e.g. primary production) depending on space ($\mathbf{x}$), time (t) and the uncertain input parameter θ (e.g. background turbidity light attenuation coefficient), and ϵ_{trunc} is the truncation error, its approximation follows:

$$f(\mathbf{x}, t, \theta) = \sum_{k=0}^{k_{max}} (a_k(\mathbf{x}, t)\ \phi_k(\theta)) + \epsilon_{trunc}(\theta) \tag{2.23}$$

Here, $a_k(x, t)$ are the expansion coefficients and $\phi_k(\theta)$ is the kth basis function. The basis functions depend on the probability distribution assigned to the uncertain input parameter and can be looked up in the literature (Mattern et al., 2012a).
The quadrature points are determined according to the order chosen for the polynomials. Defining k_{max} as the maximum order of polynomials to be used in the approximation, the number of quadrature points P_q simply is

$$P_q = k_{max} + 1 \tag{2.24}$$

The higher the maximum order of the polynomials, the smaller is the truncation error ϵ_{trunc} in the approximation. This means, the higher k_{max}, the more accurate is the approximation, but the more model runs are needed at the same time.
The polynomial chaos expansion calculates the expansion coefficients $a_k(x, t)$ by the following approximation (Mattern et al., 2012a):

$$a_k(\mathbf{x}, t) \approx \frac{1}{N_k} \sum_{i=0}^{k_max} f(\mathbf{x}, t, \theta^{(i)}) \phi_k(\theta^{(i)}) \omega_i \tag{2.25}$$

N_k is a normalization factor connected to the polynomials as well as the Gaussian quadrature weights ω_i, and $\theta^{(i)}$ are the quadrature points.
The number of quadrature points (P_q) forms the only computational restraint because it determines the number of model runs needed for the analysis. The higher the number of points,

the more model runs are needed. If more than one input parameter is assumed uncertain, the number of model runs grows potentially. Taking n uncertain parameters into account, ${P_q}^n$ model runs are needed. That means that theoretically, not only one, but all parameter values can be assumed uncertain and varied using this technique, but this will potentially lead to computational problems.
For more details about the mathematical background of the polynomial chaos expansion, refer to Wiener (1938) and Mattern et al. (2012a).
In this study, the emulator method is used for sensitivity analyses. Details on the settings for each of the experiments in this study can be found in Section 4.1.

3 Sedimentary respiration & Flux of dissolved nutrients

3.1 General approach and simulations I

At first, the effect of phosphate release from the sediment pool of dissolved phosphorus due to resuspension is assessed by comparing a run with to a run without this release. Both runs are run from 1984-2009, but only 1999-2009 are analyzed to allow for spin-up time.
To quantify the effect of the new paramnetrization of sedimentary respiration in ECOSMO, two model runs are performed: one with the former parametrization presented in Section 2.2.2 (Daewel and Schrum, 2013) and a second one with the new parametrization described in 2.4.2. For both setups, the model is run from 1948-2008.
To validate the model, resulting nutrient profiles from both runs are compared to observational data (see Section 2.3). Where necessary, nutrient concentrations are spatially averaged according to Figure 2.5.
To assess the sensitivity of the results to the chosen fraction for the different respiration pathways, two additional runs ("sensitivity I" & "sensitivity II") are performed. The fractions are changed as presented in Table 3.1. Besides the differences in the parametrization of sedimentary respiration, these two runs are identical to the other two presented in this chapter.

Table 3.1: Sensitivity runs for parametrization of sedimentary respiration. Black numbers in this table correspond to Table 2.2 on p.27. The first run ("sensitivity I", cyan) considers a smaller fraction of denitrification in anoxic settings, the second ("sensitivity II", red) a greater importance of aerobic respiration in oxic settings. Changes in the contribution of anaerobic respiration to overall respiration occur accordingly.

Regime	**Aerobic resp.** (*aero*)	**Denitrification** (*denit*)	**Anaerobic resp.** (*anaero*)
oxic	0.22/0.30	0.10	0.68/0.60
hypoxic	0.05	0.10	0.85
anoxic	0	0.10/0.20	0.90/0.80

3.2 Phosphate release

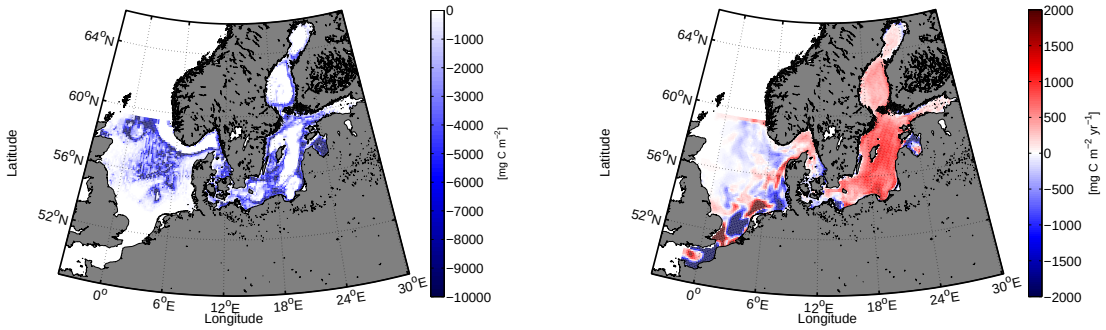

(a) Sed_2 (b) Primary Production

Figure 3.1: Comparison of runs w/ and w/o phosphate release from sediments due to resuspension: Change in average amount of Sed_2 in Figure 3.1(a), change in average vertically integrated annual primary production in Figure 3.1(b). Run without subtracted from run with phosphate release from sediments due to resuspension, so that blue colors denote decrease of the respective property in run with compared to run without this release. Averages calculated over 1999-2009.

In Daewel and Schrum (2013), phosphate is only released from the sediment pool of dissolved phosphorus as a function of bottom water oxygen concentrations (see Section 2.2.2). The wrongly missing release due to resuspension is accounted for in this study. The results in this section shall demonstrate the difference of this "old" baseline run to a new one which includes phosphate release from the sediments due to resuspension. This latter run will be considered the "baseline" run for the remains of this study. In Figure 3.1, differences in the sediment pool of dissolved phosphorus (Sed_2, left) and vertically integrated annual primary production (right) are shown, and blue colors denote a decrease of the respective property in the run with compared to the run without this release.

If phosphate is additionally released due to resuspension, the average amount of dissolved phosphorus in the sediment pool (Sed_2) is significantly reduced in all shallow coastal areas of the Baltic Sea and large areas in the central North Sea. This increased release of phosphate to the water column fuels primary production all over the Baltic Sea (see Figure 3.1(b)). Primary production in the North Sea reacts strongest in the tidal mixing zone, but shows alternating patches of increased and decreased primary production.

3.3 Sedimentary respiration

The new parametrization of sedimentary respiration accounts for the anoxic nature of sediments below a thin oxygenated surface layer and resolves different pathways of respiration. The largest impacts of these changes are on the representation of the nitrogen cycle, which will therefore be the focus in the presentation of the results.
Figure 3.2 shows Taylor diagrams for surface nitrate values for the baseline run (Figure 3.2(a)) and for the run with the new parametrization of sedimentary respiration (Figure 3.2(b)) for the different model regions as shown in Figure 2.5 (p.23).

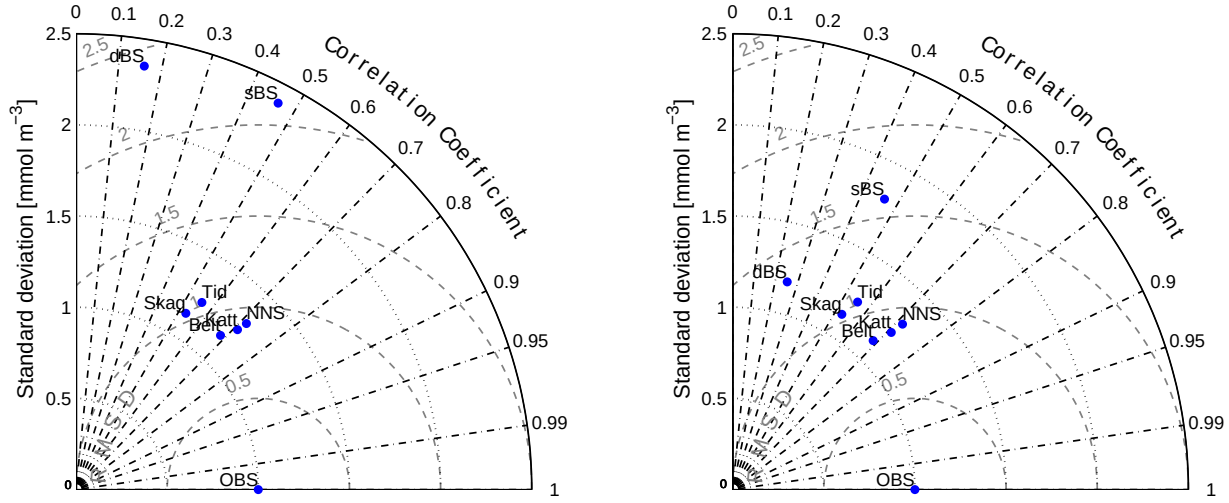

(a) Baseline

(b) New parametrization

Figure 3.2: Taylor diagrams for surface nitrate in the different subareas: Tidal mixing zone (Tid), northern North Sea (NNS), Skagerrak (Skag), Kattegat (Katt), Belt Sea (Belt), shallow Baltic Sea (sBS), and deep Baltic Sea (dBS, see Figure 2.5 for the boundaries between the regions). The model results are compared to available observations (OBS) in the respective area.

What stands out in the baseline run, is a clear difference in performance of the model when comparing the North Sea (Tidal mixing zone (Tid), northern North Sea (NNS)), for which the model performs significantly better, and the Baltic Sea (shallow Baltic Sea (sBS) and deep Baltic Sea (dBS)), where performance in simulating surface nutrients is weak.
The transition zone (Skagerrak (Skag), Kattegat (Katt) and Belt Sea (Belt)) between these two seas is closer to the values obtained for the regions in the North Sea. While root mean square differences (RMSD) of approximately 1 can be found in the areas of the North Sea and the transition zone when comparing the model output to the observations in these areas, values in the Baltic Sea are twice (sBS) or even 2.5 times as high (dBS). This better representation

of surface nitrate in the North Sea is also reflected in the correlation values (0.5-0.7 in the North Sea, about 0.15 and 0.45 in the deep and shallow Baltic Sea, respectively).
Introducing the new parametrization of sedimentary respiration does not lead to easily visible changes in the Taylor diagram in both the regions of the North Sea and the transition zone between North and Baltic Sea (see Figure 3.2(b)). Looking at the numbers in more detail reveals that changes in the correlation coefficient and RMSD in these areas occur only in the third or fourth and second or third decimal place of the two different measures, respectively.
The picture is different for both regions in the Baltic Sea. In both the shallow and the deep part of the Baltic Sea, an overall improvement of the model's representation of surface nitrate compared to the observations can be seen. Here, the most apparent changes are visible for the RMSD and the standard deviation, which both are reduced by approximately 50% in the deeper Baltic Sea and about 25% in the shallow areas.
The variability of the amplitude of surface nitrate concentrations is still overestimated (standard deviation larger than 1), but it is considerably improved by the implementation of the new parametrization of sediment respiration.
The new parametrization of sedimentary respiration does not only impact the surface nutrient concentrations, but also the vertical distribution of these. Figure 3.3 shows the temporally and spatially averaged vertical nitrate profiles for the different subareas in the model domain as defined in Figure 2.5. Solid lines denote the average profile from 1948-2008 for the observations (black), the baseline run (green), and the run with the new parametrization of sedimentary respiration (blue), respectively. The shaded areas behind each line represent the standard deviation from the average profile.
Comparing the average vertical profile of nitrate observations to the model results in the different regions of the model domain, different characteristics can be identified for the North Sea, the transition zone, and the Baltic Sea, respectively.
In both regions of the North Sea and in the Skagerrak and the Kattegat, only very small changes are observed in the vertical nitrate profile between the baseline run and the run with the new parametrization of sedimentary respiration. Comparing the modeled profiles to the observations, an overestimation of nitrate at all depth levels can be seen for the Skagerrak and the Kattegat. In the northern North Sea, a clear overestimation is visible below approximately 20 m while the modeled values at shallower depths compare somewhat better with the observations. In the shallowest area of the North Sea, the tidal mixing zone, the modeled profile seems to be shifted towards higher nitrate concentrations at all depths compared to the observational profile. In this area, the large range of observed surface nitrate concentrations has to be pointed out. The model is able to simulate this variability, but with an offset of at least 5 mmol m^{-3}.

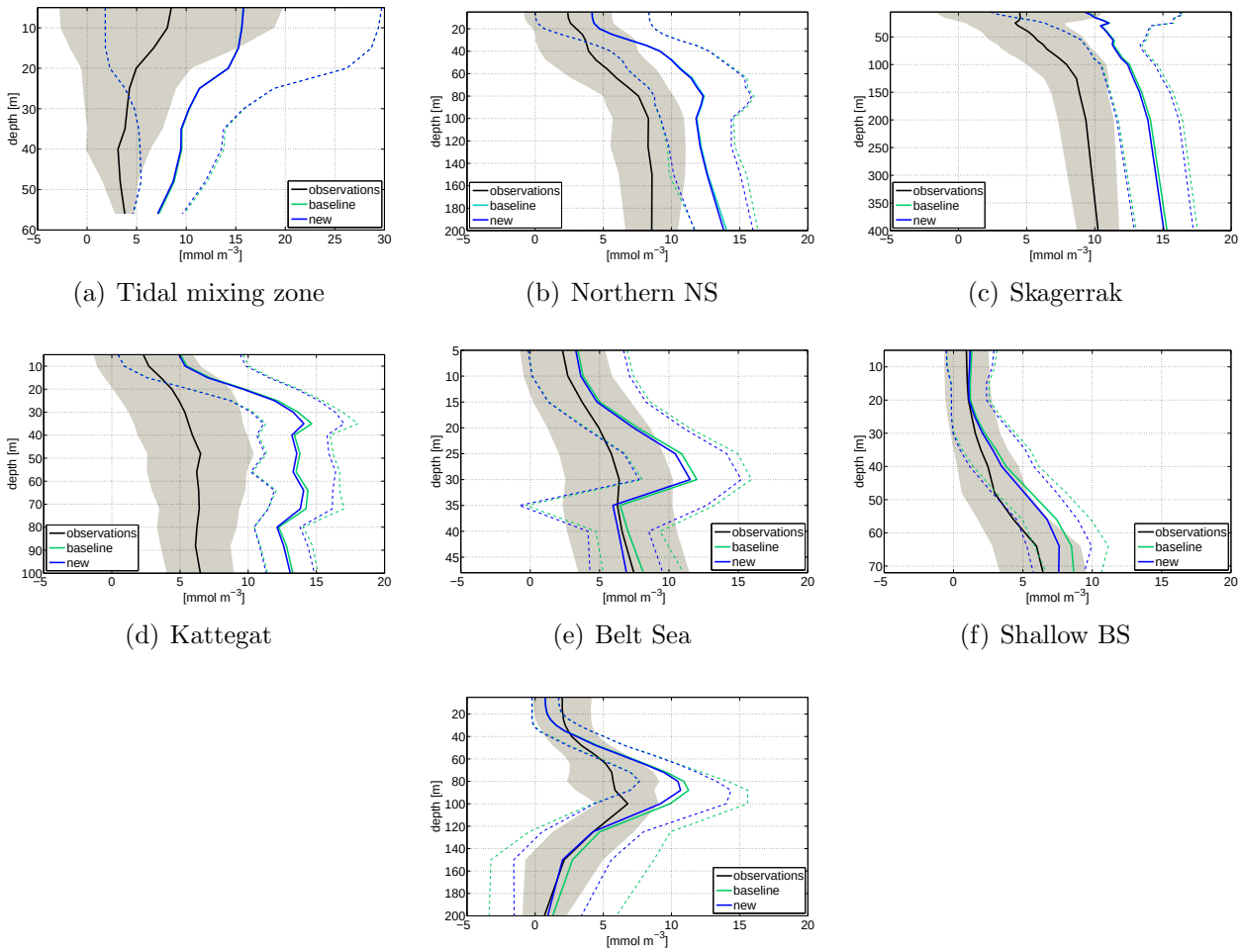

(a) Tidal mixing zone (b) Northern NS (c) Skagerrak

(d) Kattegat (e) Belt Sea (f) Shallow BS

(g) Deep BS

Figure 3.3: Average vertical profiles of nitrate in the different subareas in the model domain (see Figure 2.5). Solid lines represent the average over 1948-2008 for the observations (black), the baseline run (green) and the run with the new parametrization of sedimentary respiration (blue). The shaded areas behind each line represent the respective standard deviations from the mean.

The closer one gets to the Baltic Sea, the more changes can be seen when comparing the baseline run with the run using the new parametrization of sedimentary respiration. The model generally shows a better performance using the new parametrization while getting closer to the Baltic Sea. Overall, the implementation of the new parametrization leads to a decrease of nitrate in the whole water column. However, the changes are small except for the near bottom waters in the Belt Sea and the Baltic Sea (both shallow and deep waters).
In the Belt Sea, the region with by far the most available observational data (see Figure 2.4(b), p.22), the range of values simulated by ECOSMO agrees well with the observed range at all depths, except for a layer between 20-40 m. Here, a peak in nitrate concentrations is simulated

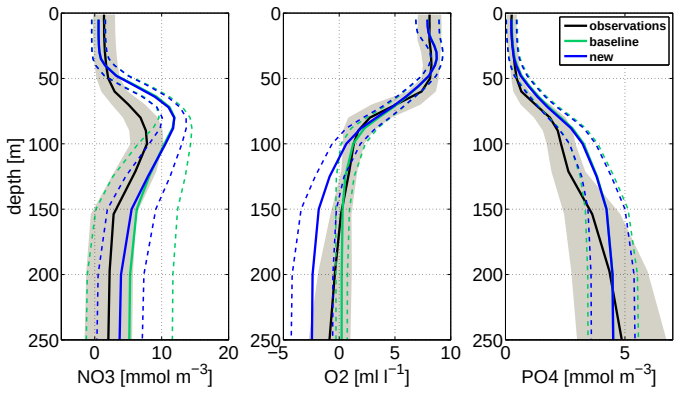

(a) BY15

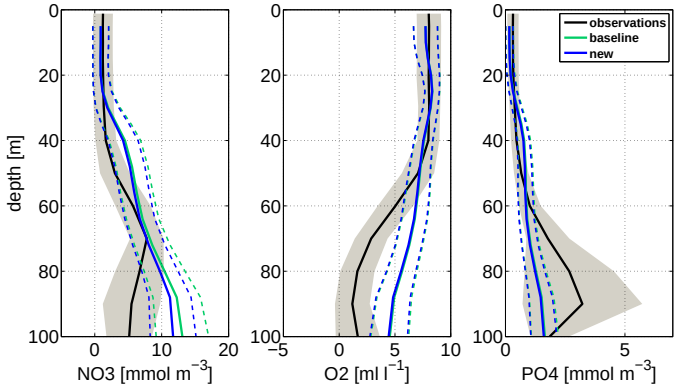

(b) BY5

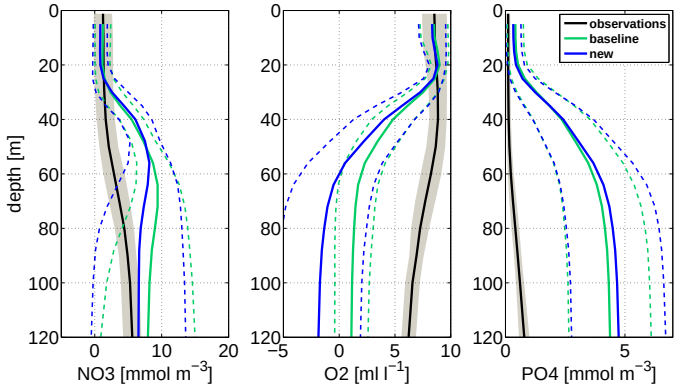

(c) F26

Figure 3.4: Average vertical profiles of nitrate, oxygen and phosphate at BY15, BY5, and F26 (see Figure 2.5 for exact locations of the stations). Solid lines represent the average over 1948-2008 for the observations (black), the baseline run (green), and the run with the new parametrization of sedimentary respiration (blue). The shaded area and the area limited by the dashed lines, respectively, represent the respective standard deviations from the mean.

by the model which is not documented in the observations. The implementation of the new parametrization of sedimentary respiration improves the representation of nitrate in and below this before mentioned layer by reducing nitrate concentrations, but does not change the overall shape of the profile. This is likely because of artificial topographic corrections applied to improve inflow characteristics of dense waters into the Baltic Sea (Schrum, personal communication).
When comparing the profiles of all regions to each other, the biggest changes with the implementation of the new parametrization arise for the Baltic Sea (see also figures 3.2(a) and 3.2(b)). The changes in the average nitrate profile are small in the upper meters. Therefore, the improvements seen in the Taylor diagrams for the regions for surface nitrate (see Figure 3.2) must stem from an improved agreement in time between model output and observations.
Below approximately 30 m, the modeled nitrate profiles with the new parametrization of sedimentary respiration in the Baltic Sea differ from the ones simulated with the old parametrization more and more the closer to the bottom it gets.
In the shallow Baltic Sea, bottom nitrate concentrations are decreased by approximately 1-2 mmol m^{-3}, thereby considerably improving the performance of the model when comparing the profile to observations. A similar result can be seen for the deep Baltic Sea. The peak in nitrate concentrations simulated at 80 m is slightly reduced, but the implementation of the new parametrization of sedimentary respiration does not change the general shape of the vertical profile which can likely, at least partly be attributed to problems of the model simulating physical characteristics of the area, such as stratification.
To get a more detailed look into the benthic-pelagic coupling in regions that have reacted sensitively to changes in the parametrization of sedimentary respiration, three stations in the Baltic Sea are analyzed. Figure 3.4 shows average vertical nitrate (left), oxygen (middle), and phosphate (right) concentrations for the monitoring stations BY15, BY5, and F26 (see Figure 2.5,p.23, for the exact positions of the locations). When interpreting the vertical profiles for these stations, it has to be kept in mind that the observations are in-situ measurements while the model data represent a larger grid box and are daily averaged (see Section 2.3).
The upper part of Figure 3.4 shows the results for the station BY15 in the Baltic Proper. Below ≈200 m, the water column is almost permanently anoxic, and nitrate concentrations are very low (1-2 mmol m^{-3}). The implementation of the new parametrization of sedimentary respiration has a comparatively large effect at this location. While no clear changes can be seen in the upper 100 m of the water column, a decrease in both nitrate and oxygen is observed with the new parametrization compared to the old one below this depth. Now, average bottom water nitrate concentrations and especially the range of simulated values are obviously closer to the observations at this location. Looking at the oxygen profiles, the new parametrization

seems to use up too much oxygen and consequently, oxygen is underestimated compared to observations with the new parametrization. However, the general deficiency of the original model version, which relates to too high bottom oxygen values is compensated. Phosphate is relatively well simluated and no change is visible for the two model runs.
Station BY5 (see Figure 3.4(b)) is located in the Bornholm Deep. Nitrate, oxygen, and phosphate values simulated by ECOSMO agree very well with observations at the surface. In deeper layers (below 40-50 m), nitrate and oxygen are generally overestimated while phosphate is underestimated by the model. The implementation of the new parametrization of sedimentary respiration does only lead to visible changes, namely a reduction, in the nitrate profile. This implies an improvement in model performance.
The third station looked at is F26, which is located in the northern Baltic Sea. After the implementation of the new parametrization of sedimentary respiration, the model is able to simulate the vertical distribution of nitrate relatively well, both close to the surface and the bottom. At intermediate depths, the modeled profile shows a peak in nitrate concentrations which the observations do not confirm. Both with the new and the old parametrization of sedimentary respiration, the model fails to reproduce both the shape of the vertical profile and the range of observed oxygen and phosphate values. Here, the new parametrization does not improve the modeled vertical profiles. Modeled oxygen concentrations are far too low and part of the too large phosphate concentration simulated by the model might be attributed to consequent sediment release. Daewel and Schrum (2013) linked this to an unsufficient ventilation of the water column in this area, potentially due to too coarsely resolved atmospheric forcing data. Additionally, no primary production in melt ponds on sea ice is included in ECOSMO. Since sea ice plays an important role in seasonal dynamics in the Gulf of Bothnia, primary production is likely underestimated in this area.
Overall, the new parametrization of sedimentary respiration does improve the model's performance in simulating nitrate in the Baltic Sea, but disagreements between modeled nitrate concentrations and observations are still present. The North Sea is not sensitive to the parametrization of sedimentary respiration, indicated by barely visible changes in modeled nitrate concentrations after the implementation of the new parametrization. Here, other reasons are responsible for the overestimation of nitrate concentrations when comparing the modeled to the observed data. A number of these potential reasons will be discussed in Section 5.1, p.72.

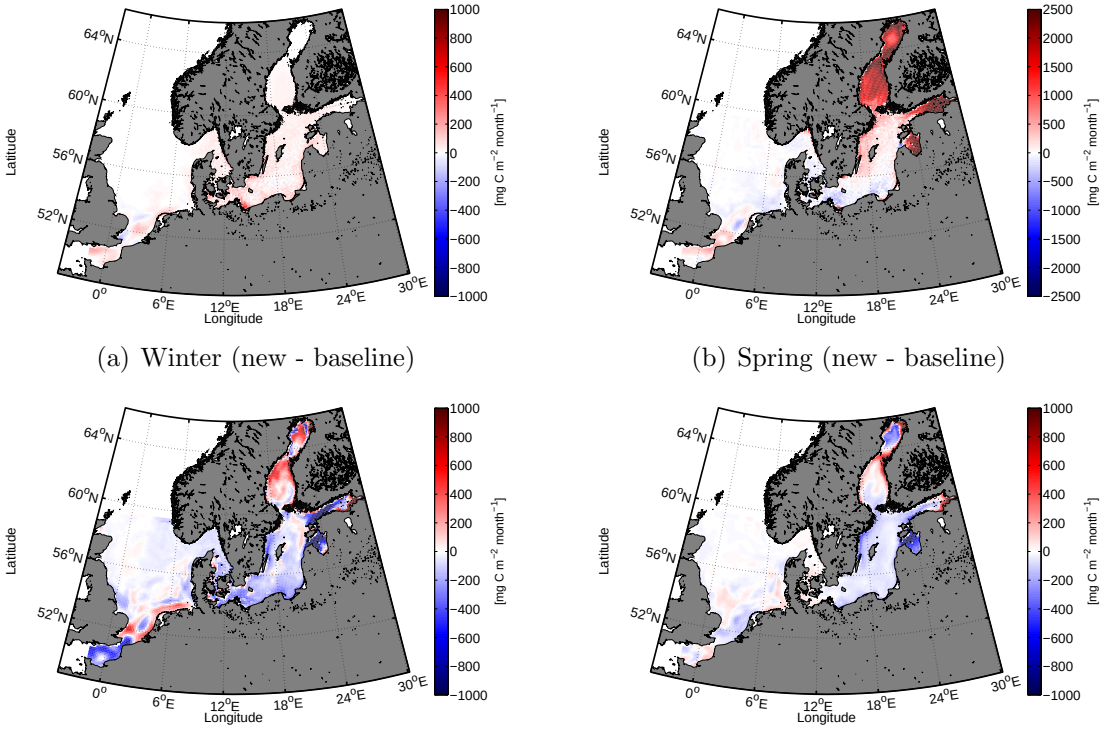

(a) Winter (new - baseline)

(b) Spring (new - baseline)

(c) Summer (new - baseline)

(d) Autumn (new - baseline)

Figure 3.5: Seasonally averaged vertically integrated primary production: Effect of the new parametrization of sedimentary respiration. Results from the baseline run are subtracted from the run with the new parametrization of sedimentary respirtaion. Red colors denote an increase in primary production with the new parametrization. All values are averaged over 1999-2009. Months included for each season: Winter = DJF, spring = MAM, summer = JJA, autumn = SON.

3.3.1 Effect on primary production

It has been shown in the previous chapters that a change in the parametrization of sedimentary respiration changes nutrient concentrations. It is therefore near by hand to suspect these changes to then impact primary production as well.

Figure 3.5 shows the seasonally averaged vertically integrated primary production as the difference between the run with the old parametrization of sedimentary respiration (see Section 2.2.2, p.20) and the run with the new one (see Section 2.4.2, p.25). Red colors denote an increase in primary production with the new parametrization.

Big differences can be seen in the sensitivity of primary production to the parametrization of sedimentary respiration between the different seasons and between the North Sea and Baltic Sea. The peak of primary production in these seas is in spring and summer (see also Figure 4.3). This is also when the biggest changes are seen in primary production when opposing

the two parametrizations. Changes in nutrient concentrations as induced by changes in sedimentary respiration processes are obviously not large enough to impact primary production in the generally less productive seasons, namely winter and fall. Especially in winter, primary production in the model domain is rather light than nutrient limited.
Accordingly with the results already presented in this chapter, primary production in the Baltic Sea is more sensitive to changes in the parametrization of sedimentary respiration. Here, it can be differentiated between the northern Baltic Sea (Guld of Bothnia) and the Baltic Proper. In the Gulf of Bothnia, primary production increases significantly when the new parametrization is introduced (locally by more than 2500 mg C $m^{-2}month^{-1}$, compare this area in Figure 4.4). Looking at Figure 3.4(c) showing the average nitrate, oxygen, and phosphate profiles for the former and the new parametrization of sedimentary respiration at the monitoring station F26 gives more insight into what is happening in this area. Oxygen is reduced leading to a consequent release of phosphate from the sediments. This is then fueling primary production which reduces nitrate in the water column.
Changing the parametrization of sedimentary respiration has an opposite effect in the Baltic Proper. Here, primary production is reduced with the new parametrization. This is likely linked to an increased removal of nitrate by denitrification in the sediment.
The link between sedimentary respiration processes, such as denitrification, and the carbonate chemistry of coastal systems via primary production has been demonstrated in Fennel et al. (2008).

3.3.2 Difference between North Sea and Baltic Sea

The fundamentally different sensitivity of the North Sea and Baltic Sea to the parametrization of sedimentary respiration as found in this part of the study was expected from the characteristic features of the two seas.
The North Sea is mostly shallower than 50 m in the southern areas and has a wide opening towards the Atlantic in the northwest (see Figure 2.1). Tidal currents are strong. This geographic setting leads to a frequent exceedance of the critical bottom shear stress causing both sediment resuspension and vertical mixing of the water column. In contrast to most areas in the Baltic Sea, no permanent stratification develops in the southern North Sea (see Section 1.3, p.9). This weaker stratification lets changes implemented into the sediment-water column exchange of dissolved matter become less visible when looking at temporally and spatially averaged vertical profiles of nitrate. Changes are rapidly mixed both vertically and horizontally. This faster exchange is also expressed by the much smaller residence time of

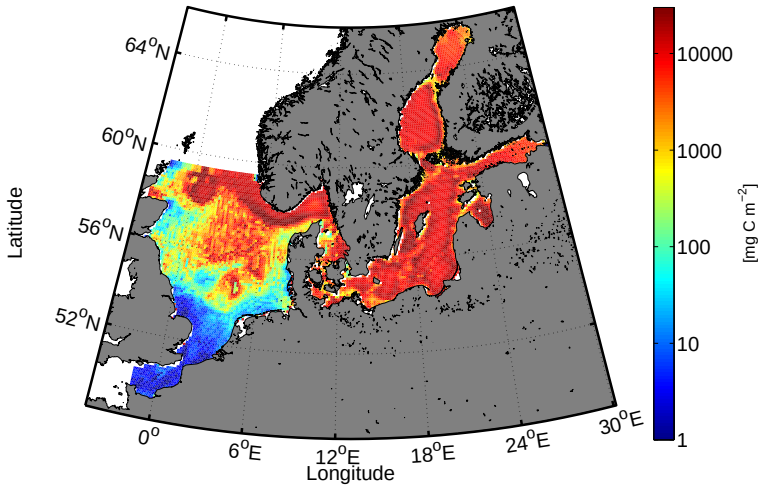

Figure 3.6: Average amount of particulate sediment (*Sed*, see Table 2.1 and Section 2.2.2 for a description of the different sediment variables) as simulated by ECOSMO. Values are taken from the baseline run in this section and averaged over 1999-2009.

waters in the North Sea (≈1 year (Rodhe et al., 2006)) compared to those in the Baltic Sea (≈30 years, see Section 1.3). This is the first reason for the difference seen between the two seas.

Resuspension of sediment increases its changes of being remineralized in the water column instead of either remineralization or burial in the sediment. The insensitvity of the North Sea to changes in the parametrization of sedimentary respiration processes suggests that in the North Sea, remineralization of organic matter is dominantly taking place in the water column. This finding is in good agreement with previous studies in the area, e.g. van Raaphorst et al. (1990). In their study, nutrients released by organic matter degradation in the sediments only contributed to a very small extent to the nutrients required by phytoplankton (if the effect of resuspension is excluded).

The frequency of resuspension events in the North Sea, especially in the southern parts, compared to the Baltic Sea is the second explanation why the sensitivity of the Baltic Sea to the parametrization of sedimentary respiration processes is so much higher. Due to resuspension, less sediment accumulates on the seabed for a prolonged period in the North Sea. This is visible in Figure 3.6 showing the average amount of sediment in ECOSMO (long baseline run, average over 1999-2008 only). The amount of sediment, the model is simulating, gradually increases as one goes from the tidal mixing zone to the northern North Sea, the transition zones, and shallow and especially deep Baltic Sea.

In the deeper basins, the depth itself and the permanent stratifiction almost fully de-couple both deeper water layers and sediment from atmospheric influence so that sediment can set-

tle undisturbed. This is why changes in the parametrization of sedimentary respiration are most visible there. Additionally, oxygen concentrations in this area frequently fall below the threshold for hypoxia as defined by Middelburg and Levin (2009). It can be assumed that the introduction of an hypoxic regime was crucial for a better simulation of vertical nutrient profiles.

3.3.3 Sensitivity of results to chosen fractions

The fractions used in the new parametrization of sedimentary respiration are based on a modeling study by Middelburg et al. (1996); Middelburg and Levin (2009), but have to be interpreted as a first educated guess for the North Sea and Baltic Sea in this study.
The sensitivity of the resulting nutrient profiles to the relative importance attributed to aerobic respiration, denitrification and other anaerobic respiration pathways, respectively, was assessed by performing two additonal runs (see Section 4.1 and Table 3.1). In the first run, the relative importance of denitrification was reduced from 20% to 10% which is compensated by a higher contribution of other anaerobic respiration processes and which corresponds to Figure 1.2 ("sensitivity I"). Secondly, the fraction for aerobic respiration was increased from 22% to 30%, again compensated by anaerobic respiration processes ("sensitivity II").
The general outcome of this part of the study, namely that the Baltic Sea is by far more sensitive to changes in the parametrization of sedimentary respiration than the North Sea, is not sensitive to the chosen fractions for the different respiration pathways. Again, the Baltic Sea shows a higher sensitivity to the relative contributions of the three pathways. Looking at Figure 3.7 (same as Figure 3.3, but with the two additional runs shown in cyan and red), hardly any changes between the different runs using the new parametrizations (blue, cyan, and red) can be seen for the North Sea and the transition zone. Compared to the deep Baltic Sea, the sensitivity in the shallow Baltic Sea is also small (variability in bottom water nitrate concentrations is $<<1\,\mathrm{mmol\,m^{-3}}$). However, nitrate concentrations in the deep Baltic Sea appear to be especially sensitive to the relative contribution of denitrification when the bottom water is anoxic. Bottom water nitrate concentrations increase by as much as 3-4 $\mathrm{mmol\,m^{-3}}$ when halving the fraction attributed to denitrification to 10%. Here, 20% as assumed in this study seems to be more realistic when comparing to the available observations (black line).
Changes applied to the fractions when the bottom water is oxic (red) do only slightly impact the simulated nitrate concentrations, which can be explained by the frequent (or in some places permanent) anoxia in the deep Baltic Sea.
Looking at the three monitoring stations BY15, BY5, and F26, the findings just described

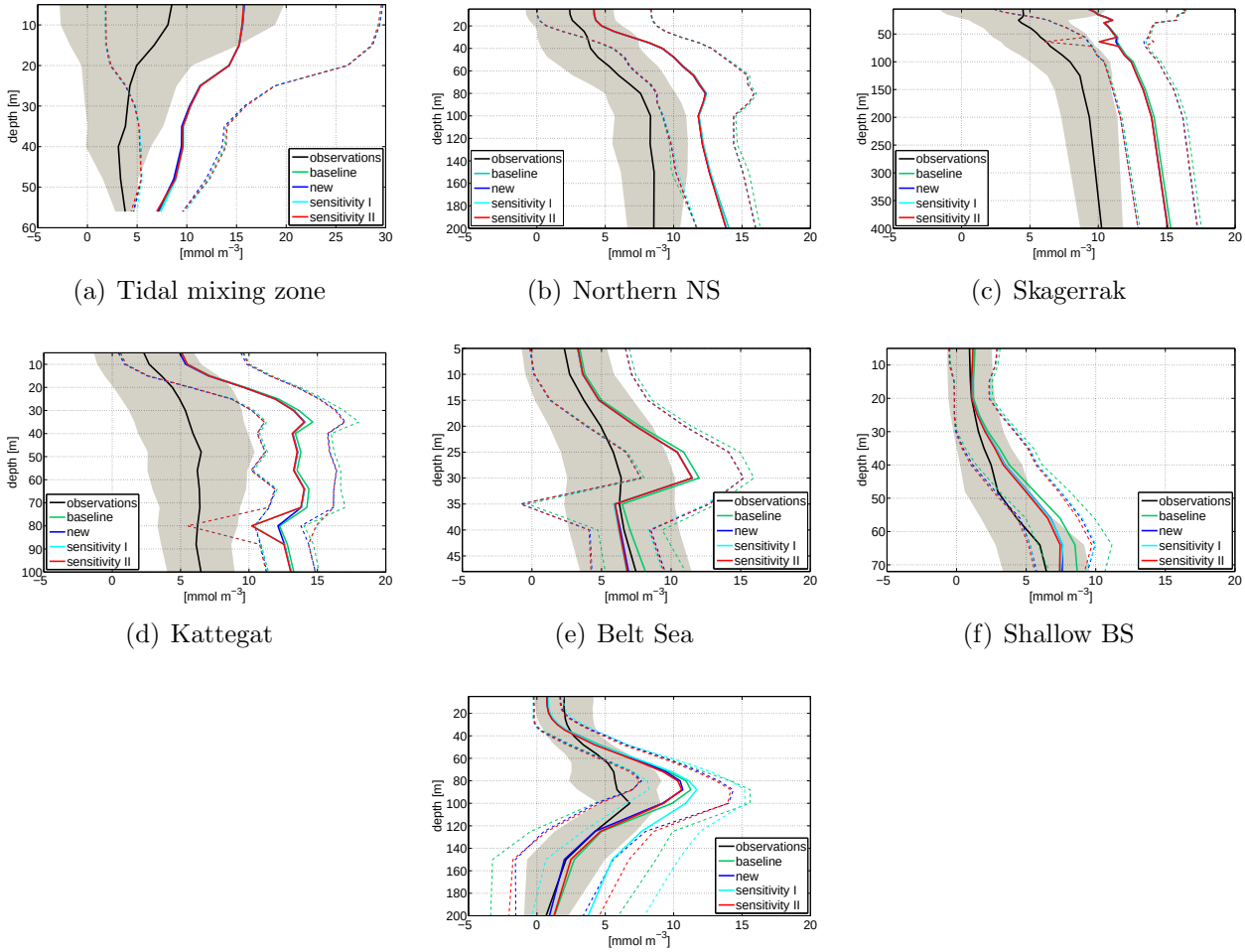

(a) Tidal mixing zone (b) Northern NS (c) Skagerrak

(d) Kattegat (e) Belt Sea (f) Shallow BS

(g) Deep BS

Figure 3.7: Sensitivity of average vertical profiles of nitrate in the different subareas in the model domain (see Figure 2.5) to fractions in new parametrization of sedimentary respiration. Solid lines represent the average over 1948-2008 for the observations (black), the baseline run (green), the run with the new parametrization of sedimentary respiration (blue) as presented in Table 2.2, and the two sensitivity runs "sensitivity I" (cyan) and "sensitivity II" (red, see also Table 3.1). The shaded area and the area limited by the dashed lines, respectively, represent the respective standard deviations from the mean.

above are confirmed. Amongst the three stations, BY15 shows the strongest sensitivity to the fraction of denitrification in anoxic settings while BY5 does not seem to be sensitive at all. At F26, the problems in simulating an oxygen and phosphate profile close to the observations are to a very small extent due to the new parametrization of sedimentary respiration. In fact, the too low oxygen concentrations and the consequently too high phosphate levels are also seen in the baseline run indicating that the aforehand mentioned too coarse atmospheric resolution (missing ventilation) and missing primary production in melt ponds are in fact more strongly

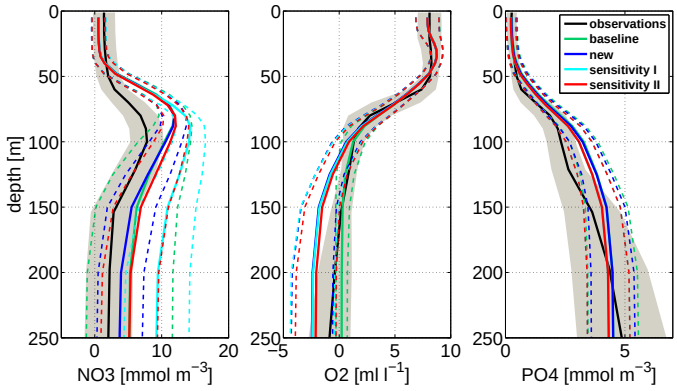

(a) BY15

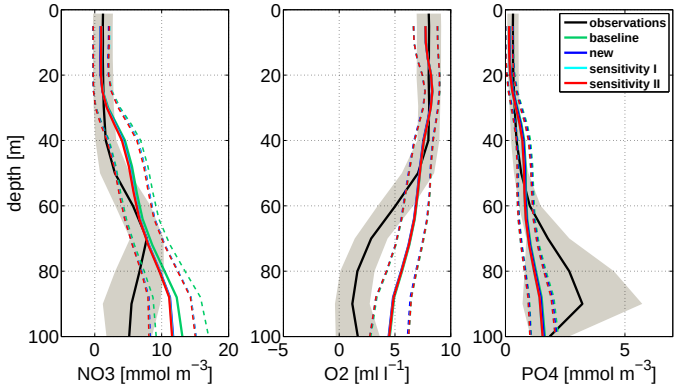

(b) BY5

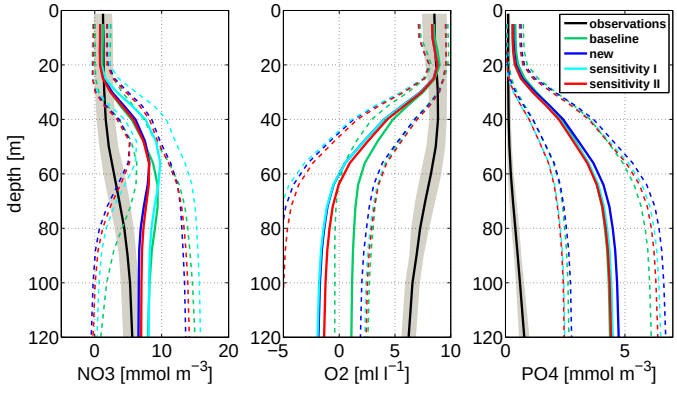

(c) F26

Figure 3.8: Sensitivity of average vertical profiles of nitrate, oxygen and phosphate at BY15, BY5, and F26 (see Figure 2.5 for exact locations of the stations) to fractions in new parametrization of sedimentary respiration. Solid lines represent the average over 1948-2008 for the observations (black), the baseline run (green), the run with the new parametrization of sedimentary respiration (blue) as presented in Table 2.2, and the two sensitivity runs "sensitivity I" (cyan) and "sensitivity II" (red, see also Table 3.1). The shaded area and the area limited by the dashed lines, respectively, represent the respective standard deviations from the mean.

impacting the vertical distribution of nutrients.
It has to be pointed out that the parametrization implemented into ECOSMO in this study was not systematically optimized. The results were not tuned against the observations to find the fractions representing the observed profiles best. To further improve the model's performance, this still needs to be done as part of future work. Additionally, the assumption that organic matter is degraded through the different respiration pathways with the same relative importance of each in the whole model domain, is potentially wrong. Past studies have shown other factors than just temperature and bottom water oxygen concentrations being important in controlling the importance of different respiration processes in overall respiration. This will be discussed in more detail in Section 5.1.

4 Resuspension & Light attenuation

4.1 General approach and simulations II

Table 4.1: Model runs performed assessing the sensitivity of primary production to resuspension and the parametrization of light attenuation. All runs are from 1984-2009, but only 1999-2009 are analyzed to allow for spin-up time. PCE exp. = Experiment using polynomial chaos expansion, see further details on setup in the text.

		Resusp.	k_{bg} [m^{-1}]	k_p [$m^2(mmolC)^{-1}$]	k_{DOM} [$m^2(gC)^{-1}$]	k_{det} [$m^2(gC)^{-1}$]
1	baseline	active	0.05	0.2	-	-
2	w/o resuspension	neglected	0.05	0.2	-	-
3-9	PCE exp. k_{bg}	active	varied	0.2	-	-
10		active	0.03	0.2	-	-
11	with DOM in light I	active	0.03	0.2	0.18	-
12	with DOM in light II	active	0.03	0.2	0.29	-
13	with DOM in light III	active	0.03	0.2	0.40	-
14	baseline II	active	0.03	0.2	0.29	0.2
15-39	PCE exp. det/DOM	active	0.03	0.2	0.29	-
40	w/o resuspension II	neglected	0.03	0.2	0.29	0.2

A stepwise procedure is applied to study the role of resuspension for productivity and carbonate chemistry. First of all, the effect of resuspension was estimated using the original ECOSMO version, which allows for consideration of the effect on nutrient conditions, but neglects the effect of resuspension on light limitation. A run without resuspension (sediment can only be deposited on the seabed, but never resuspended to the water column) is compared to a run with resuspension (run 1 & 2 in Table 4.1). Here, the original parametrization of light attenuation (attenuation due to background turbidity and phytoplankton) is used ($K = k_{bg} + k_p$, see Section 1.2.2, p.7).

Secondly, the sensitivity of the ECOSMO model with respect to the background turbidity light attenuation coefficient is investigated in different regions using the emulator method presented in Section 2.5 to address the overall sensitivity to light parametrization (run 3-9 in Table 4.1).

A literature research has resulted in a documented range of background turbidity attenuation coefficients in the model domain of $0.03\,\mathrm{m}^{-1}$ - $0.64\,\mathrm{m}^{-1}$ (Kirk, 2011; Urtizberea et al., 2013; Hommersom et al., 2009; Høyerslev, 1988). Here, the highest values have been documented for the Wadden Sea.
Based on these values, a polynomial chaos expansion with the following settings is performed:

- parameter to be varied: background turbidity attenuation coefficient
- range of uncertain parameter: $0.03\,\mathrm{m}^{-1}$ - $0.64\,\mathrm{m}^{-1}$
- probability distribution of uncertain parameter: uniform
- maximum order of polynomials: 6 ($P_q = 7$) [1]
- resolution of interpolation in parameter space: 25

As mentioned before and as demonstrated in Mattern et al. (2012a), the results obtained with the polynomial chaos expansion are sensitive to the chosen settings. This has to be kept in mind when interpreting the results. However, the settings chosen here are assumed to be a justified compromise between computational demand and the research question of interest. The analysis done in this section is meant to be a first assessment of the model's sensitivity to the background turbidity attenuation coefficient while being aware of the limitations or uncertainties the chosen settings might induce.
Thirdly, the parametrization of light attenuation is changed to consider both DOM and detritus as factors in light attenuation (runs 11-13 and run 14 in Table 4.1, respectively).
When considering DOM and detritus in the parametrization of light attenuation, the specific light attenuation coefficients used are not the only uncertainty in the setup, but the general representation of DOM and detritus in ECOSMO is dependent on a number of parameter values, such as the sinking speed of detritus, remineralization rates and partitioning of dead organic matter into DOM and detritus. A sensitivity study is done to assess the effect of the sinking speed of detritus and the detrtus/DOM partitioning on primary production in the different subareas. Details on how the choice on these two model parameters was made can be found in the appendix (see p.91). The emulator method (see Section 2.5) is used with the following settings:

- parameters to be varied: partitioning of detritus and DOM & sinking rate of detritus
- range of the uncertain parameters: 0.2 - 0.7[2] & $3\,\mathrm{m\,d}^{-1}$ - $10\,\mathrm{m\,d}^{-1}$

[1] The model is run at the following background turbidity light attenuation coefficients: $0.0455\,\mathrm{m}^{-1}$, $0.1088\,\mathrm{m}^{-1}$, $0.2112\,\mathrm{m}^{-1}$, $0.3350\,\mathrm{m}^{-1}$, $0.4588\,\mathrm{m}^{-1}$, $0.5612\,\mathrm{m}^{-1}$, $0.6245\,\mathrm{m}^{-1}$

[2] This is the fraction of DOM.

- probability distribution of uncertain parameters: uniform
- maximum order of polynomials: 4 ($P_q = 5$)[3]
- resolution of interpolation in parameter space: 25

For this experiment, the parametrization of light attenuation considering pure water, phytoplankton, and DOM is used (run 15-39 in Table 4.1). Again, the results of this study are likely to be sensitive to the settings for the polynomial chaos expansion.
To eventually quantify the effect of resuspension on light limitation in ECOSMO, the resuspension experiment (run 1 & 2 in Table 4.1) is repeated using the new parametrization of light attenuation considering phytoplankton, DOM, and detritus (run 14 & 40 in Table 4.1). In this study, the initiation of the phytoplankton spring bloom in each grid cell of ECOSMO is defined as the first day when the daily primary production exceeds the median of daily production levels of the respective year by more than 5% (Siegel et al., 2002). Subsequently, the difference in bloom initiation between the run without and the run with resuspension is analyzed.
For the analysis, spatial averages of primary production are calculated over certain subareas according to Figure 2.5.

4.2 Resuspension I: No light effect

In the first resuspension experiment, resuspended matter does not contribute to light attenuation. Therefore, only the effect of resuspension on nutrient availability in the water column is quantified for primary production and state variables of the carbonate system.

4.2.1 Effect on primary production

A run neglecting all resuspension was performed to quantify its influence on primary production and state variables of the carbonate system. Hereby, the parametrization of light attenuation only accounting for the background turbidity and phytoplankton is used (see sections 2.4.3 and 4.1).

[3]The model is run at all combinations of the following values vor the partitioning of detritus and DOM (I) and the sinking rate of detritus (II):
I: 0.2235, 0.3154, 0.45, 0.5846, 0.6765
II: 3.3284 m d^{-1}, 4.6154 m d^{-1}, 6.5 m d^{-1}, 8.3846 m d^{-1}, 9.6716 m d^{-1}

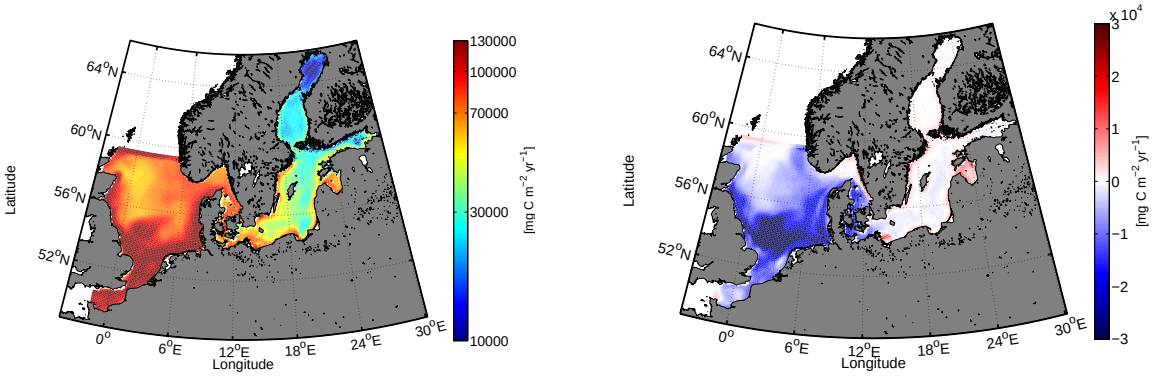

(a) Primary Production (baseline)

(b) Primary Production (w/o resuspension - baseline)

Figure 4.1: Vertically integrated annual primary production in the model domain averaged over 1999-2009. Figure 4.1(a) shows results of the baseline run, Figure 4.1(b) the difference between the run without resuspension and the baseline run (w/o resuspension - baseline). Blue colors indicate a decline in primary production when neglecting resuspension.

Figure 4.1 shows the spatial distribution of vertically integrated annual primary production in the model domain in the baseline run (Figure 4.1(a)) and the difference between the run with neglected resuspension and the baseline run (w/o resuspension - baseline, Figure 4.1(b)).
Primary production is clearly strongest in the North Sea, more specifically in the tidal mixing zone, and weakest in the northern Baltic Sea which can be attributed to frequent ice cover in this region. This pattern is valid throughout all seasons as can be seen in Figure 4.4 showing the average monthly vertically integrated primary production for each season.
In the tidal mixing zone, the strongest decrease in vertically integrated primary production is observed in the southwestern part of the North Sea, with a local decrease of up to 45%. The pattern which becomes visible in Figure 4.1 is clearly dominated by the seasons with the highest production in the North Sea, namely spring and summer (see Figure 4.4). In fall and winter, a more diverse picture is simulated by the model with regions of either increased or decreased primary production.
The effect of resuspension on vertically integrated annual primary production is clearly less pronounced in the Baltic Sea. Primary production in the shallow Baltic Sea increases when resuspension is neglected. Looking at Figure 4.1(b), this feature seems to be primarily caused by areas along the Swedish coast and the Gulf of Riga. Here, this pattern is most pronounced for summer and fall (see Figure 4.4, largest increase of locally up to ≈85% observed in fall), the effect of resuspension is smaller in winter and spring.
Averaging the effect of resuspension on vertically integrated annual primary production for the different subareas gives the picture shown in Figure 4.2. Values are averaged over 1999-2009 and the errorbars denote the standard deviation over this period. The result from the run

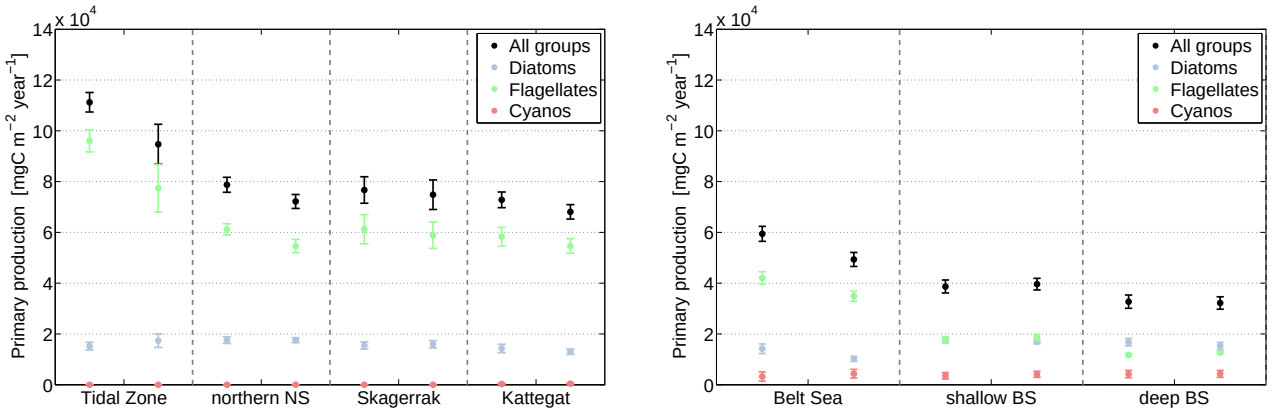

(a) (b)

Figure 4.2: Vertically integrated annual primary production with (left) and without (right) resuspension. Annual production of all phytoplankton groups (black), flagellates (green), diatoms (blue), and cyanobacteria (pink) averaged over 1999-2009 and over the respective subarea. The errorbars indicate the standard deviation over the averaged period.

with resuspension (baseline run) is on the respective left, the run without resuspension on the right side.

As already observed in Figure 4.1, overall changes in primary production induced by neglecting resuspension are larger in the North Sea than in the Baltic Sea. Given the geography of the two seas and the stronger tidal forcing in the North compared to the Baltic Sea, this result was expected (see Section 1.3, p.9). A clear decrease of approximately 15% on average in vertically integrated annual primary production can be seen for both the northern North Sea and the tidal mixing zone. In the transition zone between the North Sea and the Baltic Sea (Skagerrak, Kattegat, and Belt Sea), the change is clearly less pronounced, but neglecting resuspension still has a negative effect on primary production. In contrast, the deeper areas of the Baltic Sea seem to be almost insensitive to in-/excluding resuspension. This can easily be explained by the generally little tidal forcing in the Baltic Sea and the very little to non-existing direct influence of the wind below the mixed layer depth. In the shallow Baltic Sea, an increase of primary production is observed when resuspension is neglected. This is potentially linked to circulation. Water that is transported on-shelf from the central Baltic Sea is enriched in nutrients when resuspension is neglected and primary production is reduced in the central Baltic Sea. The direct negative effect of neglected resuspension in the shallow Baltic Sea is obviously masked by this advection of nutrient enriched water enhancing local primary production.

Besides the effect on overall annual integrated primary production, the effect of resuspension on the seasonal cycle is of interest as well. Figure 4.3 shows the average seasonal cycle for

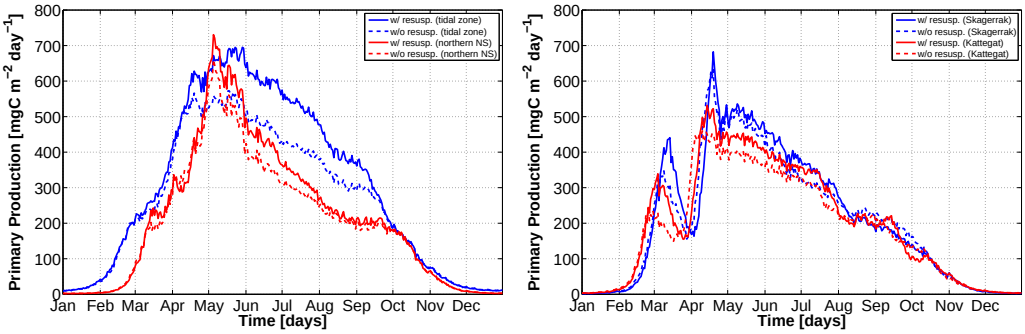

(a) Tidal mixing zone and northern NS

(b) Skagerrak and Kattegat

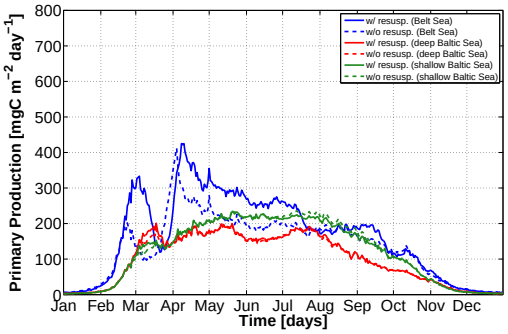

(c) Belt Sea, deep and shallow Baltic Sea

Figure 4.3: Average annual cycle of vertically integrated primary production for the different subareas in the model domain with (solid lines) and without (dashed lines) resuspension. Subareas are defined in Figure 2.5 (p.23). Annual cycle is averaged over 1999-2009.

the different subareas and reveals that neglected resuspension damps the peak of primary production, but does not influence the timing of phytoplankton bloom due to a light effect of resuspended matter. This was expected from the model setup in this first resuspension experiment. Here, light is only attenuated due to a background turbidity and phytoplankton. Resuspended matter is added to the detritus pool in ECOSMO, which is not included as a factor attenuating light here. Consequently, including or neglecting resuspension does not directly influence the local light climate in this setup. Since the results indicate a reduction of primary production for most areas when resuspension is neglected, an indirect effect of resuspended matter on the light conditions through a decreased attenuation by phytoplankton can be found.

Later in this chapter (see Section 4.3), the results of the second resuspension experiment using the parametrization of light attenuation considering pure water, phytoplankton, DOM, and detritus are presented (run 14 & 15 in Table 4.1, p.49).

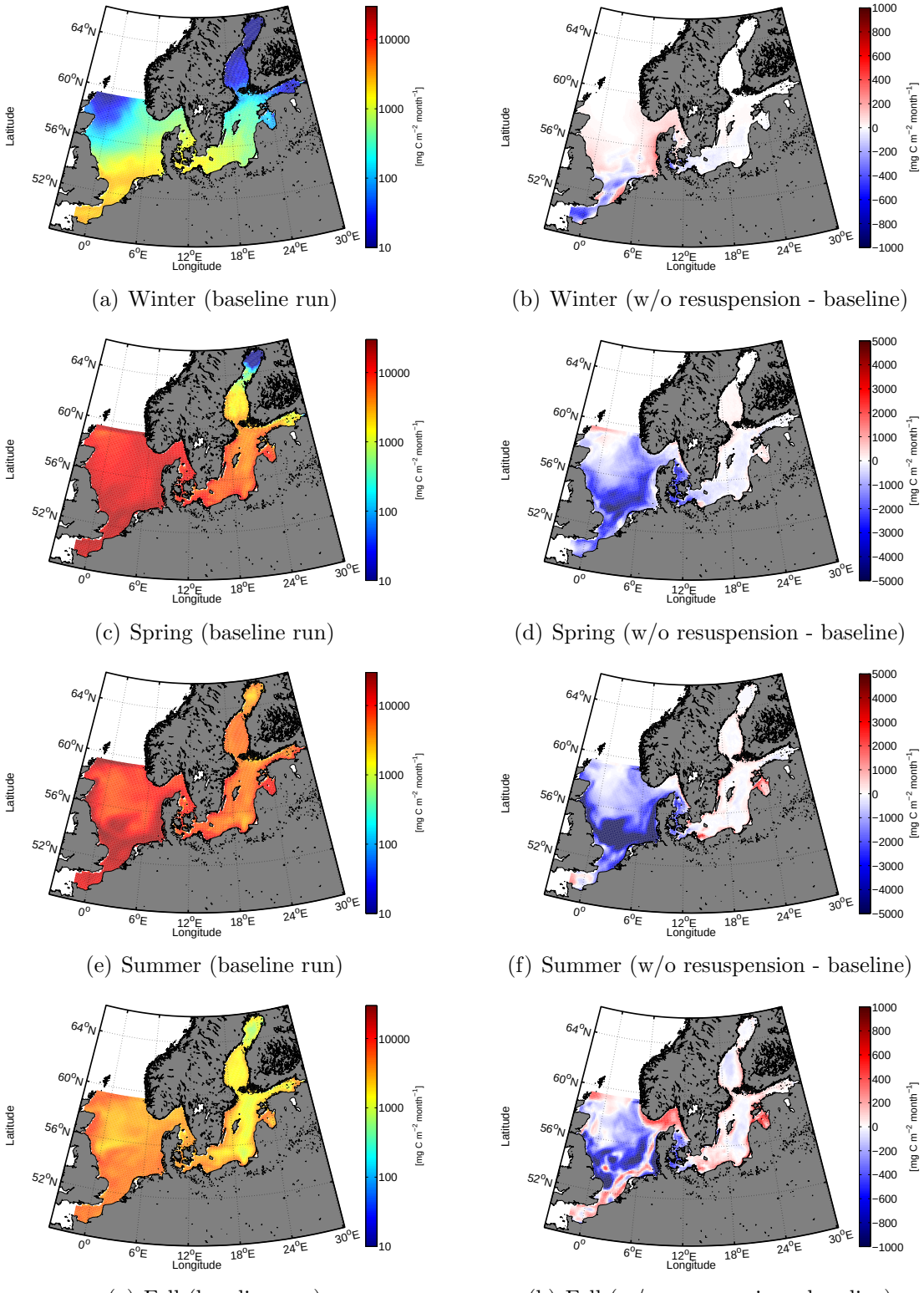

(a) Winter (baseline run)

(b) Winter (w/o resuspension - baseline)

(c) Spring (baseline run)

(d) Spring (w/o resuspension - baseline)

(e) Summer (baseline run)

(f) Summer (w/o resuspension - baseline)

(g) Fall (baseline run)

(h) Fall (w/o resuspension - baseline)

Figure 4.4: Seasonally averaged vertically integrated primary production with (left column, note logarithmic scaling) and changes when neglecting resuspension (right) for all four seasons. All values are averaged over 1999-2009. Months included for each season: Winter = DJF, spring = MAM, summer = JJA, fall = SON.

4.2.2 Effect on the carbonate system

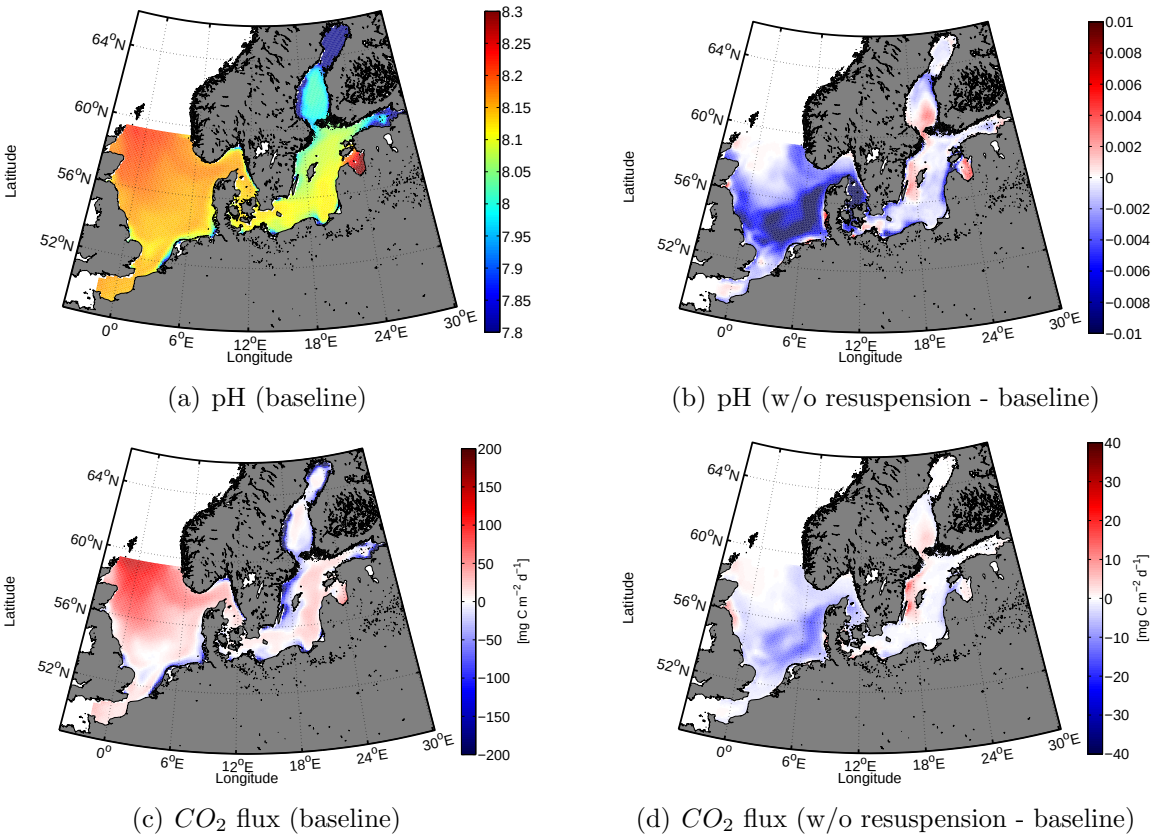

(a) pH (baseline)

(b) pH (w/o resuspension - baseline)

(c) CO_2 flux (baseline)

(d) CO_2 flux (w/o resuspension - baseline)

Figure 4.5: Surface pH and daily surface flux of CO_2 in the model domain averaged over 1999-2009. Figures 4.5(a) and 4.5(c) show results of the baseline run (in Figure 4.5(c): blue = flux ocean-atmosphere), figures 4.5(b) and 4.5(d) the difference between the run without resuspension and the baseline run (w/o resuspension - baseline).

The importance of resuspension for primary production in the model domain has been demonstrated and quantified in the previous section. Primary production is directly linked to the carbonate chemistry. Formation and degradation of organic material influences state variables of the carbonate system directly, such as for example pH, dissolved inorganic carbon (DIC) or the surface flux of CO_2. Primary production hereby increases the pH, decreases DIC and thereby potentially also changes the surface flux of CO_2.

Figure 4.5 shows the effect of resuspension on surface pH and surface flux of CO_2 in the model domain of ECOSMO. While the respective left figures show the surface pH (top) and flux of CO_2 (bottom) in the baseline run (active resuspension) averaged over 1999-2009, the respective right figures show the difference of the same variables when subtracting the results obtained with the baseline run from the run without any resuspension.

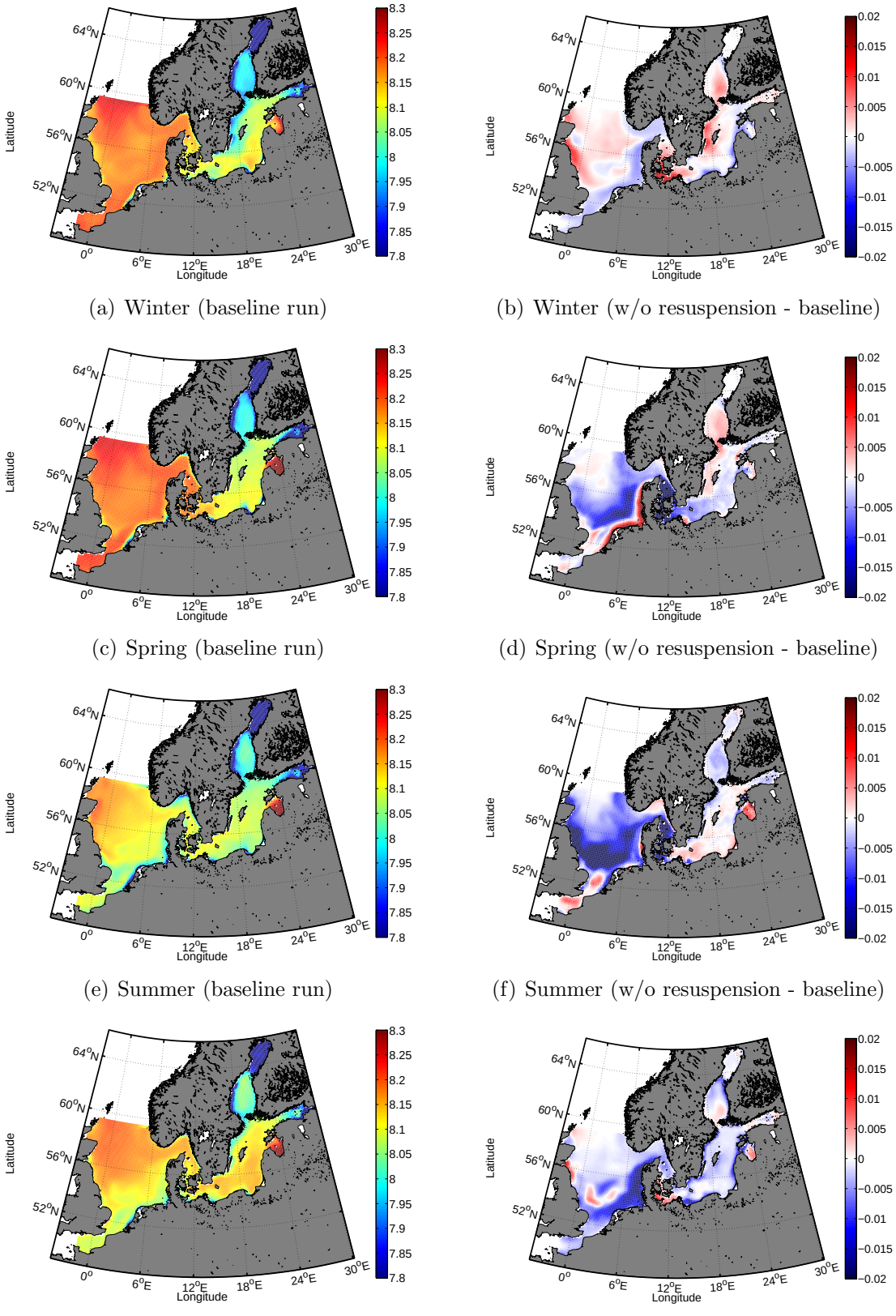

(a) Winter (baseline run)

(b) Winter (w/o resuspension - baseline)

(c) Spring (baseline run)

(d) Spring (w/o resuspension - baseline)

(e) Summer (baseline run)

(f) Summer (w/o resuspension - baseline)

(g) Fall (baseline run)

(h) Fall (w/o resuspension - baseline)

Figure 4.6: Seasonally averaged surface pH with (left column) and changes when neglecting resuspension (right). All values are averaged over 1999-2009. Months included for each season: Winter = DJF, spring = MAM, summer = JJA, fall = SON.

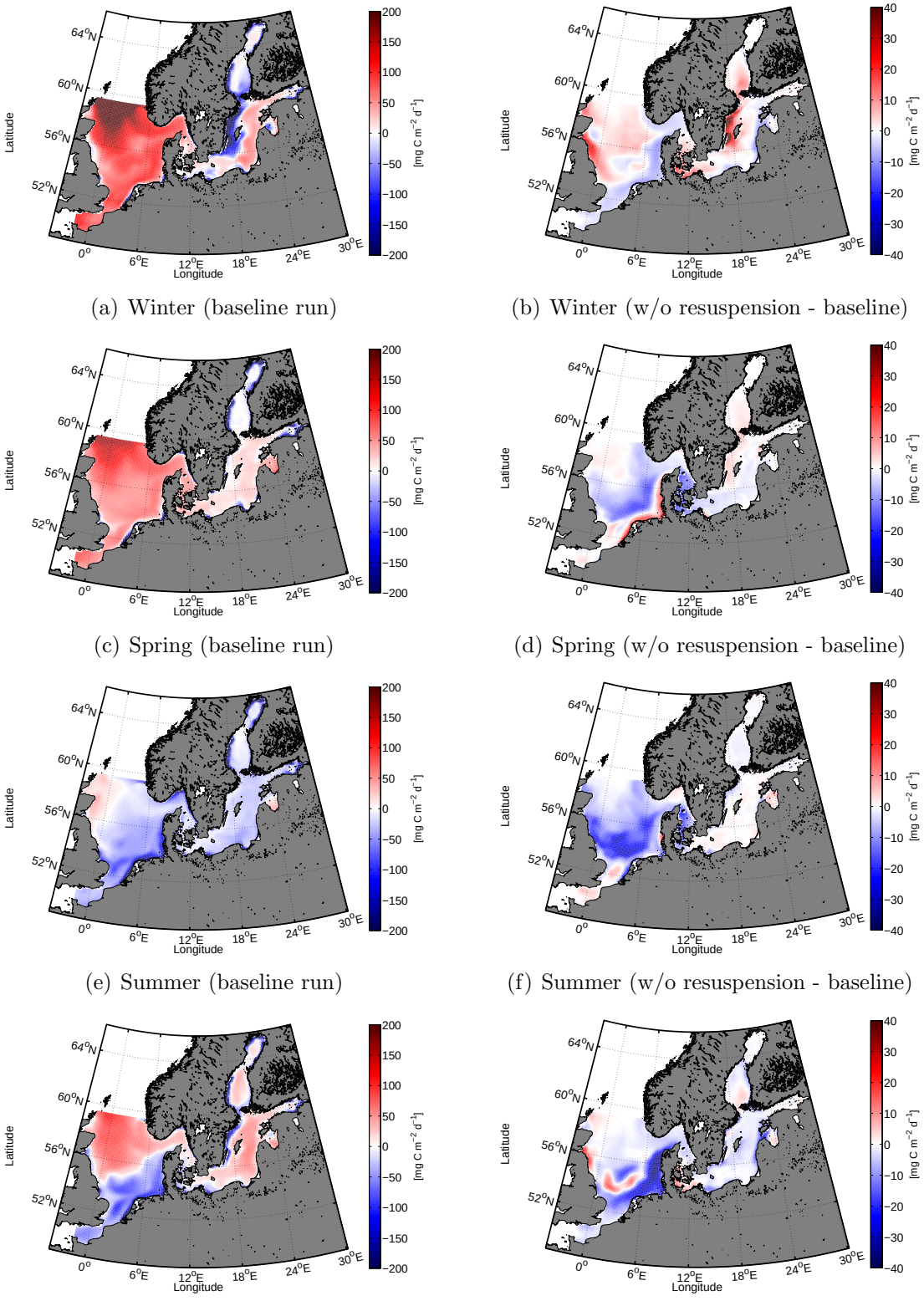

(a) Winter (baseline run)

(b) Winter (w/o resuspension - baseline)

(c) Spring (baseline run)

(d) Spring (w/o resuspension - baseline)

(e) Summer (baseline run)

(f) Summer (w/o resuspension - baseline)

(g) Fall (baseline run)

(h) Fall (w/o resuspension - baseline)

Figure 4.7: Seasonally averaged daily surface CO_2 flux with (left column) and changes when neglecting resuspension (right). All values are averaged over 1999-2009. In the left column, blue colors denote flux from ocean to atmosphere (out-gassing), red correspond to a flux from the atmosphere to ocean (in-gassing). Months included for each season: Winter = DJF, spring = MAM, summer = JJA, fall = SON.

Accordingly to the observed changes in primary production, changes in surface pH and flux of CO_2 are observed when neglecting resuspension.
Generally, the main patterns arising for both surface pH and surface flux of CO_2 correspond well to the patterns observed for primary production (compare to Figure 4.1(b)). The largest changes can be seen in the tidal mixing zone of the North Sea (decline) while in the Baltic Sea, regions with changes in both directions (increase/decrease) can be found.
Surface pH is generally higher in the North Sea than in the Baltic Sea. While surface pH in the North Sea is simulated to be around 8.2 on average, values for the Baltic Proper are around 8.1 and even below 8 in the northern Baltic Sea. This agrees well with the spatial distribution of primary production in the model domain with higher pH values corresponding to higher primary production. When resuspension is neglected, a decline of surface pH is observed in those regions where primary production is simulated to decrease as well. The biggest decrease in surface pH is observed in the tidal mixing zone with a reduction of up to 0.02 (strongest decline in most productive seasons, namely spring and summer, see Figure 4.6).
Large parts of the North and Baltic Sea are a sink for atmospheric CO_2 on average (red colors in Figure 4.5(c)). Only the regions very close to the coast are a source of CO_2 for the atmosphere (blue colors in Figure 4.5(c)).
Interpreting Figure 4.5(d) showing the change in observed surface fluxes of CO_2 when neglecting resuspension, the sign of the respective fluxes in the baseline run has to be kept in mind. The change for the majority of the North Sea which was a sink of atmospheric CO_2 in the baseline run (red colors in Figure 4.5(c)) is negative (blue colors in Figure 4.5(d)). This means that the surface flux of CO_2 can be less positive (smaller sink), neutral, or even negative (source for atmosphere) in the run with neglected resuspension. The opposite is true for the regions very close to the Swedish coast. Having been a source of CO_2 for the atmosphere in the baseline run (blue colors in Figure 4.5(c)), the change is positive for these areas when resuspension is neglected, indicating the flux is less negative (smaller source), neutral, or even positive (sink) in the run without resuspension.
Looking at the map of surface flux of CO_2 in the run without resuspension (see Figure 2(b) in the appendix, p.94), it is revealed that the flux becomes less positve (smaller sink), neutral, or even negative (source for the atmosphere) in large parts of the North Sea (see blue colors in Figure 4.5(d)) and less negative (smaller source) in the Swedish coastal areas (see red colors in Figure 4.5(d)).

4.3 Light attenuation

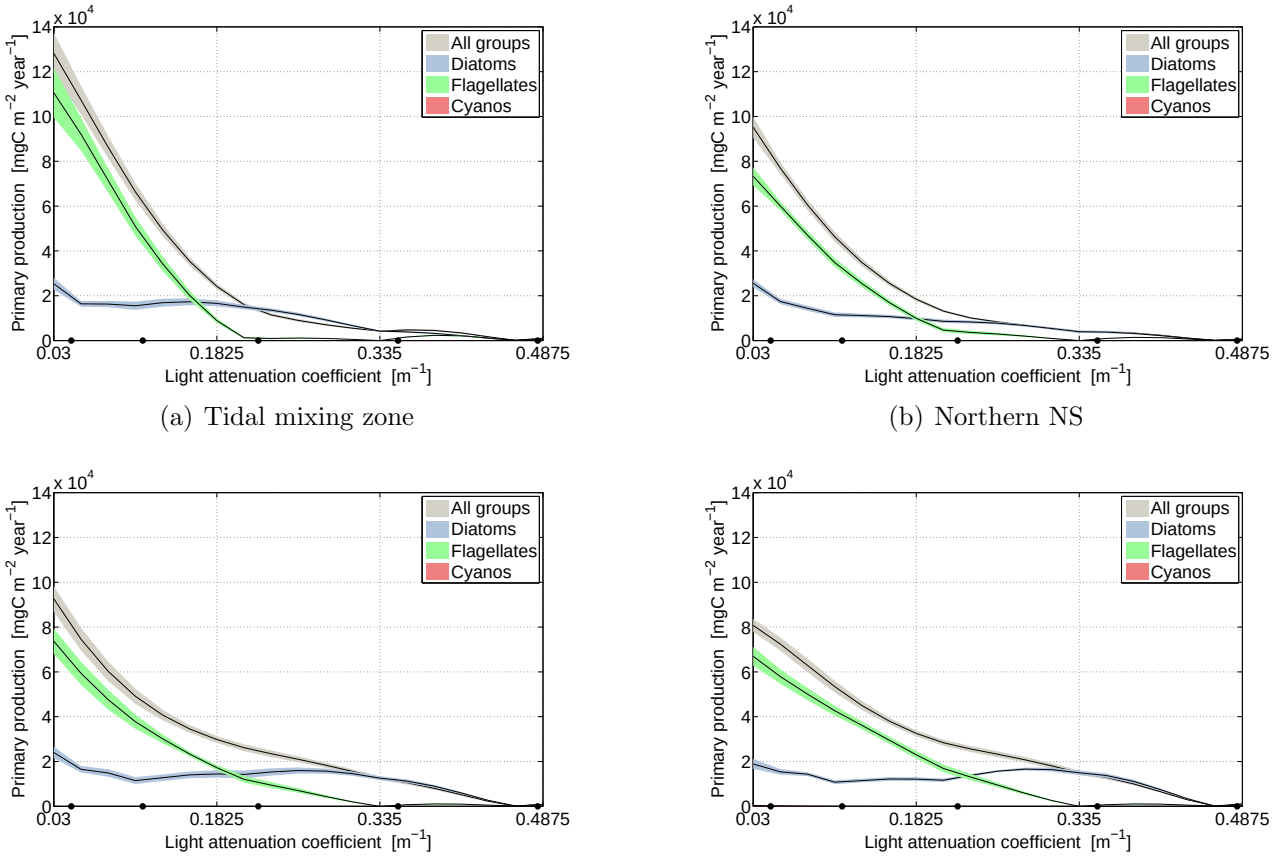

(a) Tidal mixing zone

(b) Northern NS

(c) Skagerrak

(d) Kattegat

Figure 4.8: Vertically integrated annual primary production (overall (grey), diatoms (blue), flagellates (green), and cyanobacteria (pink) only) averaged over the different subareas for different background turbidity coefficients. Results obtained using the emulator method described in 2.5 (p.31) and 4.1 (p.49). Black lines indicate the averaged annual production for 1999-2009, shaded areas the standard deviation over 1999-2009.

Primary production in ECOSMO is limited by either light or nutrients (see Section 2.2.1, p.17). In this section, the results of the study looking at the sensitivity of primary production to different parametrizations of light attenuation are presented.

In the baseline run, light in ECOSMO is attenuated due to a background turbidity ($k_{bg} = 0.05\,\mathrm{m}^{-1}$) or phytoplankton (see Section 4.1, p.49). Figure 4.8 and 4.9 show the sensitivity of vertically integrated annual primary production to different background turbidity light attenuation coefficients. Results are spatially averaged over the subareas presented in Figure 2.5 (p.23) and temporally over 1999-2009 (black lines). The shaded areas behind the black lines

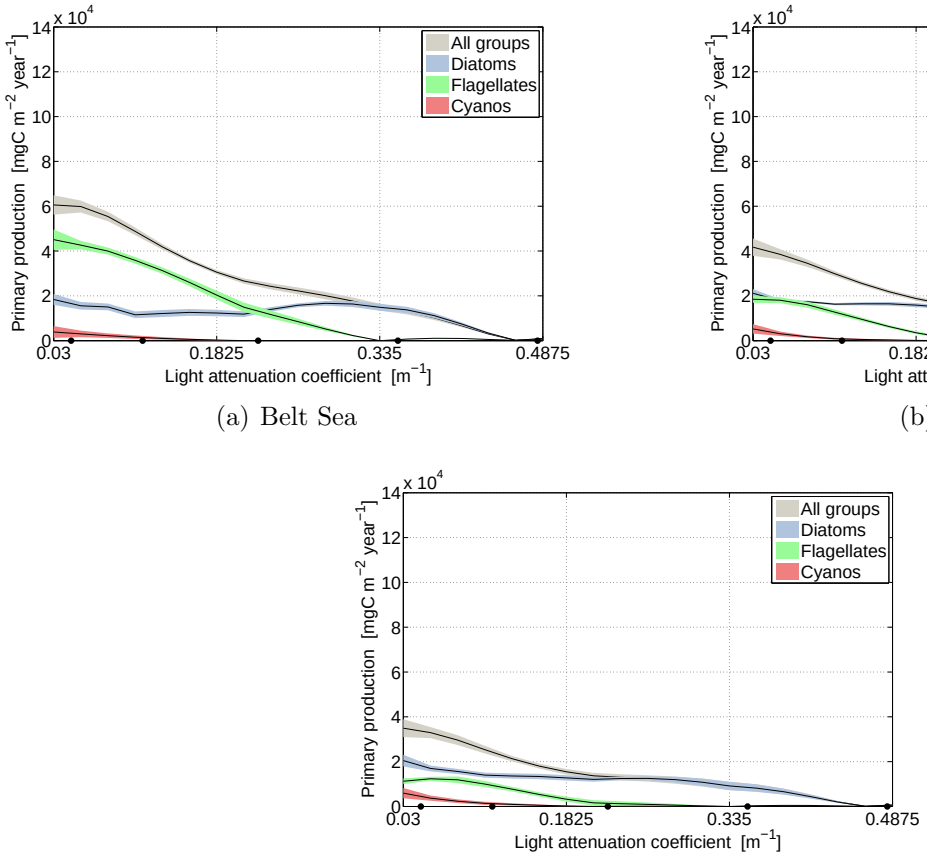

(a) Belt Sea

(b) shallow BS

(c) deep BS

Figure 4.9: Vertically integrated annual primary production (overall (grey), diatoms (blue), flagellates (green), and cyanobacteria (pink) only) averaged over the different subareas for different background turbidity coefficients. Results obtained using the emulator method described in 2.5 (p.31) and 4.1 (p.49). Black lines indicate the averaged annual production for 1999-2009, shaded areas the standard deviation over 1999-2009.

denote the standard deviation over this period for overall primary production (grey), diatoms only (green), flagellates only (blue), and cynobacteria (pink). The black dots on the x-axis denote the quadrature points in the polynomial chaos expansion setup (see Section 4.1, p.49). At larger background attenuation coefficients than shown in Figure 4.8 and 4.9, vertically integrated annual primary production is zero in all regions. For a better utilization of the space in the figures, these results are not shown here.

In agreement with Figure 4.1 and 4.2, the North Sea is generally more productive than all other areas in the model domain with maximum values of vertically integrated annual overall primary production of almost $14 \cdot 10^4$ mg C m^{-2} year^{-1} in the tidal mixing zone (lowest background turbidity attenuation coefficient). The larger the distance from the North Sea, the lower the primary production values get (maximum values in deep Baltic Sea just below

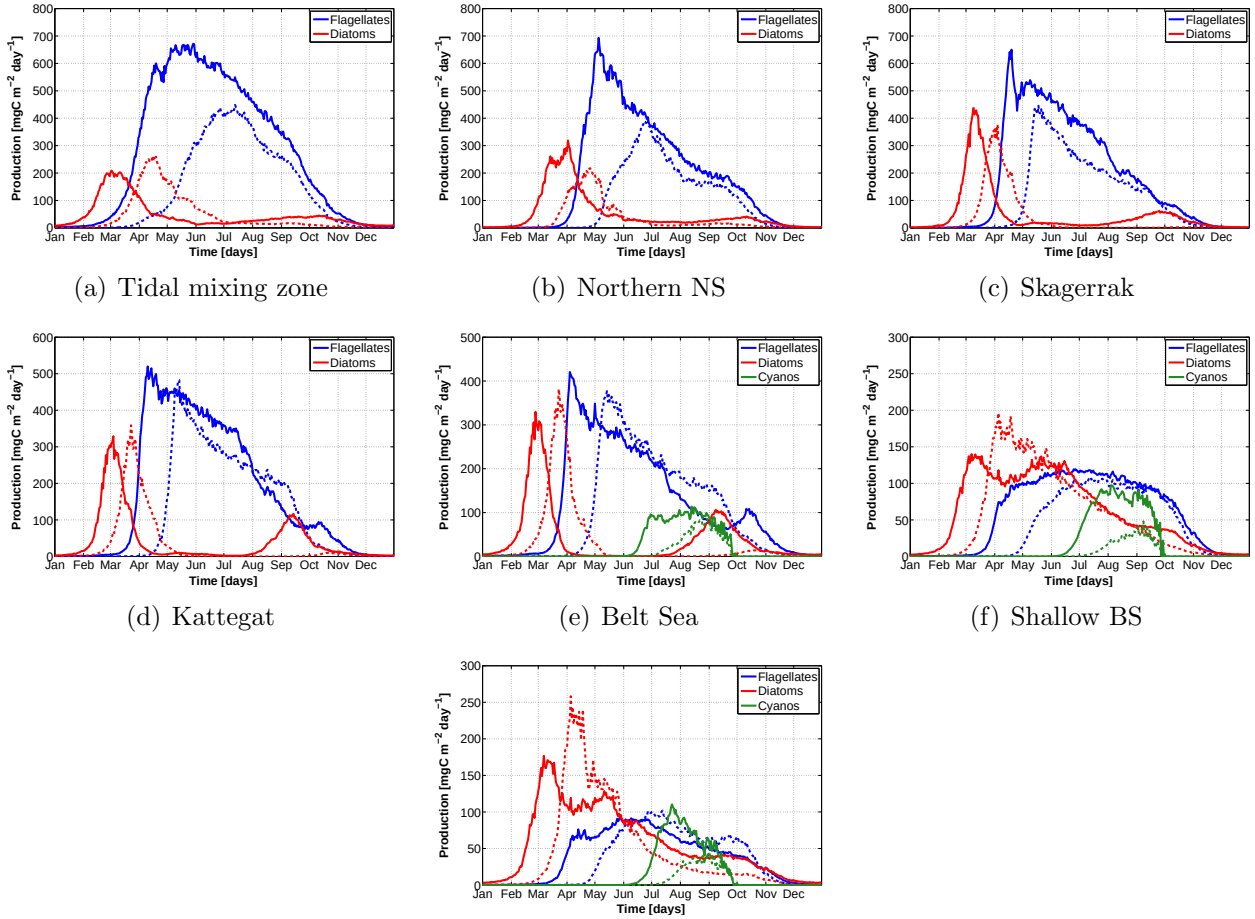

(a) Tidal mixing zone (b) Northern NS (c) Skagerrak

(d) Kattegat (e) Belt Sea (f) Shallow BS

(g) Deep BS

Figure 4.10: Seasonality of production of different phytoplankton groups in different subareas as a function of the background turbidity coefficient. Flagellate production in blue, diatom production in red, and cyanobacteria production in green. Solid line: $k_{bg} = 0.0455\,\mathrm{m}^{-1}$, dashed line: $k_{bg} = 0.1088\,\mathrm{m}^{-1}$. Seasonal cycle averaged over 1999-2009.

$4\ \cdot 10^4\,\mathrm{mg}\ C\ \mathrm{m}^{-2}\ \mathrm{year}^{-1}$).

Showing the highest primary production values, the tidal mixing zone also shows the strongest decline in primary production when the background turbidity attenuation coefficient is increased (increasing the background turbidity attenuation coefficient by a factor of 6 from $0.03\,\mathrm{m}^{-1}$ to $\approx 0.18\,\mathrm{m}^{-1}$ reduces simulated primary production to $\approx \frac{1}{6}$ of the value simulated at the lowest simulated coefficient). Flagellates make up by far the biggest part in North Sea primary production and show a much stronger sensitivity to the background turbidity attenuation coefficient than diatoms. Even though less dominant or even less abundant than diatoms in other areas of the model domain, this higher sensitivity can generally be seen. A reduction of the average vertically integrated annual production of diatoms by 50% requires an increase of the background turbidity attenuation coefficient by a factor 10, whereas the

same reduction for the production of flagellates is already achieved by only increasing the background turbidity attenuation coefficient by a factor of approximately 4-6, depending on the region. This can be explained with the timing of the production of flagellates and diatoms, respectively.

Figure 4.10 shows the effect of different background turbudity attenuation coefficients on the seasonality of production of flagellates (blue), diatoms (red), and cyanobacteria (green) examplarily for $k_{bg} = 0.0455\,\mathrm{m}^{-1}$ (solid lines) and $k_{bg} = 0.1088\,\mathrm{m}^{-1}$ (dashed lines). Irrespectively of the background turbidity attenuation coefficient, production of diatmos starts first in the year (February-March), followed by flagellates (March-April) and cyanobacteria where occurring (Belt Sea and Baltic Sea, June-July). Increasing the background turbidity attenuation coefficient and thereby reducing the amount of light at all water depths leads to changes in the seasonality of all three functional groups of phytoplankton. Generally, less light leads to a shift of initiation of production towards later times of the year. The time in winter in which light is not sufficient for production to take place is extended and hence, the time during which production is possible is shortened.

Summarized over all groups of phytoplankton and all regions, a doubling of the background turbidity attenuation coefficient as can be seen in Figure 4.10 delays the start of primary production by approximately one month. In addition, the maximum simulated production of flagellates and cyanobacteria is damped in all regions. For diatoms, the peak of production is only damped in the northern North Sea and the Skagerrak, but increases with a higher background turbidity attenuation coefficient in all other regions (dashed red lines). This can most likely be linked to the delayed initiation of flagellates production leading to a reduced competition for nutrients for diatoms for a longer time in the year. It is changes in the seasonal cycle which can explain the relatively small sensitivity of annual integrated diatom production to a change in background turbidity attenuation coefficient as seen in Figure 4.8 and 4.9.

Comparing to the values found in the literature, the background turbidity light attenuation coefficient of $0.64\,\mathrm{m}^{-1}$ as found for the Wadden Sea (see Section 4.1) appears to be by far too high when applied to the whole model domain. Even in the tidal mixing zone, all primary production is suppressed when light attenuation is this strong. It is however imaginable that a value this high is appropriate very locally and for a very specific point of time. When looking at the values suggested for the Baltic Sea (around $0.3\,\mathrm{m}^{-1}$), flagellate production does not occur anymore while diatom production seems to be almost unaffected. Overall, more information about the spatial and temporal variability of the light attenuation coefficients for both North and Baltic Sea and detailed model validation is still needed to make conclusions about what values are appropriate to use.

Considering light attenuation due to a background turbidity implies disregarding any spatial

and temporal variations in all particulate (other than phytoplankton) and dissolved matter (see Section 1.2.2, p.7). Therefore, as the next part of this sensitivity analysis, light attenuation due to a background turbidity was replaced by specific light attenuation due to pure water and DOM (see runs 11-13 in Table 4.1) and due to pure water, DOM, and detritus (run 14 in Table 4.1, see Section 4.1, p.49).

Same as Figure 4.8 and 4.9, Figure 4.11 shows the vertically integrated annual primary production for different subareas and the different functional groups averaged over 1999-2009. In Figure 4.11, 5 values are shown for each region using different parametrizations of light attenuation: the first value is the result of run 10 in Table 4.1 (p.49) accounting for light attenuation due to a background turbidity and phytoplankton. The values 2, 3 and 4 for each region are obtained using the parametrization of light attenuation considering the attenuation due to water, phytoplankton, and DOM (see runs 11-13 in Table 4.1). The three values for each region correspond to three different specific DOM attenuation coefficients k_{DOM} used (left/low value: $0.18\,\mathrm{m}^2(\mathrm{gC})^{-1}$; middle/mean value: $0.29\,\mathrm{m}^2(\mathrm{gC})^{-1}$; right/high value: $0.40\,\mathrm{m}^2(\mathrm{gC})^{-1}$). The last value for each region show the result of run 14 in Table 4.1 additionally including light attenuation due to detritus.

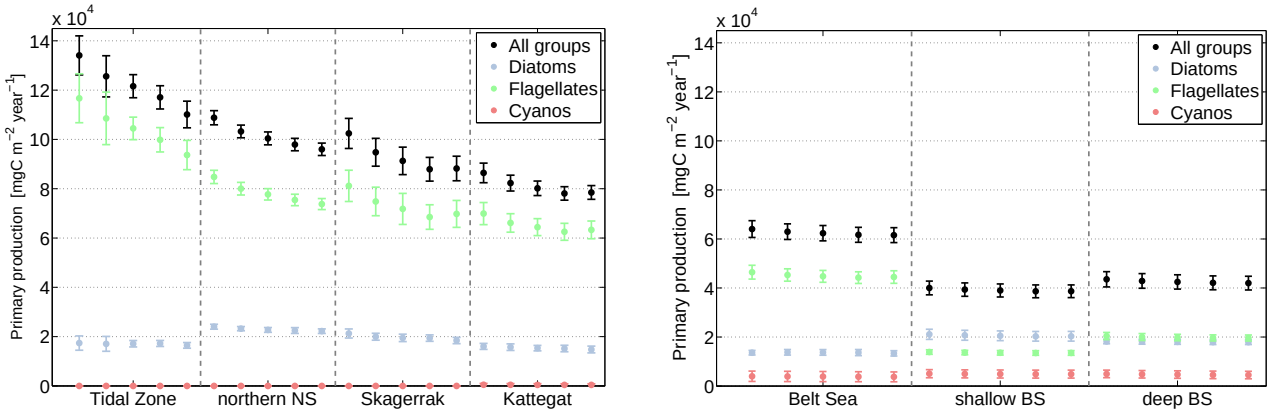

Figure 4.11: Vertically integrated annual production for different parametrizations of light attenuation (annual production averaged over 1999-2009 and over the respective region): The first value for each group and each region corresponds to run 10 in Table 4.1 (light attenuation due to water and phytoplankton), the values 2-4 to run 11-13 (light attenuation due to water, phytoplankton, and DOM) and the last value to run 14 (light attenuation due to water, phytoplankton, DOM, and detritus). The errorbars indicate the standard deviation over the averaged period.

Generally, introducing DOM and subsequently detritus as additional factors attenuating the light intensity in the water column leads to a gradual reduction of primary production in all subareas in the model domain (values 2-5 in Figure 4.11(b)).

The general impact of DOM in light attenuation and the variabiliy to different specific DOM attenuation coefficients (values 2-4) decreases as one goes from the North Sea (highest variability) to the Baltic Sea (lowest) and is controlled by the abundance of DOM in the model domain. DOM is most abundant in the water column where primary production is high, namely in the North Sea in general, and more specifically in the tidal mixing zone (see Figure 4.12(a)). The same is valid for detritus (see Figure 4.12(b)).

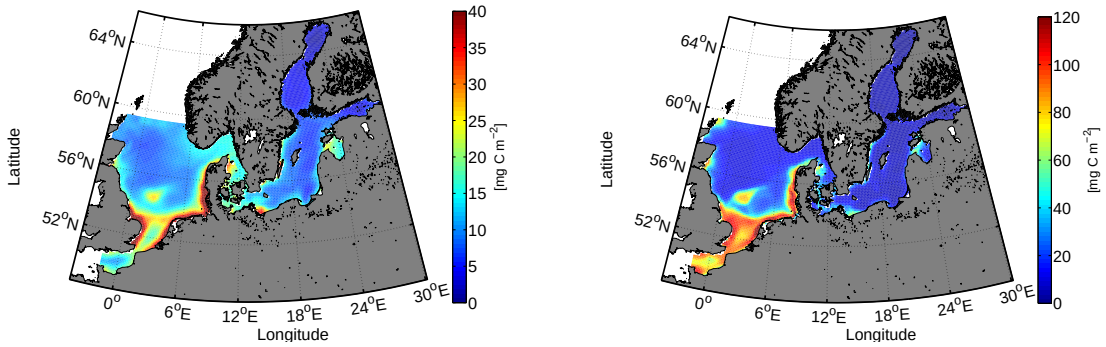

(a) DOM (b) Detritus

Figure 4.12: Average concentrations of DOM (4.12(a)) and detritus (4.12(b)) as simulated by ECOSMO. Values averaged over 1999-2009 and taken from run 1 in Table 4.1. Note the different color scaling for DOM and detritus, respectively.

Comparing the results of Figure 4.11(b) to those of the polynomial chaos expansion experiment regarding the background turbidity light attenuation coefficient (Figure 4.8 and 4.9), changes in the parametrization of light attenuation again effect flagellates (green) most. The production of diatoms (blue) is relatively insensitive to changes compared to flagellates. This can again be explained by the seasonality of diatoms versus flagellates. It has been pointed out before that diatoms are the first to start production every year when flagellates are not yet abundant. Diatom biomass is relatively small because growth is still potentially light limited at that time of the year. Before their biomass can get high enough to see the effect of added specific light attenuation coefficients of DOM (and detritus) to the parametrization of light attenuation, diatoms get outcompeted by flagellates. When flagellte production peaks later in the year (see Figure 4.3), biomass is high enough to impact light intensity which in turn negatively impacts production (negative feedback).

4.4 Detritus versus DOM

Including DOM and detritus in the parametrization of light attenuation demands a reasonably good understanding of the representation of DOM and detritus in ECOSMO. In this part of

the study, the results of the sensitivity analysis looking at the impact of parameters controlling detritus and DOM on primary production in the model are shown in Figure 4.13. The sinking rate of detritus and the partitioning of detritus and DOM were varied in a polynomial chaos expansion experiment and the resulting values of primary production interpolated in parameter space to obtain values over the whole range of both uncertain input parameters. In this experiment, the light attenuation due to water, phytoplankton, and DOM is considered (see Section 4.1 and the appendix, p.91).
Figure 4.13 shows the vetically integrated annual primary production (averaged over 1999-2009) for the different subareas of interst (note the different color scalings for the different regions). Generally, decreasing the sinking rate of detritus and increasing the fraction attributed to DOM increase primary production. This is observed for all subareas.
The fraction of dead organic matter attributed to DOM has two counteracting effects: On the one hand, since it is included in the parametrization of light attenuation, it directly diminishes the light available for primary production, thus potentially decreasing it. On the other hand, DOM is remineralized ten times fast than detritus in the model. A faster remineralization leads to an increased supply of nutrients fueling primary production. This sensitivity study shows that it is the latter effect dominating the impact of the fraction attributed to DOM on primary production.
If the sinking speed of detritus is reduced, the probability increases that it is remineralized close to where the organic matter died. This means that detritus is more likely to be remineralized where primary production can take place: in the euphotic zone. Like this, a reduced sinking speed of detritus increases primary production by a resupply of nutrients in the upper layers of the ocean. If the sinking speed is higher, remineralization of detritus is more likely to take place in deeper layers of the ocean or even in the sediment. In this case, nutrients get eventually transported upwards by turbulent mixing induced by wind or tides or diffusion.
It has to be pointed out that in the North Sea, Skagerrak and Kattegat, the resulting values in this experiment for vertically integrated annual primary production at a sinking rate of detritus of $5\,\mathrm{md}^{-1}$ and 40% of the dead organic matter attributed to DOM (corresponding to the settings in the baseline run) are up to 15% lower than the ones resulting from the baseline run. Even the highest values observed in the whole parameter range (lowest sinking rate of detritus, highest fraction attributed to DOM) are lower than the values obtained in the baseline run for the northern North Sea, the tidal mixing zone and the Skagerrak, respectively. In contrast, the values both in the Belt Sea and Baltic Sea are up to 10% higher than the values from the baseline run.
This is most likely due to an unsufficient number of model runs during the polynomial chaos expansion experiment leading to greater uncertainties during the interpolation. In this setting,

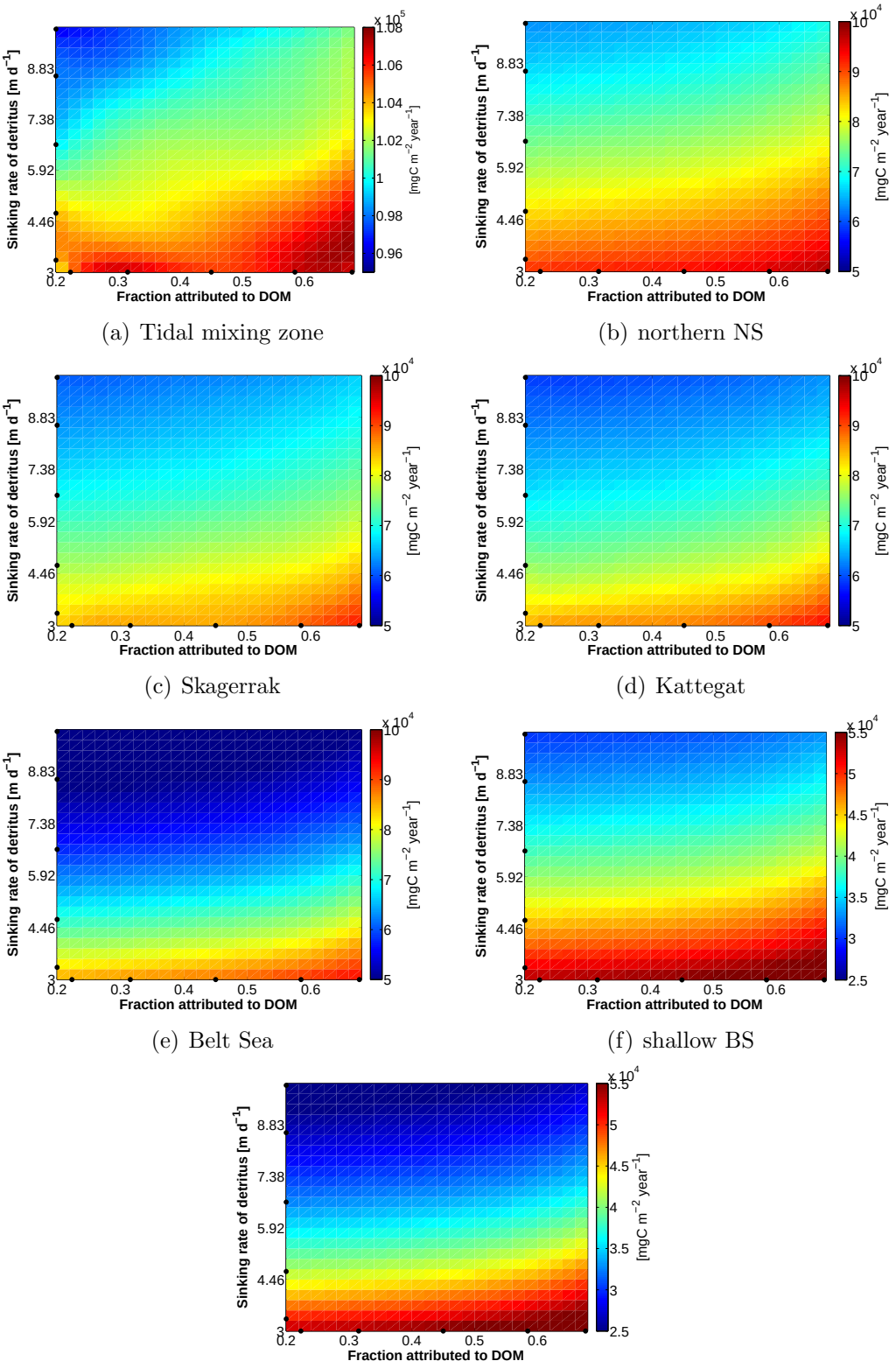

(a) Tidal mixing zone

(b) northern NS

(c) Skagerrak

(d) Kattegat

(e) Belt Sea

(f) shallow BS

(g) Deep BS

Figure 4.13: Results of the polynomial chaos expansion experiment detritus vs. DOM. Vertically integrated annual primary production averaged over the respective area and over 1999-2009 as a function of different sinking rates of detritus and fractions attributed to DOM. Black dots on x- and y-axis correspond to quadrature points at which model is run (see sections 2.5 and 4.1).

the interpolation is obviously not capable to emulate the baseline run very accurately (see also Section 5.3 for a more detailed discussion on the setup of the polynomial chaos expansion). The regions of the strongest misrepresentations of vertically integrated annual primary production are the regions showing the strongest sensitivity to the parametrization of light attenuation (see Figure 4.11), namely the tidal mixing zone and the northern North Sea. Since these regions also show the biggest primary production in general in the model domain, it is understandable that these are the regions most sensitive to any parameter influencing primary production dynamics.

4.5 Resuspension II: With light effect

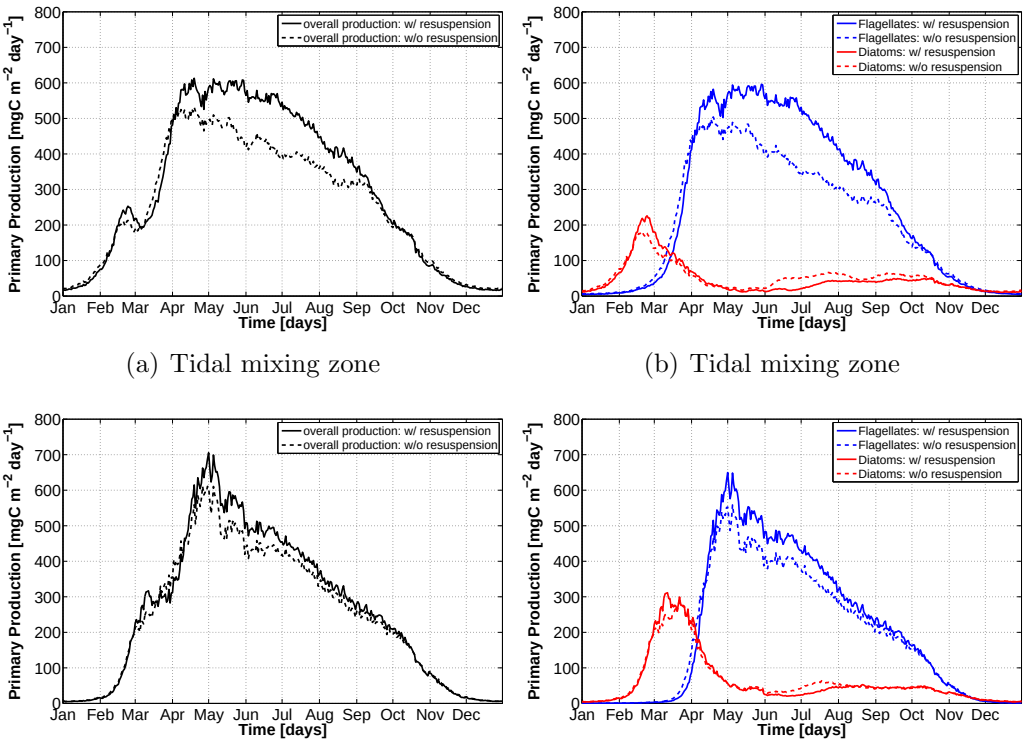

(a) Tidal mixing zone

(b) Tidal mixing zone

(c) Northern NS

(d) Northern NS

Figure 4.14: Average annual cycle of vertically integrated primary production for the tidal mixing zone and the northern NS (see Figure 2.5, p.23) with (solid lines) and without (dashed lines) resuspension when considering water, phytoplankton, detritus, and DOM in light attenuation (run 14 & 15 in Table 4.1, p.49). Overall primary production in the left, production of flagellates and diatoms in the respective right figures. Annual cycle averaged over 1999-2009.

Eventually, the resuspension experiment (see Section 4.1 for the detailed setup of the runs and

4.2.1 for the results) was repeated with the parametrization of light attenuation accounting for attenuation due to water, phytoplankton, DOM, and detritus (run 14 & 15 in Table 4.1). The spatial distribution of changes of vertically integrated annual primary production between the new baseline run and the run without resuspension does show the same patterns as Figure 4.1. It is therefore not shown here. The highest decline in primary production is again observed in the tidal mixing zone with around 45%. The results from the previous resuspension experiment have genrally shown a much higher importance of resuspension for primary production in the North Sea than in the Baltic Sea. Therefore, the presentation of the resulting seasonal cycles of the second experiment will here be restricted to the two regions in the North Sea (tidal mixing zone and northern North Sea). Figure 4.14 shows the averaged seasonal cycles with (solid lines) and without resuspension (dashed lines) when using the before mentioned parametrization of light attenuation accounting for water, phytoplankton, DOM, and detritus. The figures in the upper row show the results for the tidal mixing zone, the ones in the lower row for the northern North Sea. Overall primary production is shown in black (left figures), flagellates (blue) and diatoms (red) are presented in the respective right figures.
Comparing the seasonal cycle in the tidal mixing zone of the first resuspension experiment (Figure 4.3(a)) and this one (activated resuspension), a reduction of the peak of overall primary production from $\approx$700 mg$C$ m^{-2}d^{-1} to $\approx$600 mg$C$ m^{-2}d^{-1} can be observed. Neglecting resuspension slightly increases both overall primary production and flagellate and diatom production in the tidal mixing zone in the beginning of the year (January - April, dashed line above solid line). This can be attributed to the reduced light attenuation due to resuspended matter (detritus). This effect cannot be seen as clearly for the northern North Sea and could not be seen at all in the first resuspension experiment not accounting for DOM and detritus in light attenuation (see Figure 4.3(a)).
The results presented here are spatial averages. The effect of resuspension on primary production by limiting light availability is expected to be larger than presented here on a local scale. To assess this spatial variability, the phytoplankton bloom initiation is analyzed for the run with resuspenion (baseline II in Table 4.1) using the "5% above the median"-definition of bloom initiation as presented in Siegel et al. (2002). The resulting day is then compared to the result of the run neglecting resuspenion and are presented separately for overall primary production, diatoms, flagellates in Figure 4.15.
A latitudinal dependence of the phytoplankton spring bloom initiation is nicely simulated by ECOSMO. The spring bloom starts first in the English Channel, the southern North Sea, and the southern Baltic Sea (February) and propagates northwards with time. As can be seen in Figure 4.14, diatom production (earliest initiation in early January in the North Sea) starts before flagellate production (earliest initiation in late January in the northern Baltic Sea,

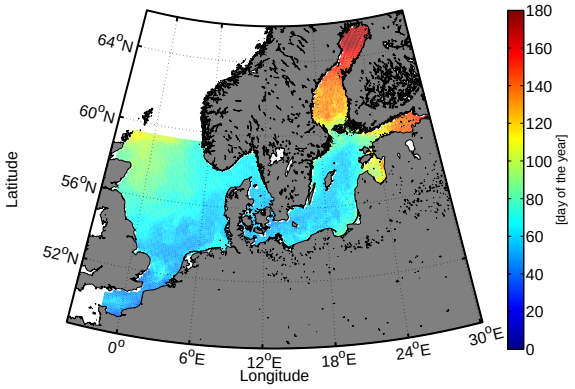

(a) All phytoplankton groups: bloom initiation

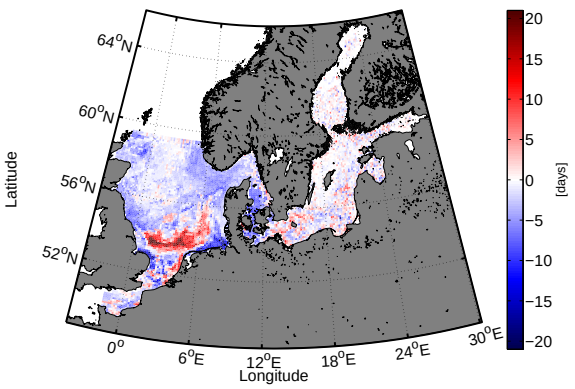

(b) All phytoplankton groups: change in bloom initiation

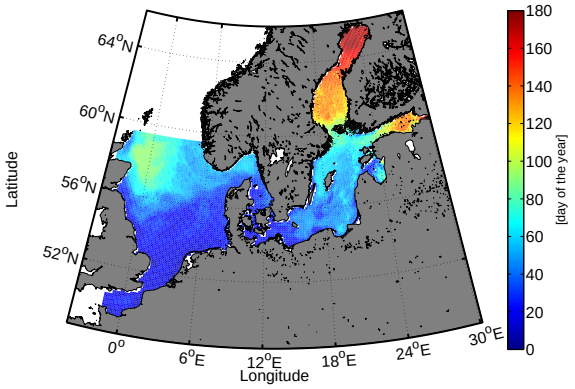

(c) Diatoms: bloom initiation

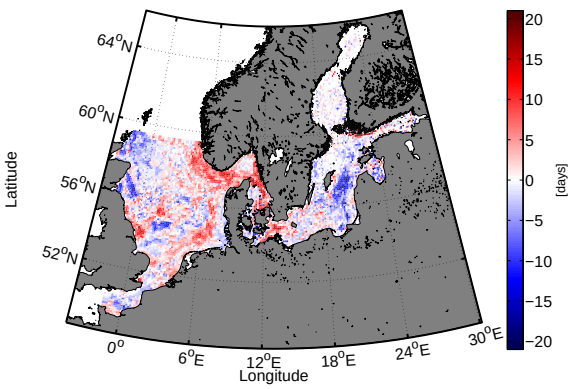

(d) Diatoms: change in bloom initiation

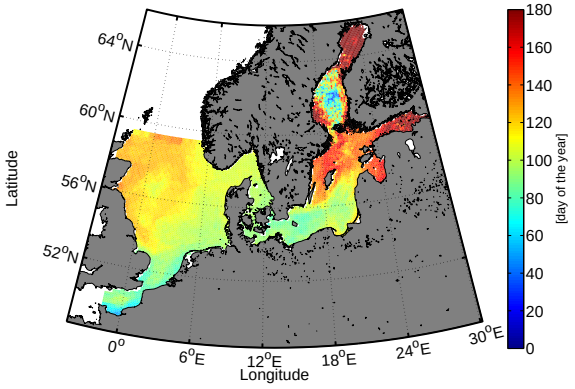

(e) Flagellates: bloom initiation

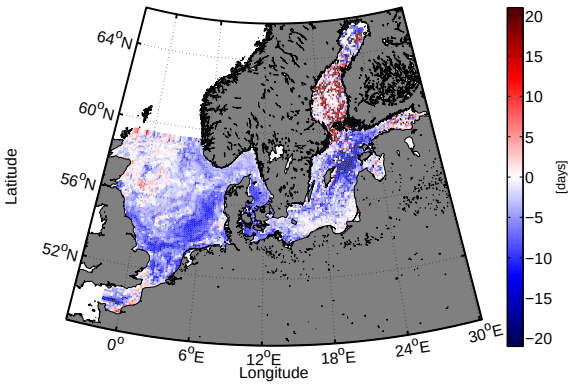

(f) Flagellates: change in bloom initiation

Figure 4.15: Effect of resuspension on phytoplankton bloom initiation. Light attenuation is due to water, phytoplankton, DOM, and detritus. Definition of bloom initiation is described in Section 4.1 (Siegel et al., 2002). Left figures show average day of bloom initiation in baseline run II (see Table 4.1), right figures show change in bloom initiation when subtracting results of this run from run without resuspension (run 40 in Table 4.1). Blue colors denote an earlier bloom initiation in run without resuspension. Results are shown for all phytoplankton groups (top), diatoms (middle), and flagellates (bottom). Results are averaged over 1999-2009.

middle of February in the English Channel, early March in Baltic Proper). The difference between the two varies spatially, but is simulated to be around at least one month.
Phytoplankton bloom initiation changes significantly when neglecting resuspension, but different spatial patterns can be found for the different phytoplankton groups.
Looking at overall primary production (Figure 4.15(b)), an earlier bloom initiation of up to about three weeks can be seen in the coastal areas of the North Sea, but a delay of bloom initiation by up to more than three weeks is simulated in an area south of the Dogger Bank in the southern North Sea. No significant pattern of change in bloom initiation is seen in the Baltic Sea. While diatom bloom initiation is generally rather delayed in the North Sea when neglecting resuspension, the flagellate bloom initiation is observed at two to three weeks earlier in the year in large areas of the North Sea and the Baltic Proper (compare Figure 4.15(d) and Figure 4.15(f))).
At first sight, the results presented in Figure 4.15 suggest that diatom and flagellate production become less separated in time when neglecting resuspension. Looking at Figure 4.14(b) and 4.14(d), it is noticeable that diatom production decreases in the first half of the year, but increases in the second half. If the increase in the second half is larger than the decline in the first half, the bloom initiation date as calculated from the measure used in this study can move to later times in the year even though the time of the spring bloom itself (e.g. the peak production) does not change at all.
This emphasizes the difficulty of the measure of bloom initiation used here to comprehensively capture changes in seasonality and has to be kept in mind when interpreting the results.
Furthermore, all results presented in this chapter are potentially sensitive to the setup of the model, i.e. how resuspended matter is treated. In ECOSMO, all resuspended matter is regarded as detritus even though it might have undergone some transformation in the sediment and might now belong to DOM whose effect on light attenuation was shown to be bigger in this study (see Figure 4.11). This analysis still needs to be done.

5 Discussion & Conclusions

5.1 Sedimentary respiration & Nutrient profiles

The new parametrization implemented into ECOSMO in this study accounts for the anoxic nature of sediments below a thin oxygenated surface layer, leading to anaerobic respiration processes being much more important than they were hypothesized to be in the original parametrization. Constant relative contributions of aerobic respiration, denitrification and other anaerobic respiration pathways to overall organic matter respiration were considered for sediments underlying oxyic, hypoxic, and anoxic bottom water. The new parametrization led to an improved representation of nutrients in the Baltic Sea, but no noticeable change was seen in the North Sea (see Section 3.3). The latter was shown to be insensitive to the relative contributions of the different respiratory pathways while the deep Baltic Sea, being frequently hypoxic or anoxic, was especially sensitive to the chosen fractions when the water column was anoxic.

In this section, the new parametrization of sedimentary respiration of this study is discussed, as well as other approaches of parametrizing respiratory processes. Furthermore, some potential reasons for the remaining disagreement between modeled and observed nutrient profiles are presented.

The newly implemented parametrization of sedimentary respiration is considered an improvement to the original representation of the processes in the model, but has its limitations and weaknesses as well. Amongst these are the following three:

- Only three oxygen regimes are defined. Within each of these, the importance of the different respiratory pathways is constant.
- Differences in respiratory pathways can only arise due to differences in bottom water oxygen concentration.
- Differences in overall respiration rates can only arise due to differences in local bottom water temperature or oxygen concentration.

To fully capture both spatial and temporal variability of sedimentary respiration in the model domain with a single parametrization, a different functional relationship between respiratory

processes in the sediment and the local conditions should be used. It has been mentioned before that bottom water temperature and oxygen concentrations are not the only factors known to contribute to the pathways and rates of organic matter degradation.
The first obvious weak point of the new parametrization is the fact that it only includes three oxygen regimes. A continuous dependency of the importance of different respiratory pathways on bottom water oxygen concentrations is given in Figure 1.2 (p.7). This continuous dependency has to be considered when aiming for a more realistic simulation respiratory processes. In the new parametrization, organic matter in any sediment underlying waters with oxygen concentrations above $63 \cdot 10^{-6}$ mol is degraded through the same partitioning of respiratory pathways. Here, the importance of aerobic respiration is the same, no matter if the bottom water oxygen concentration is just above $63 \cdot 10^{-6}$ mol or $350 \cdot 10^{-6}$ mol. The chosen fraction in this study (22% for oxic settings) seems to overestimate the importance of aerobic respiration for sediments underlying bottom water with oxygen levels below $\approx 200 \cdot 10^{-6}$mol according to Figure 1.2. Optimizing the fractions against observations might further improve the model's ability to correctly simulate the exchange of nutrients at the sediment-water column interface without increasing the complexity of the parametrization, e.g. by including a continuous dependency on bottom water oxygen or even additional variables (see also Section 3.3.3).
In the literature, numerous different approaches to parametrizing respiratory processes in general or denitrification in particular can be found. Besides considering temperature as a factor controlling respiration rates (Daewel and Schrum, 2013; Neumann et al., 2002), a number of other parameters potentially impacting respiratory processes are suggested: bottom water oxygen concentrations (as used in both the original and the new parametrization in ECOSMO) or sediment oxygen demand, bottom water nitrate concentrations, depth, and carbon loadings, hence the amount of organic matter reaching the seafloor.
Middelburg et al. (1996) used a diagenetic model to derive a parametrization of denitrification rates as a function of the carbon loadings, depth, and bottom water oxygen and nitrate concentrations. Instead of bottom water oxygen concentrations, Seitzinger and Giblin (1996) found a linear relationship between sediment oxygen demand and denitrification rates based on available observational data on continental shelves. Since only data for coupled nitrification/denitrification were included, the relationship underestimates denitrification rates and hence removal of fixed nitrogen where direct denitrification is important, e.g. in the Baltic Sea (Jensen et al., 1990). Fennel et al. (2009) re-evaluated existing parametrizations of denitrification rates in the sediment by compiling a new data set of denitrification measurements spanning both freshwater and marine systems. They found sediment oxygen demand to be a much better predictor of denitrification rates than both bottom water oxygen and nitrate con-

centrations, also better than carbon loadings in shallow regions where resuspension is highly important. They pointed out that these conclusions only hold for sediments underlying oxic bottom water, the situation is much more complex in hypoxic or anoxic conditions.
To finally conclude which parametrizations of respiratory processes is most suitable for the North and Baltic Sea, other parametrizations of sedimentary respiration have to be implemented into ECOSMO and their performance assessed in comparison to the current parametrization. Another approach would be to include a full diagenetic model, but this would make ECOSMO significantly more computationally demanding.
Comparing nutrient profiles simulated with ECOSMO to observed ones in the model domain, a disagreement is obvious (see section 3.3).
It has already been pointed out by Daewel and Schrum (2013) that ECOSMO has some deficiencies in correctly simulating nutrient dynamics in the model domain. A wrong representation of sedimentary respiration processes, which influence the exchange of dissolved nutrients and oxygen at the sediment-water column interface, was thought to be one factor contributing to this misrepresentation of nutrient concentrations in the model. The results of this study show that the implementation of a new and more realistic parametrization of sedimentary respiration does improve the performance of the model, but disagreements with the observations remain.
Several potential reasons for the misrepresentation of nutrients are identified in the biogeochemical and physical module of ECOSMO, respectively, and will be discussed in the following.
Tidal flats are not included in ECOSMO and were pointed out as a potential reason for the misrepresenation by Daewel and Schrum (2013). Tidal flats are a source of nutrients, especially phosphate, to the water column (Lillebø et al., 2004; Lübben et al., 2009). Assuming primary production to be phosphate limited in this area in ECOSMO, including tidal flats in the model could lead to an enhanced primary production which in turn reduces nitrate concentrations. This is suggested by the especially large overestimation of nitrate in the tidal mixing zone (see Figure 3.3(a), p.38).
Another reason could be river loads which are too high or too coarse in temporal resolution. If nutrient discharges from rivers were too high in the model, the overestimation of nitrate could be explained.
Uptake in primary production decreases nutrient concentrations. Therefore, the overestimation of nitrate could originate from too little primary production caused by other reasons than the possible phosphate limitation generated due to missing tidal flats. Here, potential sources of error in the parametrization of primary production are, amongst others, a wrong light or nutrient limitation or inappropriate parameter values, such as the maximum growth rates of the different functional groups of phytoplankton. Regarding the parameter values, only using

one constant value in both space and time is probably not adequate for most of the parameters used in the model, e.g. the background light attenuation coefficient which varies in both space and time in the model domain (Kirk, 2011; Urtizberea et al., 2013; Hommersom et al., 2009; Høyerslev, 1988), see also discussion of results of this part of the study in Section 4.3. When comparing ECOSMO to other regional bio-physical models of the North and Baltic Sea or observational data, it is apparent that ECOSMO is at the lower end of simulated/observed primary production values (compare, amongst others, to Conkright et al. (2001), Holt et al. (2014), and to Figure 4 in both Skogen and Moll (2000) and Moll and Radach (2003)). This indicates that too little primary production could well be at least part of the explanation why the model overestimates nitrate concentrations in the model domain, more specifically in the tidal mixing zone.

When looking for processes impacting the exchange of dissolved matter at the sediment-water column interface, two highly important processes taking place at the interface directly are not included in ECOSMO: bioturbation and bioirrigation. Bioturbation refers to the rearrangement of sediment particles by e.g. tube construction or burrowing by benthic organisms (Gruber and Sarmiento, 2006, p. 241). Middelburg and Levin (2009) pointed out that the deposition of carbon to the seafloor through bioturbation can locally be the most important source of carbon. This process is therefore highly important for the benthic-pelagic coupling, but is difficult to parametrize because its importance varies both vertically and horizontally (Gruber and Sarmiento, 2006, p. 242). Tubes contructed by benthic organisms increase the surface area between sediment and bottom water, thus leading to an enhanced diffusive flux of nutrients and oxygen in both directions and to increased mixing of pore water and bottom water (bioirrigation). Bioirrigation can lead to an increased flux of oxygen into the sediment and can bring the oxic/anoxic interface to greater depths, locally increasing the importance of aerobic respiration and coupled nitrification/denitrification in organic matter degradation (Middelburg and Levin, 2009; Laverock et al., 2011). Mermillod-Blondine (2011) pointed out that bioturbation is likely more important in "diffusion-dominated habitats" (such as the Baltic Sea), whereas it is less important in "advection-dominated habitats" (e.g. North Sea). In the North Sea, bioturbation is expected to be highly important in the tidal flats, but advective processes are assumed to be dominant elsewhere.

Another process impacting nutrient concentrations is denitrification in the water column. Studies agree that denitrification is inhibited by the presence of oxygen, but the oxygen threshold for the onset of denitrification is not well known (Peña et al., 2010). In the literature, different thresholds can be found: Eilola et al. (2009) suggest a threshold of $1\,\mathrm{ml}\ O_2\ \mathrm{l}^{-1}$ whereas Seitzinger et al. (2006) give a smaller value of $0.2\,\mathrm{mg}\ O_2\ \mathrm{l}^{-1}$ (corresponds to $\approx 0.14\,\mathrm{ml}\ O_2\ \mathrm{l}^{-1}$) while emphasizing that "completely anoxic conditions are not required". Water column deni-

trification is especially relevant in the Baltic Sea where water column oxygen concentrations frequently fall below either of these two thresholds. A recent study by Dalsgaard et al. (2013) in the Baltic Sea has shown that water column denitrification is locally at least as important for the removal of fixed nitrogen from the system as denitrification in the sediments. In the current version of ECOSMO, water column denitrification only begins when the water becomes anoxic. Therefore, ECOSMO potentially underestimates the removal of nitrate in the water column by denitrification in large areas in the Baltic Sea.
Additional processes not accounted for in ECOSMO, but potentially very relevant for the cycling of nutrients, are anaerobic ammonium oxidation (anammox) (Seitzinger et al., 2006; Dalsgaard et al., 2005) and the retention of ammonium in the sediments by adsorption to sediment particles (Rosenfeld, 1979; van Raaphorst and Malschaert, 1995; Holmboe and Kristensen, 2002).
Besides the aforementioned sources of error in the biogeochemical module of ECOSMO, several potential reasons of the disagreement between simulated and observed nutrient concentrations can be found in the setup or the physical module of the model.
It has already been pointed out that the forcing data (river inputs, atmospheric forcing) could be too coarsely resolved to capture both spatial and temporal variability.
Another reason are the twenty depth levels located at fixed depths in ECOSMO (z-coordinates, thus not terrain following). Two main problems arise from this setup with regard to water mass properties such as nutrient concentrations:

- The depth intervals are increasing with depth. This means that the deepest grid box spans a comparatively large depth interval (230 m). When comparing observational data to model output, this has to be kept in mind. While observational data points are in-situ measurements in both space and time, the simulated water properties are restricted by the resolution of the model in both space (horizontally and vertically) and time. Any property (e.g. nutrient concentrations) is considered homogeneous in each grid box and for each time step.
- The correct representation of downslope flow is prohibited by the fixed depth levels. Downslope flow of a water mass, e.g. in the transition zone between the coastal areas and the deeper basins of the Baltic Sea, cannot take place on a direct path, but occurs on a steplike path following the defined grid boxes. Here, only vertical and horizontal mixing is possible and water properties are not brought as deeply into the water column as they are in reality.

Daewel and Schrum (2013) and Barthel et al. (2012) pointed out that low numerical diffusion in the current version of ECOSMO can lead to underestimated mixing. This implies that also

nutrients are potentially mixed to a smaller extent than they are in reality.
Generally, stratification of the water column (as a proxy for vertical mixing) has a large impact on the vertical distribution of chemical properties. Fennel et al. (2013) showed this for the Gulf of Mexico and bottom water oxygen concentrations. In their model experiment, a stronger decoupling between the upper and lower layers in the water column led to a significant increase in ocurring hypoxia. This underlines the importance of correctly modeling physical properties of a model domain to correctly simultate biogeochemical dynamics.

5.2 Resuspension & Light attenuation

The role of resuspension of particulate matter from the sediment back to the water column was assessed in the second part of the study (see Section 4). It was shown that neglecting resuspension locally reduced vertically integrated annual primary production by up to 45% due to reduced nutrient availability and thereby also significantly impacted surface pH and surface flux of CO_2 (especially in the North Sea). To quantify the effect of resuspended matter on the light availability, a new parametrization resolving light attenuation due to water, phytoplankton, DOM, and detritus was implemented into ECOSMO. Primary production in the North Sea was very sensitive to this new parametrization. Neglecting resuspension in a second resuspension experiment using this newly implemented formulation of light attenuation led to significant changes in the seasonality of primary production.
Similar to ECOSMO, resuspension of sediment particles is parametrized as a function of the bottom shear stress, in both ERGOM, another bio-physical model for the North and Baltic Sea (Maar et al., 2011; Neumann, 2000), and NORWECOM, a bio-physical model for the North Sea only (Skogen et al., 2004). In the literature, regional models can be found which do not explicitly include resuspension, e.g. ECOHAM (Lorkowski et al., 2011; Pätsch and Kühn, 2008) and the bio-physical model by Fennel et al. (2006). These models do not allow sedimentation of particulate matter, but all is remineralized instantaneously when reaching the seafloor. This means that the enhanced nutrient availability caused by resuspension events is accounted for by always immediately releasing all nutrients from remineralization back into the water column.
However, resuspension is presumably not as important for open ocean primary production directly as it has been shown to be for continental shelf production in this study (see Section 4.2. This can be explained by generally greater water depths off the shelves. Therefore, most global climate models (GCMs) do not consider resuspension of sediment particles as a factor impacting organic matter cycling. NorESM (Tjiputra et al., 2013) and the bio-physical module

used by Gröger et al. (2013) - in both models, the biogeochemical part is based on HAMOCC - can be named as examples for GCMs not accounting for resuspension.
Nonetheless, continental shelves constantly interact with the open ocean which is why shelf processes do matter for the open ocean. This has been shown in Giraud et al. (2008) who used a GCM accounting for resuspension of sediment to assess the importance of coastal areas as a source of nutrients for open oceans.
In their study looking at the Northwest European shelf including the North Sea, Gröger et al. (2013) investigated the effect of increasing sea surface temperatures on primary production and carbonate chemistry, specifically carbon absorbtion, without including sediment resuspension in their model (see Ilyina et al. (2013) for their model formulation). They simulate a reduced primary production in the North Sea causing a decline in carbon absorbtion from the atmosphere. This is of high relevance because continental shelves generally play an important role in the uptake of anthropogenic CO_2 via the export of absorbed CO_2 to the open ocean (continental shelf pump).
The results of the study at hand demonstrate the importance of including resuspension of organic matter to correctly simulate primary production and carbonate chemistry in the North Sea. It is therefore expected that including resuspension as a source of nutrients for primary production on shelf seas in the study by Gröger et al. (2013) will change their results significantly.
To draw conclusions from GCMs about the effects of climate change (e.g. effects related to the carbonate chemistry or temperature), processes such as resuspension which might be irrelevant in the open ocean directly, but do matter on continental shelves, must be included in GCMs to correctly simulate interactions between the shelves and the open ocean.
Primary production has been shown to be dependent on the light parametrization in this study (see Section 4.3. To include both suspended (detritus) and dissolved organic matter (DOM) in light attenuation, two assumptions were made whose validity will be further assessed in this section:

1. DOM of oceanic origin dominates in the model domain of ECOSMO.
2. All DOM in ECOSMO is optically active, thus DOM is equal to CDOM.

The results in this part of the study are shown to be sensitive to the model parameters themselves, such as the partitioning of detritus and DOM and the sinking speed of detritus. The values these parameters adopt in ECOSMO are educated guesses from available literature, but detailed sensitivity studies and information about spatial and temporal variability are missing. The sinking speed of detritus is likely to vary in both space and time due to both the size spectrum of phytoplankton in reality and aggregation of particles while sinking. Ideally,

detritus and DOM concentrations have to be validated against observations to understand factors controlling them, but observational data are sparse. As a third assumption for this study, the parameter values used in the baseline run of ECOSMO are hypothesized to be the best to represent biogeochemical dynamics in the model domain.
DOM in the marine environment can originate from various sources (Lübben et al., 2009; Nelson and Siegel, 2013; Twardowski and Donarghay, 2001). It has already been pointed out that ECOSMO only includes DOM of oceanic origin, and that no DOM of terrestrial origin is considered.
Several studies have found a linear relationship between salinity of a water mass and its CDOM concentration (Nelson and Siegel, 2013; Twardowski and Donarghay, 2001). The higher the salinity, the lower the local CDOM concentrations, pointing towards a conservative mixing behavior of prevailing water masses with freshwater runoff. However, this relationship only holds as long as terrestrially originating CDOM is the only source of local CDOM concentrations (Lübben et al., 2009). If runoff from land is assumed constant, deviations from the linear mixing line (non-conservative mixing) can indicate additional sources (CDOM levels higher than suggested by linear relationship) or sinks (CDOM levels lower) of CDOM. Here, the following have to be mentioned (Lübben et al., 2009; Nelson and Siegel, 2013; Twardowski and Donarghay, 2001):

- photodegradation (bleaching of CDOM, which takes place especially in the upper water layers in summer and reduces their absorptive properties)
- microbial production
- decomposition of organic matter
- porewater efflux (e.g. induced by resuspension events)

The study of Lübben et al. (2009) suggests that the first assumption made in this study is nevertheless a valid first guess, at least for the North Sea. They found terrestrial runoff to be a very important source in the southernmost German Bight, but its importance decreased rapidly with only a few kilometers from the coast (see Figure 4 in Lübben et al. (2009)).
However, the aforementioned relationship between salinity and CDOM levels has been found for the Baltic Sea (Nelson and Siegel, 2013, Figure 10) which is known to be dominated by freshwater runoff from land (see Section 1.3, p.9). Due to lower primary production levels, detritus and DOM concentrations are much lower in the Baltic Sea accordingly. Primary production is therefore only to a very small extent sensitive to the introduction of DOM and detritus in light attenuation as seen in Section 4.3. In the Baltic Sea, terrestrial CDOM could be of greater relevance and its consideration in the model is part of future work.

To get a better understanding of the specific light attenuation coefficients of DOM/CDOM and detritus, including its spatial and temporal variability, more studies are needed in both North and Baltic Sea. Hereby, also the importance of suspended particulate matter of terrestrial origin (both organic and inorganic) could be quantified. Furthermore, the contribution of different sources and sinks to total CDOM could be disentangled based on the different optical properties of CDOM of marine and terrestrial origin, respectively (Lübben et al., 2009).
This could then also give a better understanding of the proportion of DOM which is optically active (thus part of the CDOM pool). In the current version of ECOSMO, this fraction is assumed to be 100%.

5.3 An emulator method: polynomial chaos expansion

The emulator method presented in Section 2.5 was used twice in this study: to assess the sensitivity of primary production to the background turbidity attenuation coefficient and the sensitivity of primary production to two parameters controlling the fate of dead organic matter in ECOSMO (see Section 4.3 and 4.4, respectively).
As aforementioned, the results obtained in this study are potentially sensitive to the settings of the polynomial chaos expansion applied in the respective experiment. Due to the scope of this thesis, this sensitivity could not be assessed further, but will only be addressed here.
It has been pointed out already in Section 4.4 that primary production is significantly under-/overestimated by the polynomial chaos expansion setup used for the detritus vs. DOM experiment. In contrast, primary production levels in the first experiment are comparatively accurately simulated suggesting the respective setup to be appropriate.
In their study first applying the same emulator method used in this study to an oceanographic research question, Mattern et al. (2012a) pointed out that results of studies which are only interested in the interpolation in parameter space itself and to a smaller degree in uncertainty estimates from the same, do only to a lesser extent depend on the probability distribution assigned to the uncertain parameter(s). They also showed that the accuracy of the emulation of the output parameter of interest is highly sensitive to the maximum order of polynomials allowed in the setup, hence the number of quadrature points defined.
This suggests that either the number of quadrature points or the resolution of the interpolation in parameter space defined for the experiment is unsufficient to emulate primary production levels of ECOSMO.
Based on the results presented in Mattern et al. (2012a), a higher number of quadrature points (equal to model runs) is very likely to change the quantitative outcome of the experiment, but

not the qualitative results. More work is needed to eventually confirm this hypothesis for this study as well.

5.4 Conclusions & Outlook

Several conclusions can be drawn and open questions can be identified from the study at hand:

- Performing sensitivity studies to assess differences of various parametrizations of sedimentary respiration is crucial for the Baltic Sea. The newly implemented parametrization in this study, which underlined the importance of denitrification and other anaerobic respiration processes, could improve the model's performance, but deficiencies in the simulation of the nutrient cycles remain. A parameter optimization of the newly implemented parametrization could lead to further improvement of the model's performance. The model could be systematically compared to observations by using the emulator method used in this study. How important the consideration of carbon loadings in sedimentary respiration processes is for the Baltic Sea still needs to be assessed.

- It seems to be justified to consider the same parametrization of sedimentary respiration for the whole model domain because in this study, the North Sea does not show any sensitivity to changes in the parametrization of sedimentary respiration.

- Even with the newly implemented parametrization of sedimentary respiration, disagreements remain between modeled and observed nutrient profiles. These have likely to be attributed to other deficiencies in the model. How for example a higher resolution, both horizontally and vertically, affects the results found here is part of future work.

- Primary production in ECOSMO is highly sensitive to the parametrization of light attenuation. More studies are needed to get a better understanding of spatial and temporal variability of the specific light attenuation coefficients of both DOM and detritus. In particular, the dynamics of CDOM must be further studied in the model domain and local sources and sinks must be identified to correctly simulate its effect on light attenuation.

- Again, it seems to be justified to use the same parametrization of light attenuation for both North and Baltic Sea because in this study, the Baltic Sea is much less sensitive to changes in the parametrization. This can be attributed to lower primary production levels and a smaller importance of resuspension. However, including CDOM of terrestrial origin in the model might have a strong impact in this outcome.

- Considering resuspension is crucial when addressing research questions about the carbonate system. Nowadays, this is often neglected in GCMs. This should be corrected due to the strong interaction of coastal areas and open oceans.

References

Artioli, Y., Blackford, J., M.Butenschï¿½n, Holt, J., Wakelin, S., H.Thomas, Borges, A., and Allen, J. The carbonate system in the North Sea: Sensitivity and model validation. *Journal of Marine Systems*, 102–104: 1–13, 2012. doi: 10.1016/j.jmarsys.2012.04.006.

Backhaus, J. and Hainbucher, D. A finite difference general circulation model for shelf seas and its application to low frequency variability on the north European shelf. *Elsevier Oceanography Series*, 45:221–244, 1987. doi: 10.1016/S0422-9894(08)70450-1. In: Three-Dimensional Models of Marine and Estuarine Dynamics.

Balckford, J. and Gilbert, F. pH variability and CO_2 induced acidification in the North Sea. *Journal of Marine Systems*, 64:229–241, 2007. doi: 10.1016/j.jmarsys.2006.03.016.

Barthel, K., Daewel, U., Pushpadas, D., Schrum, C., Årthun, M., and Wehde, H. Resolving frontal structures: on the payoff using a less diffusive but computationally more expensive advection scheme. *Ocean Dynamics*, 62:1457–1470, 2012. doi: 10.1007/s10236-012-0578-9.

Bellerby, R., Olsen, A., Furevik, T., and Anderson, L. *Response of the Surface Ocean CO_2 System in the Nordic Seas and Northern North Atlantic to Climate Change, in The Nordic Seas: An integrated perspective (eds H. Drange, T. Dokken, T. Furevik, R. Gerdes and W. Berger).* American Geophysical Union, Washington, D. C, 2005. doi: 10.1029/158GM13.

Borges, A. and Gypens, N. Carbonate chemistry in the coastal zone responds more strongly to eutrophication than to ocean acidification. *Limnology and Oceanography*, 55(1):346–353, 2010. doi: 10.4319/lo.2010.55.1.0346.

Bozec, Y., Thomas, H., Elkalay, K., and de Baar, H. The continental shelf pump for CO_2 in the North Sea - evidence from summer observations. *Marine Chemistry*, 93:131–147, 2005. doi: 10.1016/j.marchem.2004.07.006.

Brzezinski, M. The Si:C:N ratio of marine diatoms: Interspecific variability and the effect of some environmental variables. *Journal of Phycology*, 21:347–357, 1985. doi: 10.1111/j.0022-3646.1985.00347.x.

Claussen, U., Zevenboom, W., Brockmann, U., Topcu, D., and Bot, P. Assessment of the eutrophication status of transitional, coastal and marine waters within OSPAR. *Hydrobiologia*, 629:49–58, 2009. doi: 10.1007/s10750-009-9763-3.

Colling, A. *Ocean Circulation.* The Open University, 2. Edition, 2001. 286 pp.

Conkright, M., Locarnini, R., Garcia, H., O'Brien, T., Boyer, T., Stephens, C., and Antonov, J. World Ocean Atlas 2001: objective analyses, data statistics and figures (CD-ROM documentation). *National Oceanographic Data Center, Silver Spring, MD*, p.17, 2001.

Daewel, U. and Schrum, C. Simulating long–term dynamics of the coupled North Sea and Baltic Sea ecosystem with ECOSMO II: Model description and validation. *Journal of Marine Systems*, 119–120:30–49, 2013. doi: 10.1016/j.jmarsys.2013.03.008.

Daewel, U., Schrum, C., Primo, R. C., and Thomas, H. Impacts of ecosystem dynamics on carbon cycles of the North Sea and Baltic Sea. *in prep.*, 2014.

Dalsgaard, T., Thamdrup, B., and Canfield, D. Anaerobic ammonium oxidation (anammox) in the marine environment. *Research in Microbiology*, 156:457–464, 2005. doi: 10.1016/j.resmic.2005.01.011.

Dalsgaard, T., Brabandere, L. D., and Hall, P. Denitrification in the water column of the central Baltic Sea. *Geochemica et Cosmochimica Acta*, 106:247–260, 2013. doi: 10.1016/j.gca.2012.12.038.

Davies, A. and Kwong, C. Tidal energy fluxes and dissipation on the European continental shelf. *Journal of Geophysical Research*, 105:969–989, 2000. doi: 10.1029/2000JC900078.

Doney, S. C., Fabry, V. J., Feely, R. A., and Kleypas, J. A. Ocean acidification: The other CO_2 problem. *Annual Review of Marine Sciences*, 1:169–192, 2009. doi: 10.1146/annurev.marine.010908.163834.

Eilola, K., Meier, H., and Almroth, E. On the dynamics of oxygen, phosphorus and cyanobacteria in the Baltic Sea; A model study. *Journal of Marine Systems*, 75:163–184, 2009. doi: 10.1016/j.jmarsys.2008.08.009.

Eilola, K., Hansen, J., Meier, H., Molchanov, M., Ryabchenko, V., and Skogen, M. Eutrophication Status Report of the North Sea, Skagerrak, Kattegat and the Baltic Sea: A model study: Years 2001-2005. Rapport Oceanogrfi 110, SMHI, Norrköping Sweden, 2011. 55pp.

Eilola, K., Hansen, J., Meier, H., Molchanov, M., Ryabchenko, V., and Skogen, M. Eutrophication Status Report of the North Sea, Skagerrak, Kattegat and the Baltic Sea: A model study: Present and future climate. Rapport Oceanogrfi 115, SMHI, Norrköping Sweden, 2013. 38pp.

Fennel, K., Wilkin, J., Levin, J., Moisan, J., O'Reilly, J., and Haidvogel, D. Nitrogen cycling in the Middle Atlantic Bight: Results from a three–dimensional model and implications for the North Atlantic nitrogen budget. *Global Biogeochemical Cycles*, 20:GB3007, 2006. doi: 10.1029/2005GB002456.

Fennel, K., Wilkin, J., Previdi, M., and Najjar, R. Denitrification effects on air–sea CO_2 flux in the coastal ocean: Simulations for the northwest Atlantic. *Geophysical Research Letters*, 35:L24608, 2008. doi: 10.1029/2008GL036147.

Fennel, K., Brady, D., DiToro, D., Fulweiler, R., Gardner, W. S., Giblin, A., McCarthy, M., Rao, A., Seitzinger, S., Thouvenot-Korpoo, M., and Tobias, C. Modeling denitrification in aquatic sediments. *Biogeochemistry*, 93:159–178, 2009. doi: 10.007/s10533-008-9270-z.

Fennel, K., Hu, J., Laurent, A., Marta-Almeida, M., and Hetland, R. Sensitivity of hypoxia predictions for the northern Gulf of Mexico to sediment oxygen consumption and model nesting. *Journal of Geophysical Research: Oceans*, 118:1–13, 2013. doi: 10.1002/jgrc.20077.

Gattuso, J., Frankignoulle, M., and Wollast, R. Carbon and carbonate metabolism in coastal aquatic ecosystems. *Annual Review of Ecology and Systematics*, 29:405–433, 1998. doi: 10.1146/annurev.ecolsys.29.1.405.

Giraud, X., Quéré, C. L., and da Cunha, L. Importance of coastal nutrient supply for global ocean biogeochemistry. *Global Biogeochemical Cycles*, 22(GB2025), 2008. doi: 10.1029/2006GB002717,.

Glud, R. Oxygen dynamics of marine sediments. *Marine Biology Research*, 4:243–289, 2008. doi: 10.1080/17451000801888726.

Gröger, M., Maier-Reimer, E., Mikolajewicz, U., Moll, A., and Sein, D. NW European shelf under climate warming: implications for open ocean-shelf exchange, primary production, and carbon absorption. *Biogeosciences*, 10:3767–3792, 2013. doi: 10.5194/bg-10-3767-2013.

Gruber, N. *Nitrogen in the Marine Environment*, volume 21. Elsevier, 2nd edition, 2008. The marine nitrogen cycle: overview and challenges, pp. 1–50.

Gruber, N. and Sarmiento, J. *Ocean Biogeochemical Dynamics*. Princeton University Press, 1st edition, 2006. 503 pp.

Heip, C., Goosen, N., Herman, P., Kromkamp, J., Middelburg, J., and Soetaert, K. Production and consumption of biological particles in temperate tidal estuaries. *Oceanography and Marine Biology - an Annual Review*, 33:1–149, 1995.

HELCOM. Helcom map and data service. http://helcom.fi/baltic-sea-trends/data-maps/helcom-map-and-data-service, 2014. Website, called up on: 12.05.2014.

Henson, S., Cole, H., Beaulieu, C., and Yool, A. The impact of global warming on seasonality of ocean primary production. *Biogeosciences*, 10:4357–4369, 2013. doi: 10.5194/bg-10-4357-2013.

Hjalmarsson, S., Wesslander, K., Anderson, L., Omstedt, A., Perttilï¿½, M., and Mintrop, L. Distribution, long–term development and mass balance calculation of total alkalinity in the Baltic Sea. *Continental Shelf Research*, 28:593–601, 2008.

Holmboe, N. and Kristensen, E. Ammonium adsorption in sediments of a tropical mangrove forest (Thailand) and a temperate Wadden Sea area (Denmark). *Wetland Ecology and Management*, 10:453–460, 2002. doi: 10.1023/A:1021301918564.

Holt, J., Schrum, C., Cannaby, H., Daewel, U., Allen, I., Artioli, Y., Bopp, L., Butenschon, M., Fach, B., Harle, J., Pushpadas, D., Salihoglu, B., and Wakelin, S. Physical processes mediating climate change impacts on regional sea ecosystems. *Biogeosciences Diescussion*, 11:1909–1975, 2014. doi: 10.5194/bgd-11-1909-2014.

Hommersom, A., Peters, S., Wernand, M., and de Boer, J. Spatial and temporal variability in bio-optical properties of the Wadden Sea. *Estaurine, Coastal and Shelf Sciences*, 83:360–370, 2009. doi: 10.1016/j.ecss.2009.03.042.

Høyerslev, N. Natural occurrences and optical effects of gelbstoff. Technical Report 50, University of Copenhagen (Institute of Physical Oceanography), 1988.

ICES. ICES - Oceanography: CTD and Bottle data. http://ocean.ices.dk/HydChem/, 2014. Website, called up on: 06.04.2014.

Ilyina, T., Six, K., Segschneider, J., Maier-Reimer, E., Li, H., and Nuñez-Riboni, I. Global ocean biogeochemistry model HAMOCC: Model architecture and and performance as component of the MPI-Earth system model in different CMIP5 experimental realizations. *Journal of Advances in Modeling Earth Systems*, 5: 287–315, 2013. doi: 10.1029/2012MS000178.

Ingri, N., Kakolowicz, W., Sillén, L., and Warnqvist, B. High-speed computers as a supplement to graphical methods - V: HALTAFALL, a general program for calculating the composition of equilibrium mixtures. *Talanta*, 14:1261–1286, 1967. doi: 10.1016/0039-9140(67)80203-0.

Jähne, B., Münnich, K., Bösinger, R., Dutzi, A., Huber, W., and Libner, P. On the Parameters Influencing Air-Water Gas Exchange. *Journal of Geophysical Research*, 92(C2):1937–1949, 1987. doi: 10.1029/JC092iC02p01937.

Janssen, F., Schrum, C., and Backhaus, J. A climatological data set of temperature and salinity for the Baltic Sea and North Sea. *Deutsche Hydrographische Zeitschrift*, 51:5–245, 1999. doi: 10.1007/BF02933676.

Jensen, M., Lomstein, E., and Sørensen, J. Benthic NH_4^+ and NO_3^- flux following sedimentation of a spring phytoplankton bloom in Aarhus Bight, Denmark. *Marine Ecology Progress Series*, 61:87–96, 1990.

Jilbert, T., Slomp, C., Gustaffson, B., and Boer, W. Beyond the fe–p–redox connection: preferential regeneration of phosphorus from organic matter as a key control on Baltic Sea nutrient cycles. *Biogeosciences*, 8: 1699–1720, 2011. doi: 10.5194/bg-8-1699-2011.

Kirk, J. *Light and Photosynthesis in Aquatic Ecosystems*. Cambridge University Press, 3rd edition, 2011. 662 pp.

Laverock, B., Gilbert, J., Tait, K., Osborn, A., and Widdicombe, S. Bioturbation: impact on the marine nitrogen cycle. *Biochemical Society Transactions*, 39:315–320, 2011. doi: 10.1042/BST0390315.

Lee, K., Tong, L., Millero, F. J., Sabine, C., Dickson, A., C.Goyet, Park, G.-H., Wanninkhof, R., Feely, R., and Key, R. Global relationships of total alkalinity with salinity and temperature in surface waters of the world's oceans. *Geophysical Research Letters*, 33:LI9605, 2006. doi: 10.1029/2006GL027207.

Lillebø, A., Neto, J., Flindt, M., Marques, J., and Pardal, M. Phosphorous dynamics in a temperate intertidal estuary. *Estuarine, Coastal and Shelf Science*, 61:101–109, 2004. doi: 10.1016/j.resmic.2005.01.011.

Lohse, L., Malschaert, J., Slomp, C., Helder, W., and van Raaphorst, W. Nitrogen cycling in North Sea sediments: interaction of denitrification and nitrification in offshore and coastal areas. *Marine Ecology Progress Series*, 101:283–296, 1993.

Lorkowski, I., Pätsch, J., Moll, A., and Kühn, W. Interannual variability of carbon fluxes in the north sea from 1976 to 2006 - Competing effects of abiotic and biotic drivers on the gas–exchange of CO_2. *Estuarine, Coastal and Shelf Science*, 100:38–57, 2011. doi: 10.1016/j.ecss.2011.11.037.

Lübben, A., Dellwig, O., Koch, S., Beck, M., Badewien, T., Fischer, S., and Reuter, R. Distributions and characteristics of dissolved organic matter in temperate coastal waters (Southern North Sea). *Ocean Dynamics*, 59:263–275, 2009. doi: 10.1007/s10236-009-0181-x.

Lund-Hansen, L. Diffuse attenuation coefficients $k_d(par)$ at the estuarine North Sea - Baltic Sea transition: time-series, partitioning, absorption and scattering. *Estuarine, Coastal and Shelf Science*, 61:251–259, 2004. doi: 10.1016/j.ecss.2004.05.004.

Maar, M., Møller, E. F., Larsen, J., Madsen, K. S., Wan, Z., She, J., Jonasson, L., and Neumann, T. Ecosystem modelling across a salinity gradient from the North Sea to the Baltic Sea. *Ecological Modelling*, 222:1696–1711, 2011. doi: 10.1016/j.ecolmodel.2011.03.006.

MATLAB. MATLAB Documentation. http://www.mathworks.de/products/matlab/description1.html, 2013. Website, called up on: 06.03.2013.

Mattern, J., Fennel, K., and Dowd, M. Estimating time–dependent parameters for a biological ocean model using an emulator approach. *Journal of Marine Systems*, 96–97:32–47, 2012a. doi: 10.1016/j.jmarsys.2012.01.015.

Mattern, J., Fennel, K., and Dowd, M. Sensitivity and uncertainty analysis of model hypoxia estimates for Texas–Louisiana shelf. *Journal of Geophysical Research: Oceans*, 118:1316–1332, 2012b. doi: 10.1002/jgrc.20130.

Mattila, J. and Kankaanpää, H. Estimation of recent sediment accumulation rates in the Baltic Sea using artificial radionuclides ^{137}Cs and ^{239,240}Pu as time markers. *Boreal Environment Research*, 11:95–107, 2006.

Mermillod-Blondine, F. The functional significance of bioturbation and biodeposition on biogeochemical processes at the water-sediment interface in freshwater and marine ecosystems. *Journal of the North American Benthological Society*, 30:770–778, 2011. doi: 10.1899/10-121.1.

Michaelis, L. and Menten, M. Die Kinetik der Invertinwirkung. *Biochemische Zeitschrift: Beiträge zur chemischen Physiologie und Pathologie*, 49:333–369, 1913.

Middelburg, J. and Levin, L. Coastal hypoxia and sediment biogeochemistry. *Biogeosciences*, 6:1273–1293, 2009. doi: 10.5194/bg–6–1273–2009.

Middelburg, J. and Soetaert, K. Chapter 11: The role of sediments in shelf ecosystem dynamics. *The Sea*, 13: 353–373, 2004.

Middelburg, J., Soetaert, K., Herman, P., and C.H.R.Heip. Denitrification in marine sediments: A model study. *Global Biogeochemical cycles*, 10:661–673, 1996. doi: 10.1029/96GB02562.

Moll, A. and Radach, G. Review of three–dimensional ecological modelling related to the North Sea shelf system, Part I: models and their results. *Progress in Oceanography*, 57:175–217, 2003. doi: 10.1016/S0079–6611(03)00067–3.

NCEP/NCAR. The NCEP/NCAR Reanalysis Project. http://www.esrl.noaa.gov/psd/data/reanalysis/reanalysis.shtml, 2013. Website, called up on: 23.08.2013.

Nelson, N. and Siegel, D. The global distribution and dynamics of chromophoric dissolved organic matter. *Annual Review of Marine Science*, pages 447–476, 2013. doi: 10.1146/annurev-marine-120710-100751.

Neumann, T. Towards a 3D–ecosytem model of the Baltic Sea. *Journal of Marine Systems*, 25:405–419, 2000. doi: 10.1016/S0924–7963(00)00030–0.

Neumann, T., Fennel, W., and Kremp, C. Experimental simulations with an ecosystem model of the Baltic Sea: A nutrient load reduction experiment. *Global Biogeochemical Cycles*, 16(3), 2002. doi: 10.1029/2001GB001450.

Parsons, T., Takahashi, M., and Hargrave, B. *Biological Oceanographic Processes (Pergamon International Library of Science, Technology, Engin)*. Pergamon, 3rd edition, 1984. 344 pp.

Pätsch, J. and Kühn, W. Nitrogen and carbon cycling in the North Sea and exchange with the North Atlantic - A model study. Part I. Nitrogen budgets and fluxes. *Continental Shelf Research*, 28:767–787, 2008. doi: 10.1016/j.csr.2007.12.013.

Peña, M., Katsev, S., Oguz, T., and Gilbert, D. Modeling dissolved oxygen dynamics and hypoxia. *Biogeosciences*, 7:933–957, 2010. doi: 10.5194/bg–7–933–2010.

Porter, E., Mason, R., and Sanford, L. Effect of tidal resuspension on benthic-pelagic coupling in an experimental ecosystem study. *Marine Ecology Progress Series*, 413:33–53, 2010. doi: 10.3354/meps08709.

Redfield, A. On the Proportions of Organic Derivations in Sea Water and their Relation to the Composition of Plankton. *James Johnston Memorial Volume*, pages 163–184, 1934.

Rodhe, J., Tett, P., and Wulf, F. Chapter 26 . The Baltic and North Seas: A regional review of some important physical–chemical–biological interaction processes(20, S). *The Sea*, 14 B:1029–1072, 2006. Harvard University Press.

Rosenfeld, J. Ammonium adsorption in nearshore anoxic sediments. *Limnology and Oceanography*, 24(2): 356–364, 1979. doi: 10.4319/lo.1979.24.2.0356.

Schallenberg, M. and Burns, C. Effects of sediment resuspension on phytoplankton production: teasing apart the influence of light, nutrients and algal entrainment. *Freshwater Biology*, 49:143–159, 2004. doi: 10.1046/j.1365-2426.2003.01172.x.

Schrum, C. and Backhaus, J. Sensitivity of atmosphere–ocean heat exchange and heat content in the North Sea and Baltic Sea. *Tellus*, 51A:526–549, 1999.

Schrum, C., Siegismund, F., and John, M. S. Decadal variations in the stratification and circulation patterns of the North Sea. Are the 1990s unusual? *ICES Marine Science Symposia*, 219:121–131, 2003.

Schrum, C., Alekseeva, I., and John, M. S. Development of a coupled physical–biological ecosystem model ECOSMO, Part I: Model description and validation for the North Sea. *Journal of Marine Systems*, 61: 79–99, 2006. doi: 10.1016/j.jmarsys.2006.01.005.

Seitzinger, S., Harrison, J., Bohlke, J., Bouwman, A., Lowrance, R., Petersoon, B., Tobias, C., and van Drecht, G. Denitrification across landscapes and waterscapes: A synthesis. *Ecological Applications*, 16:2064–2090, 2006. doi: 10.1890/1051-0761(2006)016[2064:DALAWA]2.0.CO;2.

Seitzinger, S. and Giblin, A. Estimating denitrification in North Atlantic continental shelf sediments. *Biogeochemistry*, 35:235–260, 1996.

Siegel, D., Doney, S., and Yoder, J. The North Atlantic spring phytoplankton bloom and Sverdrup's critical depth hypothesis. *Science*, 296:730–733, 2002. doi: 10.1126/science.1069174.

Skogen, M. and Moll, A. Interannual variability of the North Sea primary production: comparison from two model studies. *Continental Shelf Research*, 20:129–151, 2000. doi: 10.1016/S0278-4343(99)00069-2.

Skogen, M., Søiland, H., and Svendsen, E. Effects of changing nutrint loads to the North Sea. *Journal of Marine Systems*, 46:23–38, 2004. doi: 10.1016/j.jmarsys.2003.11.013.

Soetaert, K., Middelburg, J., Herman, P., and Buis, K. On the coupling of benthic and pelagic biogeochemical models. *Earth–Science Reviews*, 51:173–201, 2000. doi: 10.1016/S0012-8252(00)00004-0.

Stedmon, C., Markager, S., and Kaas, H. Optical Properties and Signatures of Chromophoric Dissolved Organic Matter (CDOM) in Danish Coastal Waters. *Estaurine, Coastal and Shelf Science*, 51:267–278, 2000. doi: 10.1006/ecss.2000.0645.

Stigebrandt, A. and Wulff, F. A model for the dynamics of nutrients and oxygen in the Baltic proper. *Journal of Marine Research*, 45:729–759, 1987.

Taylor, K. Summarizing multiple aspects of model performance in a single diagram. *Journal of Geophysical Research*, 106:7183–7192, 2001. doi: 10.1029/2000JD900719.

Thomas, H., Bozec, Y., Elkalay, K., de Baar, H., Borges, A., and Schiettecatte, L.-S. Controls of the surface water partial pressure of CO_2 in the North Sea. *Biogeosciences*, 2:323–334, 2005. doi: 10.5194/bg-2-323-2005.

Thorpe, S. *An Introduction to Ocean Turbulence*. Cambridge University Press, 2007. 240 pp.

Tian, T., Merico, A., Su, J., Staneva, J., Wiltshire, K., and Wirtz, K. Importance of resuspended sediment dynamics for the phytoplankton spring bloom in a coastal marine ecosystem. *Journal of Sea Research*, 62: 214–228, 2009. doi: 10.1016/j.seares.2009.04.001.

Tjiputra, J., Roelandt, C., Bentsen, M., Lawrence, D., Lorentzen, T., Schwinger, J., Seland, Ø., and Heinze, C. Evaluation of the carbon cycle components in the Norwegian Earth System Model (NorESM). *Geoscientific Model Development*, 6:301–325, 2013. doi: 10.5194/gmd-6-301-2013.

Treude, T. *Cellular Origin, Life in Extreme Habitats and Astrobiology: Anoxia*, volume 21. Springer, 2012. Part I: General Introduction: Biogeochemical Reactions in Marine Sediments Underlying Anoxic Water Bodies.

Turrell, W. R., Slesser, G., Payne, R., Adams, R. D., and Gillibrand, P. A. Hydrography of the East Shetland Basin in relation to decadal North Sea variability Hydrography of the East Shetland Basin. *ICES Journal of Marine Science*, 53:899–916, 1996.

Twardowski, M. and Donarghay, P. Separating in situ and terrigenous sources of absorption by dissolved materials in coastal waters. *Journal of Geophysical Research*, 106(C2):2545–2560, 2001. doi: 10.1029/1999JC000039.

Urtizberea, A., Depont, N., Rosland, R., and Aksnes, D. Sensitivity of euphotic zone properties to CDOM variations in marine ecosystem models. *Ecological modelling*, 256:16–22, 2013. doi: 10.1016/j.ecolmodel.2013.02.010.

van Raaphorst, W. and Malschaert, J. Ammonium adsorption in superficial North Sea sediments. *Continental Shelf Research*, 16(11):1415–1435, 1995. doi: 10.1016/0278-4343(95)00081-X.

van Raaphorst, W., Kloosterhuis, H., Cramer, A., and Bakker, K. Nutrient early diagenesis in the sandy sediments of the Dogger Bank area, North Sea: pore wate results. *Netherlands Journal of Sea Research*, 26 (1):25–52, 1990.

Vihma, T. and Haapala, J. Geophysics of sea ice in the Baltic Sea: A review. *Progress in Oceanography*, 80: 129–148, 2009.

von Liebig, J. and Playfair, L. *Chemistry in Its Application to Agriculture and Physiology.* T. B. Peterson, Philadelphia, 1847.

Wanninkhof, R. Relationship Between Wind Speed and Gas Exchange Over the Ocean. *Journal of Geophysical Research*, 97(C5):7373–7382, 1992. doi: 10.1029/92JC00188.

Wiener, N. The Homogeneous Chaos. *American Journal of Mathematics*, 60:897–936, 1938.

Winsor, P., Rodhe, J., and Omstedt, A. Baltic Sea ocean climate: an analysis of 100 yr of hydrographic data with focus on the freshwater budget. *Climate Research*, 18:5–15, 2001.

Wright, J. *Seawater: its composition, properties and behaviour.* The Open University, 2. Edition, 1995. 168 pp.

Wright, J., Colling, A., Park, D., and Brown, E. *Waves, tides and shallow water processes.* The Open University, 2. Edition, 1999. 227 pp.

Wulff, F., Sokolov, A., and Savchuk, O. *Nest - a decision support system for management of the Baltic Sea. A user manual.* Technical Report No. 10, Baltic Nest Institute, Stockholm University Baltic Sea Centre, 2008. http://apps.nest.su.se/nest/ (14.02.2014).

Zeebe, R. and Wolf-Gladrow, D. *Encyclopedia of Paleoclimatology and Ancient Environments (Chapter: Carbn dioxide, dissolved (ocean)).* Kluwer Academic Publishers, Earth Science Series, 2008. edited by V. Gornitz.

Appendix A: Detritus versus DOM - additional information

The fate of dead organic matter in ECOSMO is dependent on a number of model parameters, amongst which a few are of special interest for this sensitivity study:

- partitioning of detritus and DOM (Det/DOM, in baseline run: 0.6/0.4)
- factor accounting for increased remineralization rates of DOM compared to detritus (remin. factor, in baseline run: 10)
- sinking rate of detritus (sinking rate, in baseline run: $5\,\mathrm{m\ d^{-1}}$)

Due to computational restraints, the maximum possible number of uncertain variables for the emulator method presented in section 2.5 is two for this study. The two of the above mentioned parameters the average integrated annual primary prouction (averaged over 1999-2009) is most sensitive to are chosen for the polynomial chaos expansion experiment. To identify them, six model runs are performed as described in Table 1. The percentaged change in average integrated annual primary production for the different runs compared to the respective baseline runs using the values for the parameters in question as presented above is calculated for the different areas in the model domain (see Figure 2.5) and averaged over the whole mdoel domain.
To assess whether the choice of parameters is sensitive to the parametrization of light attenuation, both the parametrization only resolving light attenuation due to a background turbidity and phytoplankton and the parametrization considering water, phytoplankton, and DOM are tested. The detailed results are presented in Table 2. T
For both parametrizations of light attenuation, the two parameters primary production is most sensitive to are the partitioning of detritus and DOM and the sinking rate of detritus. These two are the uncertain parameters varied during the polynomial chaos expansion performed here. In the following, only the parametrization of light attenuation considering pure water, phytoplankton, and DOM as presented in section 4.1 is used.

Table 1: Model runs performed assessing the sensitivity of primary production to three parameters controlling the dynamics of dead organic matter in ECOSMO, detritus and DOM. Two different parametrizations of light attenuation are used. See section 4.1 and 2.4.3 (p.49 and p.30, respectively) for more details.

	k_{bg} / k_w $[m^{-1}]$	k_p $[m^2(mmolC)^{-1}]$	k_{DOM} $[m^2(gC)^{-1}]$	**Changed parameter**
1	0.03	0.2	0.29	DET/DOM: 0.4/0.6
2	0.03	0.2	0.29	remin. factor: 20
3	0.03	0.2	0.29	sinking rate: $10\,md^{-1}$
4	0.05	0.2	-	DET/DOM: 0.4/0.6
5	0.05	0.2	-	remin. factor: 20
6	0.05	0.2	-	sinking rate: $10\,md^{-1}$

Table 2: Parameter identification for sensitivity experiment: Detritus vs. DOM. Runs 1-6 are described in Table 1. Run 1-3 are with DOM in the parametrization of light attenuation (see Figure 1(a)), 4-6 without (see Figure 1(b)). Changes compared to respective baseline run are given in % for vertically integrated averaged annual primary production for the different areas and for the whole model domain (last column). Biggest changes are observed for the partitioning of detritus and DOM (run 1 & 4) and the sinking rate of detritus (run 3 & 6).

Run	**Tidal**	**NNS**	**Skag.**	**Katt.**	**Belt Sea**	**deep BS**	**shallow BS**	**All regions**
1	2.25	13.16	9.17	11.68	31.59	36.14	28.08	**18.87**
2	5.38	4.31	5.59	4.49	1.87	1.49	1.92	3.58
3	-2.49	-4.34	-4.23	-4.12	-6.31	-5.99	-4.42	**-4.56**
4	6.22	20.10	20.69	22.38	37.08	43.49	30.48	**25.78**
5	0.10	0.56	0.73	1.10	0.78	0.09	0.69	0.58
6	-2.71	-5.08	-5.43	4.51	-6.13	-6.51	4.80	**-5.02**

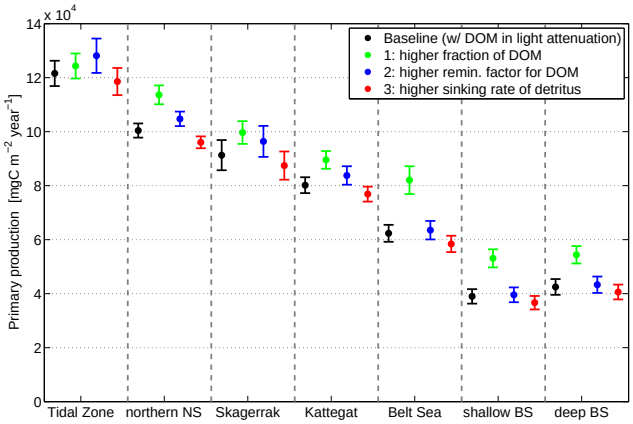

(a)

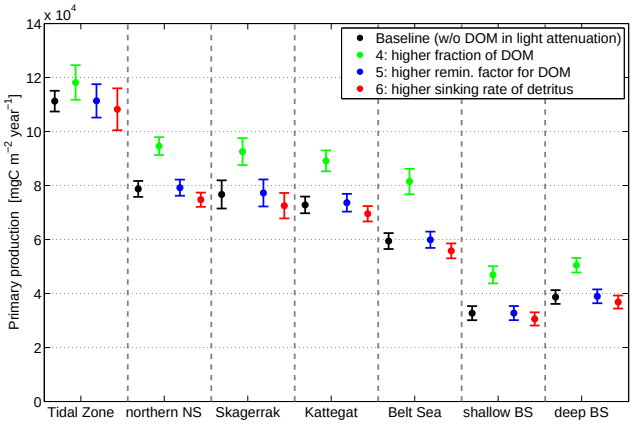

(b)

Figure 1: Parameter identification for sensitivity experiment: Detritus vs. DOM. Vertically integrated annual primary production in the different subareas. Values are averaged over 1999-2009. Errorbars denote standard deviation over the same period.

Appendix B: Resuspension experiment - additional figures

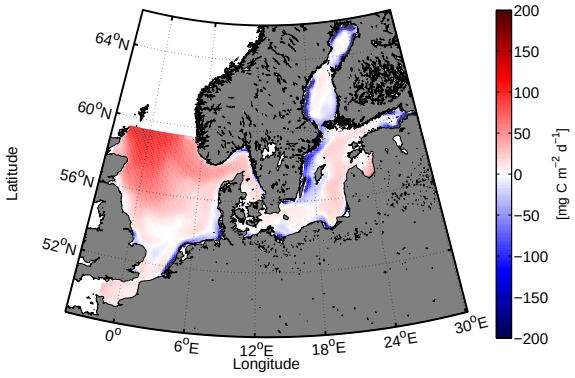

(a) baseline run

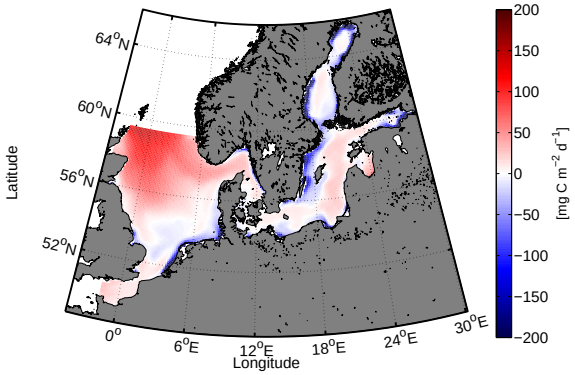

(b) run w/o resuspension

Figure 2: Annually averaged daily surface flux of CO_2 in the model domain averaged over 1999-2009. Figure 2(a) shows results of the baseline run (run 1 in table 4.1), figure 2(b) the result of the run without resuspension (run 2 in table 4.1). Blue color indicates a flux of CO_2 from the ocean to the atmosphere, red vice versa. Results are averaged over 1999-2009.

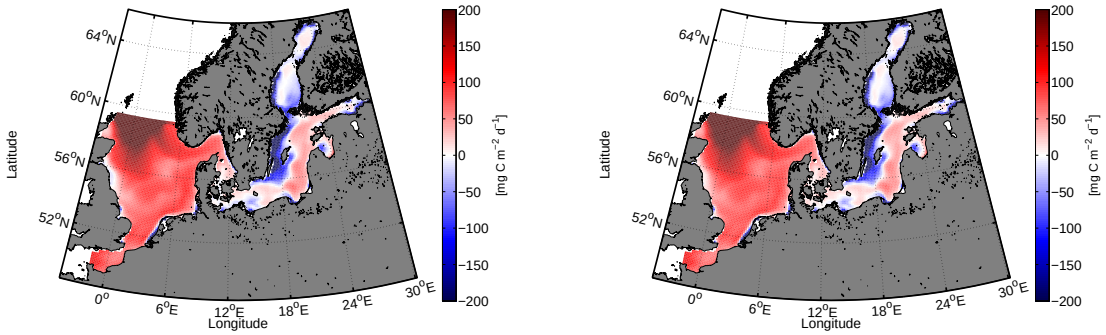

(a) Winter (baseline run)

(b) Winter (run w/o resuspension)

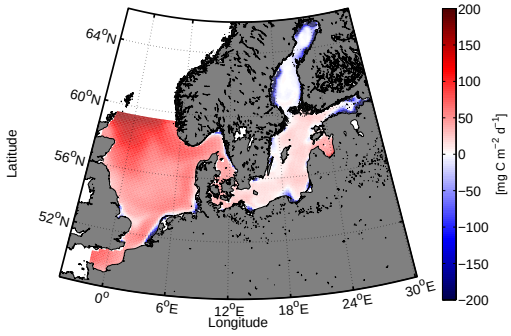

(c) Spring (baseline run)

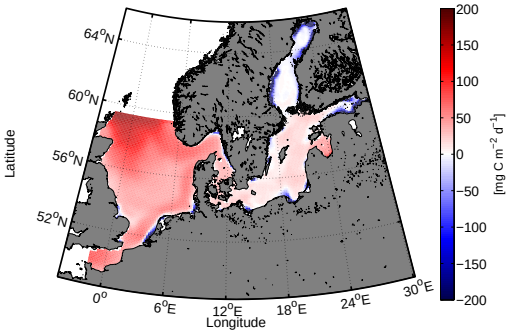

(d) Spring (run w/o resuspension)

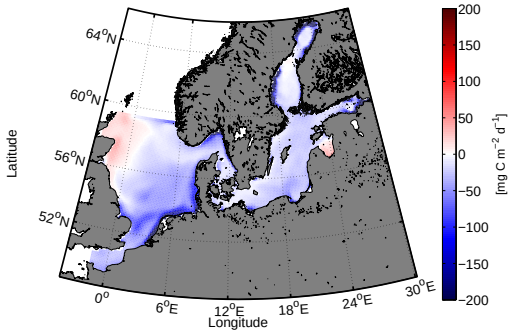

(e) Summer (baseline run)

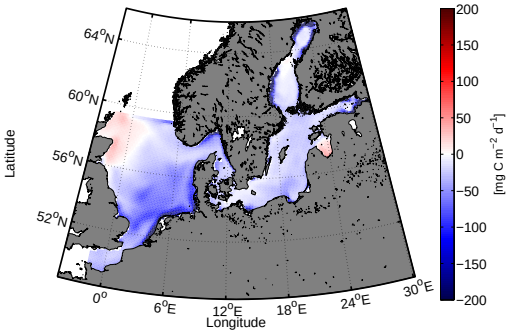

(f) Summer (run w/o resuspension)

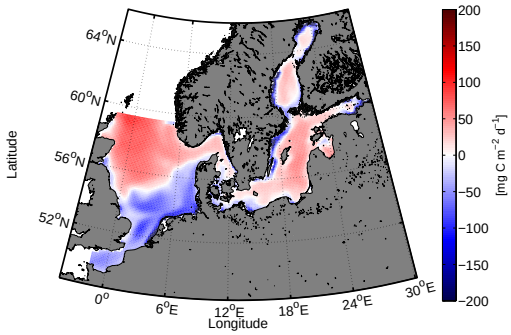

(g) Autumn (baseline run)

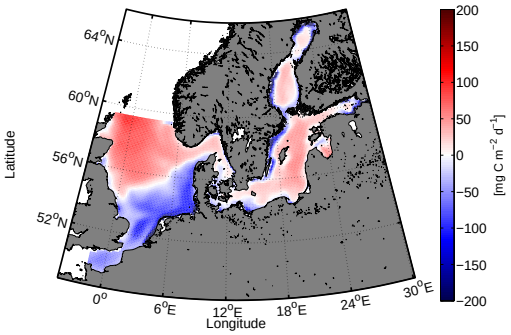

(h) Autumn (run w/o resuspension)

Figure 3: Daily surface flux of CO_2 in the model domain averaged over the respective season and over 1999-2009. The figures in the left column are the results from the baseline run (active resuspension), the figures in the right those from the run with neglected resuspension. Blue color indicates a flux of CO_2 from the ocean to the atmosphere, red vice versa. Months included for each season: Winter = DJF, spring = MAM, summer = JJA, autumn = SON.

Appendix C: Model equations

In this chapter, the model equations of the biogeochemical module of ECOSMO are presented. The equations correspond to the version of ECOSMO presented in Daewel and Schrum (2013). Changes applied to ECOSMO in this study are applied to the equations presented here and are presented in the main body of this thesis.
To activate/deactivate certain processes under the absence or presence of bottom water oxygen or nitrate, θ is defined as follows:

$$\theta(x) = \begin{cases} 1 \;\; if \; x > 0 \\ 0 \;\; if \; x \leq 0 \end{cases} \tag{1}$$

Primary & Secondary production

The reaction term R_C (see Equation 2.2, p.18) for the three phytoplankton groups P_l, P_s and P_{bg} (see Table 2.1, p.18) is a function of production, grazing by zooplankton (Z_l and Z_s) and mortality following:

$$R_{P_j} = \sigma_j \Psi_{P_j} C_{P_j} - \sum_{i=1}^{2} G_i P_j C_{Z_i} - m_{P_j} C_{P_j} \tag{2}$$

Here, $j = 1, 2, 3$ and $P_{1,2,3}$ denote the three phytoplankton groups $P_{l,s,bg}$ and $Z_{1,2}$ the two zooplankton groups $Z_{l,s}$ as presented in Table 2.1 (p.18).
Primary production ($\Psi_{P_{1,2,3}}$) in ECOSMO is a function of the maximum growth rate ($\sigma_{P_{1,2,3}}$) of the respective phytoplankton group and is additionally limited by either light or nutrients. Its parametrization is based on Liebig's law (Parsons et al., 1984; von Liebig and Playfair,

1847). The equations are:

$$\Psi_{P_1} = \Psi_{P_1}(PAR, NH_4, NO_3, PO_4) \qquad = min(\alpha(I), \beta_N, \beta_P) \tag{3}$$

$$\Psi_{P_2} = \Psi_{P_2}(PAR, NH_4, NO_3, PO_4, SiO_2) = min(\alpha(I), \beta_N, \beta_P, \beta_{Si}) \tag{4}$$

$$\Psi_{P_3} = \begin{cases} \Psi_{P_3}(PAR, PO_4) & = min(\alpha(I), \beta_P)\big|_{z=1} \\ \Psi_{P_3}(PAR, NH_4, NO_3, PO_4) & = min(\alpha(I), \beta_P, \beta_N)\big|_{z>1} \end{cases} \tag{5}$$

$$\Psi_{P_3} = \begin{cases} \Psi_{P_3} \forall\ Salinity > 11.5\ \&\ I_s(x,y) > 120\,\mathrm{W\,m^{-2}} \\ 0 \end{cases} \tag{6}$$

including terms for the light limitation ($\alpha(I)$), photosynthetically active radiation ($I(x, y, z, t)$), nitrogen (β_N including β_{NO_3} and β_{NH_4}), phosphorus (β_P) and silicate limitation (β_{SiO_2}) according to:

$$\alpha(I) = tanh(\alpha \cdot I(x, y, z, t)) \tag{7}$$

$$I(x, y, z, t) = \frac{I_s(x, y)}{2} exp(-k_w z - k_{phyto} \int_z^0 \sum_{i=1}^{3} C_{P_j} \partial z) \tag{8}$$

$$\beta_N = \beta_{NH_4} + \beta_{NO_3} \tag{9}$$

$$\beta_{NH_4} = \frac{NH_4}{r_{NH_4} + NH_4} \tag{10}$$

$$\beta_{NO_3} = \frac{NO_3}{r_{NO_3} + NO_3} exp(-\Psi \cdot NH_4) \tag{11}$$

$$\beta_P = \frac{PO_4}{r_{PO_4} + PO_4} \tag{12}$$

$$\beta_{Si} = max\Big(0, \frac{SiO_2 - Rr_{SiO_2}}{r_{SiO_2} + SiO_2}\Big) \tag{13}$$

The two zooplankton groups are distinguished by their feeding behaviour: one group is herbivorous (feeding on phytoplankton and detritus only), the other omnivorous (additionally feeding on the first zooplankton group). Grazing rates by zooplankton (G_i) are calculated with the help of the Michaelis-Menten equation (Michaelis and Menten, 1913). Food preferences of zooplankton follow the most commonly used partitioning according to Daewel and Schrum (2013) and are described in Table 3.

Sinks for the zooplankton biomass are caused by excretion and mortality. For the two zoo-

Table 3: Coefficients of food preference $a_{i,X}$.

Food source (X)	P_1	P_2	P_3	Z_1	D
Zooplankton group (i)	$\sigma_{i,X}/a_{i,X}$	$\sigma_{i,X}/a_{i,X}$	$\sigma_{i,X}/a_{i,X}$	$\sigma_{i,X}/a_{i,X}$	$\sigma_{i,X}/a_{i,X}$
Z_1	1.0/0.7	1.0/0.25	0.3/0.3	0	1.0/0.1
Z_2	0.8/0.1	0.8/0.85	0.3/0.3	0.5/0.15	0.8/0.1

plankton groups Z_1 and Z_2 follows for the term R_C in Equation 2.2:

$$R_{Z_1} = \gamma_1 C_{Z_1} \sum_{j=1}^{3} G_1 C_{P_j} + \gamma_2 G_1 C_D C_{Z_1} - G_2 C_{Z_1} C_{Z_2} - \mu_1 C_{Z_1} - m_{Z_1} C_{Z_1} \tag{14}$$

$$R_{Z_2} = \gamma_1 C_{Z_2} \sum_{j=1}^{3} G_2 C_{P_j} + \gamma_1 G_2 C_{Z_1} C_{Z_2} + \gamma_2 G_2 C_D C_{Z_2} - \mu_2 C_{Z_2} - m_{Z_2} C_{Z_2} \tag{15}$$

with

$$G_i(C_X) = \sigma_{i,X} \frac{a_{i,X} C_X}{r_i + F_i} \tag{16}$$

$$F_i = \sum_X a_{i,X} C_X \tag{17}$$

describing the respective grazing rates (X include all state variables serving as zooplankton prey).

Degradation products

Three degradation products are included in ECOSMO:
Detritus (D):

$$R_D = (1 - a_{DOM}) \cdot R_D^+ - R_D^- + \big[\frac{1}{dz}(RR \cdot SED_1 - SR \cdot D)\big]_{z=bottom} \tag{18}$$

$$
\begin{aligned}
R_D^+ = &(1-\gamma_1)\Big[\sum_{i=1}^{2} Z_i \sum_{j=1}^{3} G_i P_j + G_2 Z_1\Big] \\
&+ (1-\gamma_2)\sum_{i=1}^{2} Z_i G_i D + \sum_{j=1}^{3} m_{Pj} P_j + \sum_{i=1}^{2} m_{Zi} Z_i
\end{aligned} \tag{19}
$$

$$
R_D^- = \sum_{i=1}^{2} Z_i G_i D + \epsilon_D(T) \cdot D \tag{20}
$$

$$
\epsilon_D(T) = 0.006\,\mathrm{d}^{-1} \cdot \left(1 + 20 \cdot \left(\frac{T^2}{T_{ref}^2 + T^2}\right)\right) \tag{21}
$$

Dissolved Organic Matter (DOM):

$$
R_{DOM} = a_{DOM} \cdot R_D^+ - \epsilon_{DOM}(T) \cdot DOM \tag{22}
$$

$$
\epsilon_{DOM}(T) = 10 \cdot \epsilon_D(T) \tag{23}
$$

Opal ($Opal$):

$$
\begin{aligned}
R_{Opal} = &\frac{1}{REDF_{C:Si}}\Big[\sum_{i=1}^{2} G_i P_l Z_i + m_2 P_2 - \epsilon_{Si} \cdot Opal\Big] \\
&+ \Big[RR \cdot \frac{Sed_3}{dz} - SR \cdot Opal\Big]_{z=bottom}
\end{aligned} \tag{24}
$$

In contrast to D and DOM, biogenic opal is remineralized at a constant rate (ϵ_{Si}).

Sediments

Respiration processes in the sediment ($\epsilon_{Sed}(T)$) are described as a function of temperature by (Neumann et al., 2002):

$$
\epsilon_{Sed}(T) = 2 \cdot 0.001\,\mathrm{d}^{-1} \cdot e^{0.15^\circ\mathrm{C}^{-1} \cdot T} \tag{25}
$$

It follows for the three sediment variables:

$$\begin{aligned} R_{Sed1} = & SR \cdot D - RR \cdot Sed_1 - \delta_{burial} \cdot Sed_1 \\ & - \theta(O_2) \cdot \epsilon_{Sed}(T) \cdot Sed_1 - \theta(-O_2) \cdot \epsilon_{Sed}(T) \cdot Sed_1 \end{aligned} \tag{26}$$

$$\begin{aligned} R_{Sed2} = & - RR \cdot Sed_2 + \theta(O_2) \cdot (\epsilon_{Sed}(T) \cdot Sed_1 - \epsilon_{Sed}(T) \cdot Sed_2 \cdot (1 - 0.15\lambda)) \\ & + \theta(-O_2) \cdot (\epsilon_{Sed}(T) \cdot Sed_1 - \epsilon_{Sed}(T) \cdot Sed_2) \end{aligned} \tag{27}$$

$$\lambda = \frac{(\frac{O_2}{375})^2}{0.1^2 + (\frac{O_2}{375})^2} \tag{28}$$

$$\begin{aligned} R_{Sed3} = & SR \cdot Opal - RR \cdot Sed_3 - \delta_{burial} \cdot Sed_3 \\ & - \epsilon_{sed_3} \cdot Sed_3 \end{aligned} \tag{29}$$

It has to be pointed out that here, resuspension is considered in the equation for the second sediment pool (R_{Sed2}). In this, the model used here as a baseline deviates from the version presented in Daewel and Schrum (2013).

Nutrients

Nutrient concentrations change over time through uptake in primary production by phytoplankton, respiration processes in the water column and in the sediments and excretion by zooplankton.
Oxygen concentrations are further controlled by transfer across the sea surface (see Daewel and Schrum (2013) for further details) and nitrification ($\Omega(O_2, T)$). The latter also changes nitrate and ammonium concentrations.
The occurence of hydrogen sulfide as a product of sulfate reduction in organic matter degradation is accounted for by allowing negative oxygen concentrations.

$$
\begin{aligned}
R_{PO4} = & \frac{1}{REDF_{C:P}} \left[-\sum_{j=1}^{3} \sigma_j \Phi_{P_j} P_j + \epsilon_D(T) \cdot D + \sum_{i=1}^{2} \mu_i Z_i \right] \\
& + RR \cdot \frac{Sed_2}{dz} \\
& + \theta(O_2) \cdot \epsilon_{Sed} \cdot \frac{Sed_2}{dz}(1 - 0.15\lambda)\Big|_{z=bottom} \\
& + \theta(-O_2) \cdot \epsilon_{Sed} \cdot \frac{Sed_2}{dz}\Big|_{z=bottom}
\end{aligned} \tag{30}
$$

$$
\begin{aligned}
R_{NO3} = & \frac{1}{REDF_{C:N}} \left[-\frac{\beta_{NO3}}{\beta_N} \sum_{j=1}^{3} \sigma_j \Phi_{P_j} P_j \right] \\
& + \Omega(O_2, T) \cdot NH_4 \\
& - \theta(-O_2)\theta(NO_3) \cdot a_{denit} \cdot \epsilon_D(T) \cdot D \\
& - \theta(-O_2)\theta(NO_3) \cdot a_{denit} \cdot \epsilon_{Sed}(T) \cdot \frac{Sed_1}{dz}\Big|_{z=bottom}
\end{aligned} \tag{31}
$$

$$
\begin{aligned}
R_{NH4} = & \frac{1}{REDF_{C:N}} \left[-\frac{\beta_{NH4}}{\beta_N} \sum_{j=1}^{3} \sigma_j \Phi_{P_j} P_j + \epsilon_D(T) \cdot D + \sum_{i=1}^{2} \mu_i Z_i + a_{DOM} \cdot R_D^+ \right] \\
& - \Omega(O_2, T) \cdot NH_4 \\
& + (\theta(O_2) \cdot \frac{1}{2} \cdot \epsilon_{Sed}(T) + \theta(-O_2) \cdot \epsilon_{Sed}(T)) \cdot \frac{Sed_1}{dz})\Big|_{z=bottom}
\end{aligned} \tag{32}
$$

$$
\begin{aligned}
R_{SiO2} = & \frac{1}{REDF_{C:Si}} \left[-\Psi_2 \sigma_2 P_2 + \epsilon_{Si} \cdot Opal \right] \\
& + \epsilon_{Sed_3} \cdot \frac{Sed_3}{dz}\Big|_{z=bottom}
\end{aligned} \tag{33}
$$

$$
\begin{aligned}
R_{O_2} = & \left[\sum_{j=1}^{3} \sigma_j \Phi_{P_j} P_j \frac{6.625\beta_{NH4} + 8.125\beta_{NH4}}{\beta_N} - \theta(O_2)(6.625(\epsilon_D(T) \cdot D \right. \\
& \left. + a_{DOM} \cdot R_D^+ + \sum_{i=1}^{2} \mu_i Z_i) + 2(\Omega(O_2, T) \cdot NH_4)) \right] + SurfO_2 \\
& - \left[\frac{1}{REDF_{C:O_2} REDF_{C:N}} \left(\theta(O_2) \cdot (6.625 \cdot \epsilon_{Sed} \cdot \frac{Sed_1}{dz} \right. \right. \\
& \left. \left. + 2 \cdot \Omega(O_2, T) \cdot \epsilon_{Sed} \cdot \frac{Sed_1}{dz}) + \theta(-O_2)\theta(-NO_3) \cdot 6.625 \cdot \epsilon_{Sed} \frac{Sed_1}{dz} \right) \right]_{z=botom}
\end{aligned} \tag{34}
$$

$$\Omega(O_2, T) = \theta(O_2) \cdot 0.1\, d^{-1} \cdot e^{0.11°C^{-1} \cdot T} \cdot \frac{O_2}{0.01 + O_2} \tag{35}$$

$$SurfO_2 = \frac{\nu_p}{O_{2sat}(T, S) - O_2} \tag{36}$$

The equation for $\Omega(O_2, T)$ is taken from Stigebrandt and Wulff (1987).

Carbonate chemistry

The carbonate chemistry is an implementation of the Haltafall speciation code (Balckford and Gilbert, 2007; Ingri et al., 1967).
DIC and TA are prognostic variables and local changes occur due to physical (advection or turbulent diffusion) or reactive processes (see Equation 2.2).
The reaction term of DIC changes with primary production, degradation of organic matter and excretion by zooplankton following:

$$R_{DIC} = -\Psi_{P_{1,2,3}} + \mu_{Z1} \cdot Z_1 + \mu_{Z2} \cdot Z_2 \tag{37}$$

$$+ \epsilon_D \cdot D + \epsilon_{DOM} \cdot DOM + \epsilon_{Sed} \cdot Sed \tag{38}$$

TA depends on river discharge and is parametrized as a function of salinity. Relations between salinity and total alkalinity have been identified for different regions of the world's oceans by performing a regression analysis on observations (Lee et al., 2006). River discharge for the Baltic Sea is taken from Hjalmarsson et al. (2008) and for the North Sea from Artioli et al. (2012). At the open boundaries, the alkalinity-salinity relationship from Bellerby et al. (2005) is used.
The flux of CO_2 at the surface of the ocean (fCO_2) is calculated as a function of the difference in pCO_2 between atmosphere and ocean, the solubility of CO_2 in seawater and wind speed (Daewel et al., 2014):

$$fCO_2 = r_{tr} \cdot C_{Henry} \cdot (pCO_{2atm} - pCO_{2ocean}) \tag{39}$$

with

$$r_{tr} = (0.222 \cdot wind^2 + 0.33 \cdot wind) \cdot (\frac{Sc}{660})^{-\frac{1}{2}} \tag{40}$$

$$Sc = 2073.1 - 125.62 \cdot T + 3.6276 \cdot T^2 - 0.0432190 \cdot T^3 \tag{41}$$

Here, C_{Henry} is the Henry's Law Constant (function of teperature T and salinity S). The parametrization for the Schmidt number (Sc) is taken from Wanninkhof (1992), the one for the gas transfer rate (r_{tr}) from Jähne et al. (1987). *wind* denotes the wind speed in ms^{-1}.

Parameter values

Table 4: Parameters for primary and secondary production state variables.

Abbr.	Definition	Value	Units
$\sigma_{1,2,3}$	$P_{1,2,3}$ maximumm growth rate	1.1/1.3/1.0	d^{-1}
$m_{P1,2,3}$	$P_{1,2,3}$ mortality rate	0.08/0.05/0.08	d^{-1}
$I_s(x,y)$	Short wave radiation		$W\,m^{-2}$
α	Photosynthesis efficiency parameter	0.01	$W\,m^{-2-1}$
k_w	Water extinction coefficient	0.05	m^{-1}
k_{phyto}	Phytoplankton extinction parameter	0.2	$m^2(mmol\ C)^{-1}$
Φ	NH_4 inhibition parameter	3.00	$m^3(mmol\ C)^{-1}$
r_{NO3}	NO_3 half saturation constant	0.50	$mmol\ N\ m^{-3}$
r_{NH4}	NH_4 half saturation constant	0.20	$mmol\ N\ m^{-3}$
r_{PO4}	PO_4 half saturation constant	0.05	$mmol\ P\ m^{-3}$
r_{SiO2}	SiO_2 half saturation constant	0.50	$mmol\ Si\ m^{-3}$
Rr_{SiO2}	SiO_2 constant	1.00	$mmol\ Si\ m^{-3}$
r_Z	Z_1, Z_2 half saturation constant	3.3	$mmol\ C\ m^{-3}$
$m_{Z1,2}$	$Z_{1,2}$ mortality rate	0.2/0.1	d^{-1}
$\mu_{Z1,2}$	$Z_{1,2}$ excretion rate	0.08/0.06	d^{-1}
γ_1	Assimilation efficiency (grazing on $P_{1,2,3}$, Z_1)	0.75	-
γ_2	Assimilation efficiency (grazing on D)	0.30	-

Table 5: Parameters for degradation products state variables.

Abbr.	Definition	Value	Units
a_{DOM}	Fraction of DOM of total "new" dead material	0.4	-
SR	Sedimentation rate (if $\tau < \tau_{crit}$)	3.5	md^{-1}
RR	Resuspension rate (if $\tau \geq \tau_{crit}$)	25	d^{-1}
τ_{crit}	Critical bottom shear stress	0.007	$N\ m^{-2}$
γ_1	Assimilation efficiency (grazing on $P_{1,2,3}$, Z_1)	0.75	-
γ_2	Assimilation efficiency (grazing on D)	0.30	-
$m_{P1,2,3}$	Mortality rates of $P_{1,2,3}$	0.2/0.1	d^{-1}
$m_{Z1,2}$	Mortality rates of $Z_{1,2}$	0.08/0.05/0.08	d^{-1}
T_{ref}	D remineralization reference temperature	13	°C
w_D	D and Opal sinking speed	5.00	$m\ d^{-1}$

Table 6: Parameters for sediment state variables.

Abbr.	Definition	Value	Units
SR	Sedimentation rate (if $\tau < \tau_{crit}$)	3.5	m d^{-1}
RR	Resuspension rate (if $\tau \geq \tau_{crit}$)	25	d^{-1}
τ_{crit}	Critical bottom shear stress	0.007	N/m^2
δ_{burial}	Burial rate	10^{-5}	d^{-1}
ϵ_{sed_3}	Sediment remineralization SiO_2	0.0002	d^{-1}

Table 7: Parameters for nutrient state variables.

Abbr.	Definition	Value	Units
$\sigma_{1,2,3}$	$P_{1,2,3}$ maximumm growth rate	1.1/1.3/1.0	d^{-1}
$\mu_{1,2}$	$Z_{1,2}$ excretion rate	0.08/0.06	d^{-1}
a_{denit}	reduced nitrate/oxydized detritus	5.3	-
ϵ_{Si}	Si regeneration rate	0.015	d^{-1}
ν_p	Oxygen piston velocity	5.0	md^{-1}
$REDF_{C:P}$	Redfield Ratio (C:P)	106	mol C (mol P)$^{-1}$
$REDF_{C:N}$	Redfield Ratio (C:N)	6.625	mol C (mol N)$^{-1}$
$REDF_{C:Si}$	Redfield Ratio (C:Si)	6.625	mol C (mol Si)$^{-1}$
$REDF_{C:O_2}$	Redfield Ratio (C:O_2)	12.01	mg C (mmol C)$^{-1}$